
000
001
002
003
004
005
006
007
008
009
010
011
012
013
014
015
016
017
018
019
020
021
022
023
024
025
026
027
028
029
030
031
032
033
034
035
036
037
038
039
040
041
042
043
044
045
046
047
048
049
050
051
052
053

FROM GEOMETRY TO DYNAMICS: LEARNING OVERDAMPED LANGEVIN DYNAMICS FROM SPARSE OBSERVATIONS WITH GEOMETRIC CONSTRAINTS

Anonymous authors

Paper under double-blind review

ABSTRACT

How can we learn the laws underlying the dynamics of stochastic systems when their trajectories are sampled sparsely in time? Existing methods either require temporally resolved high-frequency observations, or rely on geometric arguments that apply only to conservative systems, limiting the range of dynamics they can recover. Here, we present a new framework that reconciles these two perspectives by reformulating inference as a stochastic control problem. Our method uses geometry-driven path augmentation, guided by the geometry in the system's invariant density to reconstruct likely trajectories and infer the underlying dynamics without assuming specific parametric models. Applied to overdamped Langevin systems, our approach accurately recovers stochastic dynamics even from extremely undersampled data, outperforming existing methods in synthetic benchmarks. This work demonstrates the effectiveness of incorporating geometric inductive biases into stochastic system identification methods.

1 INTRODUCTION

How can we discover the underlying driving forces that govern the behaviour of complex, stochastic systems when we only measure their state at discrete time points? From pollen motion in a liquid medium (Einstein, 1905) and chemical reactions (Li, 2020) to population dynamics (Silva-Dias and López-Castillo, 2018; Fisher and Mehta, 2014) and cell growth (Alonso et al., 2014), many natural processes evolve following stochastic dynamics, best described by Langevin or stochastic differential equations (SDEs) of the form

$$d\mathbf{X}_t = \mathbf{f}(\mathbf{X}_t) dt + \boldsymbol{\sigma} d\mathbf{W}_t. \quad (1)$$

Under this formalism, the deterministic part of the equation $\mathbf{f}(\cdot) : \mathcal{R}^d \rightarrow \mathcal{R}^d$, the *drift* function, captures the long-term evolution of the state variables, while the stochastic part $\boldsymbol{\sigma} : \mathcal{R}^d \times \mathcal{R}^d$, the *diffusion*, accounts for the contribution of unresolved degrees of freedom. In practice, however, we rarely observe these systems at the fine time scales required by existing inference methods.

Recent advances in dynamical system inference have delivered valuable tools for identifying continuous-time *deterministic* systems from observations (Cremers and Hübler, 1987; Brunton et al., 2016; Daniels and Nemenman, 2015; McGoff et al., 2015; Kantz and Schreiber, 2004; Schmidt and Lipson, 2009). **Data-driven** (or **nonparametric**, or **equation-free**) approaches seek to reconstruct the governing equations of observed systems directly from state observations, without imposing explicit assumptions or inductive biases about the underlying dynamical models. They rely on function approximation to infer the system's structure from observations, such as basis functions (Acosta, 1995; Small and Tse, 2002; Judd and Mees, 1995; Small and Judd, 1998; Brückner et al., 2020; Frishman and Ronceray, 2020), symbolic regression (Kaiser et al., 2018; Brunton et al., 2016; Bongard and Lipson, 2007; Daniels and Nemenman, 2015), spectral approximations (Kevrekidis et al., 2003; Theodoropoulos et al., 2000), Gaussian processes (Alvarez et al., 2009; Sanguinetti et al., 2006; Särkkä, 2019), or neural networks (Teng, 2018; Bhattoo et al., 2022; Jingling et al., 2019). However, extending these methods to *stochastic* systems remains difficult. In this setting, inference must disentangle the influence of underlying deterministic forces from random fluctuations, a task that is particularly difficult when sampling rates are low.

Two dominant perspectives for stochastic inference. Data-driven system identification for stochastic systems largely follows two tracks. **Temporal methods** (Fig. 1A.) rely on the tempo-

054
055
056
057
058
059
060
061
062
063
064
065
066
067

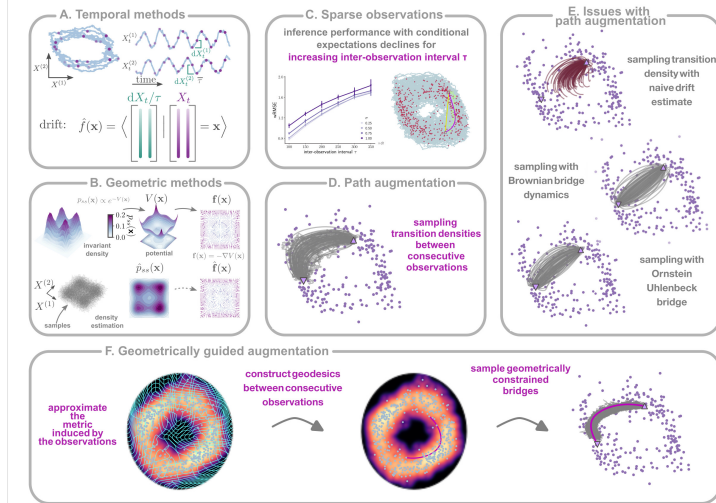


Figure 1

Temporal and geometric perspectives for discovering stochastic dynamics and proposed inference with geometrically guided augmentation. (A.) Temporal methods consider the time-ordering of observations $\{\mathcal{O}_k\}_{k=1}^K$ (purple dots) to approximate the drift $f(\mathbf{x})$ with conditional rescaled state increments $\hat{f}(\mathbf{x}) = \langle \frac{d\mathbf{X}_t}{\tau} | \mathbf{X}_t = \mathbf{x} \rangle$. (B.) Geometric methods assume a conservative drift $f(\mathbf{x}) = -\nabla V(\mathbf{x})$ as the gradient of a potential. (C.) With increasing inter-observation interval τ performance of temporal methods degrades because Euclidean distances ignore the curvature of the latent continuous path between consecutive observations. (D.) Path augmentation alternates between state estimation - by sampling diffusion bridges for each inter-observation interval - and drift inference. (E.) Commonly used path augmentation methods employ Brownian or Ornstein-Uhlenbeck bridges that increasingly deviate from the unobserved path as τ grows. (lower) Illustration of the ground truth (neon green) and geodesic (magenta) continuous path between two observations and of that assumed during inference with Gaussian likelihood (yellow line). (F.) Geometrically guided augmentation approximates first the metric induced by the invariant density, constructs geodesics connecting consecutive observations, and samples geometrically constrained diffusion bridges.

ral ordering of measurements, regressing state increments against states to estimate the drift, which works when the inter-observation interval (τ) is small (Batz et al., 2018; Friedrich and Peinke, 1997; Ragwitz and Kantz, 2001). **Geometric methods** on the other hand, approximate the **invariant density** (Batz et al., 2016; Gu et al., 2021) or eigenstructure of the infinitesimal generator of the diffusion process (Singer and Coifman, 2008; Nüske et al., 2021; Ionides et al., 2006; Talmon and Coifman, 2015; Dsilva et al., 2016; Berry and Harlim, 2018)) (Fig. 1B.), but are nevertheless limited to systems with conservative forces (Berry and Harlim, 2015; Batz et al., 2016) or decoupled state variables (Singer and Coifman, 2008). Each perspective has limitations: temporal approaches deteriorate with increasing inter-observation intervals (Fig. 1C.), whereas geometric methods are restricted to conservative flows.

A unifying perspective: reconcile temporal and geometric methods by constraining with most probable paths extracted from the invariant density. Here, we recast inference into a stochastic control problem and introduce **geometry-aware path augmentation**. Our method follows a simple premise that incorporates **geometric inductive biases** informed by the system's *invariant density* into dynamical inference: we postulate that the augmented paths should lie **in the vicinity of geodesic curves** (Fig. 1F. middle, magenta line) that connect consecutive measurements on the **empirical manifold** induced by the observations. To achieve this, (i) we approximate the Riemannian metric induced by the observations (Fig. 1F) without the need to predefined the dimensionality of the empirical manifold, (ii) compute geodesics between consecutive observations through nonparametric approximation of shortest path distances between consecutive observations according to the approximated metric, and (iii) estimate the unobserved path between consecutive observations by generating **geometrically constrained diffusion bridges** that both respect temporal order and are guided toward identified geodesics (Fig. 1 F.). Nonparametric estimation of the drift function based on the augmented paths within an Expectation Maximisation framework (E.M.) (Dempster et al., 1977) results in accurate approximations of the underlying

108

109

110

111

112

stochastic dynamics. Extensive numerical experiments demonstrate the effectiveness of our proposed method in recovering the true stochastic dynamics, even in challenging scenarios where existing approaches fail.

113

2 SETUP AND BACKGROUND

114

115

116

117

Setting. We consider a system whose state evolves according to Eq. 1. Here, $\mathbf{X}_t \in \mathcal{R}^d$ denotes the state of the system, $\mathbf{f}(\cdot) : \mathcal{R}^d \rightarrow \mathcal{R}^d$ is the drift function, σ stands for the diffusion constant or matrix, and $\mathbf{W}_t \in \mathcal{R}^d$ is a d -dimensional Wiener process representing random noise input or unresolved degrees of freedom.

118

119

Data. We observe the system state at discrete time points $t_k = k\tau$ at **inter-observation intervals** of τ time units, obtaining a time-ordered set of observations $\{\mathcal{O}_k \doteq \mathbf{X}_{t_k}\}_{k=1}^K$.

120

121

Goal. Our goal is to estimate the drift function $\mathbf{f}(\cdot)$ representing the deterministic forces acting on the system of interest from the discrete state observations $\{\mathcal{O}_k\}_{k=1}^K$.

122

123

124

125

Background. Common inference methods for this setting consider observations from the system path $\mathbf{X}_{0:T}$ in (nearly) continuous time (Batz et al., 2018; Friedrich and Peinke, 1997). Under such conditions, the infinitesimal transition probability of the SDE between observations \mathbf{X}_t and \mathbf{X}_{t+dt} is Gaussian

126

127

$$P_f(\mathbf{X}_{0:T} \mid \mathbf{f}) \propto \exp \left(-\frac{1}{2dt} \sum_t \|\mathbf{X}_{t+dt} - \mathbf{X}_t - \mathbf{f}(\mathbf{X}_t)dt\|_D^2 \right), \quad (2)$$

128

129

130

131

132

where $\|\mathbf{u}\|_D \doteq \mathbf{u}^\top \cdot \mathbf{D}^{-1} \cdot \mathbf{u}$, denotes the weighted norm with $\mathbf{D} \doteq \sigma \sigma^\top$ indicating the noise covariance. The likelihood for the drift \mathbf{f} given the path $\mathbf{X}_{0:T}$ observed during $[0, T]$, results from the Radon-Nykodym derivative (likelihood ratio) between $P_f(\mathbf{X}_{0:T} \mid f)$ and the transition probability of a Wiener path $P_W(\mathbf{X}_{0:T}) = \exp \left(-\frac{1}{2dt} \sum_t \|\mathbf{X}_{t+dt} - \mathbf{X}_t\|_D^2 \right)$ as (Liptser and Shiryaev, 2013)

133

134

135

$$\mathcal{L}(\mathbf{X}_{0:T} \mid \mathbf{f}) = \exp \left(-\frac{1}{2} \sum_t \|\mathbf{f}(\mathbf{X}_t)\|_D^2 dt + \sum_t \langle \mathbf{f}(\mathbf{X}_t), \mathbf{X}_{t+dt} - \mathbf{X}_t \rangle_D \right). \quad (3)$$

136

137

138

This likelihood has a quadratic form in terms of the drift function. This makes **Gaussian process** priors a natural and widely employed approach for modelling \mathbf{f} (Ruttor et al., 2013; Hostettler et al., 2018; Zhao et al., 2020).

139

140

141

142

143

144

145

However, these approaches rely on *small* inter-observation intervals τ (Batz et al., 2018). As τ increases, the EuM approximation becomes inaccurate: transition densities are not Gaussian, and higher-order remainder terms related to the curvature of the flow field become important (see further theoretical analysis in Sec. H.2 and c.f. Fig. 5). Attempts to mitigate this problem by introducing bridge sampling to infer the unobserved path between observations (Batz et al., 2018; Sermaidis et al., 2013) provide small improvements, because these methods rely on linearised or otherwise simplified bridge dynamics that do not match the true transition densities (c.f. Sec. E).

146

147

148

Here, we target this large inter-observation interval setting by merging insights from both temporal and geometric perspectives. Specifically, our approach combines **nonlinear** bridge sampling with **a geometric approximation of the system's invariant density** as detailed in the following.

149

150

3 METHODOLOGY

151

152

153

154

155

156

157

158

159

Core idea. The invariant density of the observed system imposes a low-dimensional structure on the state space, within which the observations are confined. We propose that this low-dimensional structure is well approximated by a Riemannian manifold $\mathcal{M}_\infty \in \mathcal{R}^{m \leq d}$ in the ambient space (Sec. G), and that the ensemble of observations $\{\mathcal{O}_k\}_{k=1}^K$ offers a reliable discrete approximation to \mathcal{M}_∞ . We term this observation-based approximation the *empirical manifold* \mathcal{M} . The central premise of our approach is that **unobserved paths between successive observations will be lying either on or in the vicinity of the empirical manifold \mathcal{M}** . In particular, we postulate that unobserved paths should lie **in the vicinity of geodesics that connect consecutive observations** on \mathcal{M} .

160

161

However, while this view of a lower dimensional manifold embedded in a higher dimensional ambient space helps to build intuition, for practical purposes we adopt a complementary view of the low dimensional manifold inspired by (Fröhlich et al., 2021). According to this view, we consider

the entire observation space \mathcal{R}^d as a smooth Riemannian manifold, $\mathcal{M} \doteq \mathcal{R}^d$, characterised by a Riemannian metric \mathfrak{h} . The effect of the nonlinear geometry of the observations is then captured by the metric \mathfrak{h} . Thus to approximate the geometric structure of the system's invariant density, we learn the Riemannian metric tensor $H : \mathcal{R}^d \rightarrow \mathcal{R}^{d \times d}$ and compute the geodesics between consecutive observations according to the learned metric. Intuitively according to this view the observations $\{\mathcal{O}_k\}_{k=1}^K$ introduce distortions in the way we compute distances on the state space. The advantage of this approach is that we do not have to estimate the dimensionality of the empirical manifold, which would have been difficult due to the presence of fluctuations in the system's dynamics. Instead, we still operate in the original space and the empirical manifold introduces distortions in the estimated metric (see Fig. 1F.i.).

Inference framework. Our approach comprises three steps: **(α .)** Approximation of the geometric structure of the system’s invariant density with metric learning, **(β .)** estimation of the (latent) system state between consecutive observations guided by the invariant density (**path augmentation**), and **(γ .)** data-driven estimation of the drift function (Fig. 1). We perform the two final steps in an iterative manner within an Expectation Maximisation (**E.M.**) framework (Dempster et al., 1977).

(a) Approximating the Riemannian geometry induced by the observations. Although there are many methods for approximating Riemannian manifolds (Tenenbaum et al., 2000; Balasubramanian and Schwartz, 2002; Mead, 1992; Roweis and Saul, 2000), our objective is to obtain a representation that acts as a *local* constraint for subsequent state estimation between consecutive observations. We achieve this in two steps: **(i.)** We approximate in the ambient space \mathcal{R}^d the metric \mathfrak{h} induced by the observations (see Fig. 1F.i.). This identifies regions of the state space with high observation density (represented with small metric values). **(ii.)** We construct geodesics between consecutive observations on the empirical manifold $(\mathcal{M} \dot{=} \mathcal{R}^d, \mathfrak{h})$ (see Fig. 1F.ii.). The geodesics identify the most probable paths between consecutive observations, and each such path subsequently functions as a constraint during latent state estimation.

(i) Approximation of the invariant metric. To approximate the (local) metric \mathfrak{h} in a nonparametric form at locations \mathbf{x} of the state space, we follow Arvanitidis et al. (2019), and consider the inverse of the weighted local diagonal covariance computed on the K observations as

$$H_{dd}(\mathbf{x}) = \left(\sum_{k=1}^K w_k(\mathbf{x}) \left(\mathcal{O}_k^{(d)} - x^{(d)} \right)^2 + \epsilon \right)^{-1}, \quad (4)$$

with weights $w_k(\mathbf{x}) = \exp\left(-\frac{\|\mathcal{O}_k - \mathbf{x}\|_2^2}{2\sigma_{\mathcal{M}}^2}\right)$, and $A^{(d)}$ denoting the d -th dimensional component of the vector \mathbf{A} for $\mathbf{A} \in \{\mathbf{x}, \mathcal{O}_k\}$. The parameter $\epsilon > 0$ is a small value ensuring non-zero diagonals of the weighted covariance matrix, while $\sigma_{\mathcal{M}}$ is a hyper-parameter characterising the curvature of the approximated manifold.

(ii) Constructing geodesics between consecutive observations. To compute the geodesic curves connecting consecutive observations on the empirical manifold, we employ the approximated metric tensor $\mathbf{H}(\mathbf{x})$. We identify the geodesic curve $\gamma_{t'}^k$ between \mathcal{O}_k and \mathcal{O}_{k+1} as the curve with minimum energy that connects these two points, i.e., as the minimiser of the kinetic energy functional $\mathcal{E}(\gamma_{t'}^k) = \int_0^1 L_{\mathcal{M}}(\gamma_{t'}^k, \dot{\gamma}_{t'}^k) dt'$

$$\gamma_{t'}^{k*} = \arg \min_{\gamma_{t'}^k, \dot{\gamma}_{t'}^k} \int_0^1 L_{\mathcal{M}}(\gamma_{t'}^k, \dot{\gamma}_{t'}^k) dt', \quad \text{with} \quad \int_0^1 L_{\mathcal{M}}(\gamma_{t'}^k, \dot{\gamma}_{t'}^k) dt' = \frac{1}{2} \int_0^1 \|\dot{\gamma}_{t'}^k\|_{\mathfrak{h}}^2, \\ \gamma_0^k = \mathcal{O}_k, \gamma_1^k = \mathcal{O}_{k+1} \quad (5)$$

where $L_{\mathcal{M}}(\gamma_{t'}^k, \dot{\gamma}_{t'}^k)$ is an appropriately constructed Lagrangian. The minimising curve of this functional is the same as the minimiser of the curve length functional $\ell(\gamma_{t'})$ (c.f. Eq. 33), i.e., the geodesic (Do Carmo and Flaherty Francis, 1992). This results in a system of second order differential equations (Eq. 36) (Arvanitidis et al., 2017; Do Carmo and Flaherty Francis, 1992) (Sec. A.3.2) with boundary conditions $\gamma_0^k = \mathcal{O}_k$ and $\gamma_1^k = \mathcal{O}_{k+1}$ that we solve with a probabilistic differential equation solver as in (Arvanitidis et al., 2019).

(B.) Latent state estimation: Geometry-guided augmentation. To estimate the unobserved system state between consecutive observations \mathcal{O}_k and \mathcal{O}_{k+1} , we perform variational inference (Beal, 2003)(see Sec. A.3). Given a prior diffusion process with drift $\hat{f}(\cdot) : \mathcal{R}^d \rightarrow \mathcal{R}^d$ and diffusion σ ,

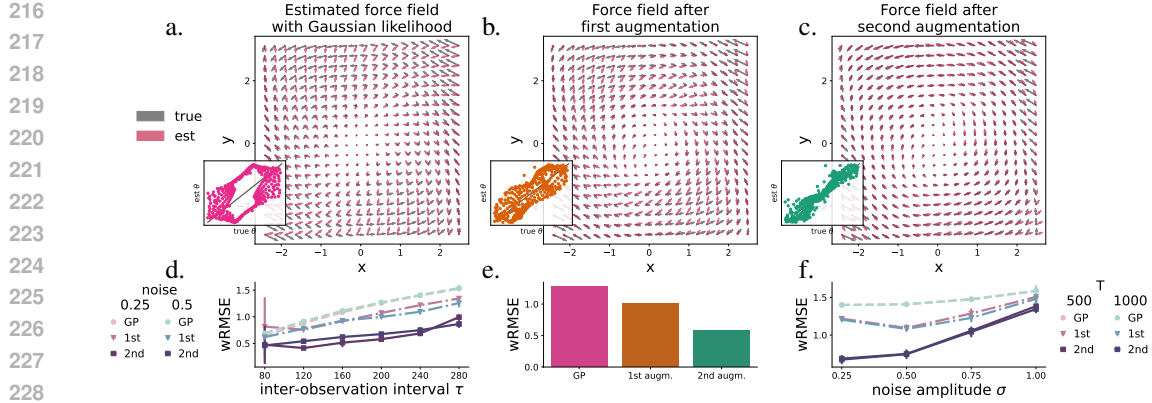


Figure 2

Geometry-aware path augmentation improves drift inference after two iterations. Estimated (red) vs. true (grey) force field with a.) Gaussian likelihood, b.) after one, and c.) after two augmentations. (Insets) True vs. estimated angles at grid points. d.) Weighted (by observation density) root mean square error (wRMSE) vs. inter-observation interval τ for different noise levels $\sigma = \{0.25, 0.5\}$ for drift estimated with a Gaussian likelihood (gaus-circles), after first augmentation (1st-triangles), and after second augmentation (2nd-squares) for $T = 500$ (time units). e.) wRMSE across iterations for the presented example. f.) wRMSE vs. noise amplitude σ for different trajectory durations $T = \{500, 1000\}$ (time units) for inter-observation interval $\tau = 240$ (dt). Markers in d.) and f.) indicate augmentation steps. Error bars: one standard deviation over five independent runs.

we construct an **approximating process** conditioned **i.)** to pass through the observations, and **ii.)** to respect the local geometry of the invariant density as it is represented by the geodesics. The conditioned process is also a diffusion process with the same diffusion constant and an effective drift function $\mathbf{g}(\mathbf{x}, t)$ (Chetrite and Touchette, 2015; Majumdar and Orland, 2015). The path probability measure $Q_X(\mathbf{X}_{0:T})$ induced by the approximating process

$$Q_X(\mathbf{X}_{0:T}) : d\mathbf{X}_t = \mathbf{g}(\mathbf{X}_t, t) dt + \sigma d\bar{\mathbf{W}}_t = \left(\hat{\mathbf{f}}(\mathbf{X}_t) + \mathbf{u}(\mathbf{X}_t, t) \right) dt + \sigma d\bar{\mathbf{W}}_t, \quad (6)$$

provides an approximation to the unobserved continuous system state. In Eq. 6 $\mathbf{u}(\cdot, \cdot) : \mathcal{R}^d \times \mathcal{R}^+ \rightarrow \mathcal{R}^d$ is a time-dependent control term that guides the approximating path distribution through the observations, while staying in the vicinity of the corresponding geodesics between them.

More precisely, we obtain the controlled drift $\mathbf{g}(\mathbf{X}_t, t)$ from the solution of the variational problem of minimising the functional (see Sec. A.3.1)

$$\begin{aligned} \mathcal{F}[Q_X] &= \mathcal{KL}\left(Q_X(\mathbf{X}_{0:T}) \mid\mid \mathbf{P}(\mathbf{X}_{0:T} \mid \hat{\mathbf{f}})\right) - \sum_{k=1}^K \left\langle \ln \mathbf{P}(\mathcal{O}_k \mid \mathbf{X}_{t_k}) \right\rangle_Q + \left\langle \|\boldsymbol{\Gamma}_t - \mathbf{X}_{0:T}\|^2 \right\rangle_Q \\ &= \frac{1}{2} \int_0^T \int \left[\|\mathbf{g}(\mathbf{x}, t) - \hat{\mathbf{f}}(\mathbf{x})\|_{\mathbf{D}}^2 + U_{\mathcal{O}}(\mathbf{x}, t) + \beta U_{\mathcal{G}}(\mathbf{x}, t) \right] q_t(\mathbf{x}) d\mathbf{x} dt, \end{aligned} \quad (7)$$

where $\boldsymbol{\Gamma}_t$ denotes the sequence of K geodesics indexed by time t , $\boldsymbol{\Gamma}_t \doteq \{\boldsymbol{\gamma}_{t'}^k\}_{t=(k-1)\tau+t'\tau}$, where $\boldsymbol{\gamma}_{t'}^k$ is the geodesic connecting \mathcal{O}_k and \mathcal{O}_{k+1} , and $t' \in [0, 1]$ denotes a rescaled time variable, and β is a weighting term. In Eq. 7, the term $U_{\mathcal{O}}(\mathbf{x}, t) = -\sum_{t_k} \ln \mathbf{P}(\mathcal{O}_k \mid \mathbf{x}) \delta(t - t_k)$ **forces the augmentation to pass through the observations at each bridge boundary**, while $U_{\mathcal{G}}(\mathbf{x}, t) \doteq \|\boldsymbol{\Gamma}_t - \mathbf{x}\|^2$ **guides the latent path towards the identified geodesics**.

This minimisation can be construed as a stochastic control problem (Opper, 2019) with the objective to identify a time-dependent drift adjustment $\mathbf{u}(\mathbf{x}, t) := \mathbf{g}(\mathbf{x}, t) - \hat{\mathbf{f}}(\mathbf{x})$ for the system with drift $\hat{\mathbf{f}}(\mathbf{x})$ so that the controlled dynamics fulfil the path constraints $U_{\mathcal{O}}(\mathbf{x}, t)$ and $U_{\mathcal{G}}(\mathbf{x}, t)$.

270 The optimal time-dependent control for
 271 the interval between \mathcal{O}_k and \mathcal{O}_{k+1} results
 272 from the solution of the backward equation
 273 (Kappen, 2005a; Maoutsas and Opper,
 274 2022)

$$275 \frac{\partial \phi_t(\mathbf{x})}{\partial t} = -\mathcal{L}_f^\dagger \phi_t(\mathbf{x}) + U_G(\mathbf{x}, t) \phi_t(\mathbf{x}), \quad (8)$$

278 with terminal condition $\phi_{t_{k+1}}(\mathbf{x}) =$
 279 $\chi(\mathbf{x}) = \delta(\mathbf{x} - \mathcal{O}_{k+1})$ and with \mathcal{L}_f^\dagger
 280 denoting the adjoint Fokker-Planck operator
 281 for the process of Eq. 26. As shown
 282 in Maoutsas and Opper (2022) the optimal
 283 drift adjustment $\mathbf{u}(\mathbf{x}, t)$ can be expressed
 284 in terms of the difference of the logarithmic
 285 gradients of two probability flows

$$286 \mathbf{u}^*(\mathbf{x}, t) = \mathbf{D} \left(\nabla \ln q_{T-t}(\mathbf{x}) - \nabla \ln \rho_t(\mathbf{x}) \right), \quad (9)$$

289 where ρ_t fulfills the forward (filtering) par-
 290 tial differential equation (PDE)

$$291 \frac{\partial \rho_t(\mathbf{x})}{\partial t} = \mathcal{L}_f \rho_t(\mathbf{x}) - U_G(\mathbf{x}, t) \rho_t(\mathbf{x}), \quad (10)$$

294 while q_t is the solution of a time-reversed PDE with initial condition $q_0(\mathbf{x}) \propto \rho_T(\mathbf{x}) \chi(\mathbf{x})$

$$295 \frac{\partial q_t(\mathbf{x})}{\partial t} = -\nabla \cdot \left[\left(\mathbf{D} \nabla \ln \rho_{T-t}(\mathbf{x}) - \hat{\mathbf{f}}(\mathbf{x}, T-t) \right) q_t(\mathbf{x}) \right] + \frac{\mathbf{D}}{2} \nabla^2 q_t(\mathbf{x}). \quad (11)$$

300 Thus, for each interval $[\mathcal{O}_k, \mathcal{O}_{k+1}]$ we identify the posterior path measure (minimiser of Eq. 37) by
 301 solving such a stochastic control problem for the time-varying control $\mathbf{u}(\mathbf{x}, t)$ of Eq. 9. This results
 302 in a set of $K-1$ independent optimal control problems, that are solved in parallel for efficiency.

303 **(γ.) Estimating the drift.** We approximate the drift function in a model independent framework
 304 by imposing a Gaussian process prior on the function values $\mathbf{f} \sim P_o(\mathbf{f}) = \mathcal{GP}(\mathbf{m}^f, k^f)$, where \mathbf{m}^f
 305 and k^f denote the mean and covariance function of the Gaussian process. The optimal measure for
 306 the drift Q_f is a Gaussian process given by (Batz et al., 2018)

$$307 Q_f \propto P_o \exp \left(-\frac{1}{2} \int \| \mathbf{f}(\mathbf{x}) \|_D^2 A(\mathbf{x}) - 2 \langle \mathbf{f}(\mathbf{x}), B(\mathbf{x}) \rangle_D d\mathbf{x} \right), \quad (12)$$

309 with $A(\mathbf{x}) \doteq \int_0^T q_t(\mathbf{x}) dt$ and $B(\mathbf{x}) \doteq \int_0^T q_t(\mathbf{x}) \mathbf{g}(\mathbf{x}, t) dt$, where $q_t(\mathbf{x})$ denotes the marginal density
 310 of the constrained process' state obtained by the state estimation. The function $\mathbf{g}(\mathbf{x}, t)$ denotes the
 311 effective (time-dependent) drift of the constrained process (Eq. 6), resulting from the solution of the
 312 individual control problems accounting for the observations and the invariant geometry.

314 RESULTS

315 **Revealing stochastic dynamics in model systems.** To demonstrate the effectiveness of our ap-
 316 proach, we inferred the stochastic dynamics of model systems, and compared the resulting estimates
 317 to those obtained from: **(i.)** Gaussian process regression without state estimation (**GP**), **(ii.)** path
 318 augmentation with Ornstein-Uhlenbeck dynamics (**OU**) (Batz et al., 2018), **(iii.)** sparse variational
 319 inference with state estimation (**SVISE**) (Course and Nair, 2023a), **(iv.)** basis function approxima-
 320 tion of Kramers-Moyal coefficients, i.e. the drift function (**KM-basis**) (Nabeel et al., 2025), and **(v.)**
 321 latent SDE inference with amortized reparameterization with (**LatentSDE+GP-pre**) and without
 322 pre-training (**LatentSDE**) (Course and Nair, 2023b), **(vi.)** metric flow matching (**MFM**) (Kapus-
 323 niak et al., 2024) (with RBF (Arvanitidis et al., 2021) and LAND metric (Arvanitidis et al., 2019)
 324 metric approximations), **(vii.)** generalized Schrödinger bridge matching (**GSBM**) (Liu et al., 2023),

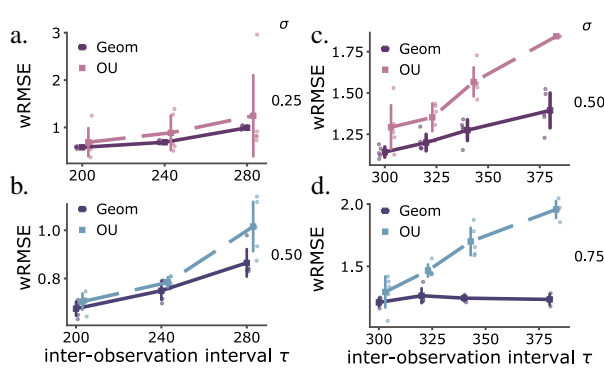


Figure 3

Comparison of geometry-aware inference against inference with Ornstein-Uhlenbeck augmentation. Weighted root mean square error (wRMSE) vs. different inter-observation intervals τ for different noise amplitudes for moderate inter-observation intervals with a.) $\sigma = 0.25$ and b.) $\sigma = 0.50$, and for large inter-observation intervals with c.) $\sigma = 0.50$ and d.) $\sigma = 0.75$, where only one observation per oscillation period is available. Error bars indicate one standard deviation over five independent runs.

Van der Pol								
wRMSE ↓	total duration T	$\tau = 80 \times dt$	$\tau = 120 \times dt$	$\tau = 160 \times dt$	$\tau = 200 \times dt$	$\tau = 240 \times dt$	$\tau = 280 \times dt$	
$\sigma = 0.25$								
GP	500	0.642 ± 0.006	0.879 ± 0.005	1.083 ± 0.015	1.258 ± 0.011	1.399 ± 0.003	1.528 ± 0.0153	
SVISE	500	1.465 ± 0.009	0.857 ± 0.021	0.740 ± 0.072	0.592 ± 0.026	0.587 ± 0.112	0.824 ± 0.003	
KM-basis	500	0.368 ± 0.054	0.452 ± 0.011	0.671 ± 0.023	1.588 ± 0.021	1.751 ± 0.008	1.735 ± 0.020	
LatentSDE	500	1.091 ± 0.316	1.091 ± 0.039	1.098 ± 0.023	1.089 ± 0.036	1.088 ± 0.038	1.091 ± 0.039	
LatentSDE+GP-pre	500	1.095 ± 0.038	1.085 ± 0.039	1.101 ± 0.034	1.089 ± 0.038	1.106 ± 0.045	1.102 ± 0.039	
GSBM	500	1.518 ± 0.033	1.435 ± 0.055	-	-	-	-	
[SF]2M	1500	1.741 ± 0.304	1.801 ± 0.226	1.745 ± 0.322	1.583 ± 0.132	1.816 ± 0.228	1.721 ± 0.094	
MFM _{RBF}	1500	1.462 ± 0.007	1.469 ± 0.005	1.470 ± 0.012	1.469 ± 0.008	1.469 ± 0.006	1.466 ± 0.008	
MFM _{LAND}	1500	1.463 ± 0.007	1.469 ± 0.005	1.469 ± 0.012	1.469 ± 0.008	1.469 ± 0.006	1.467 ± 0.008	
Geometric_{RBF} (our)	500	0.419 ± 0.052	0.458 ± 0.063	0.493 ± 0.031	0.517 ± 0.022	0.657 ± 0.040	1.001 ± 0.077	
Geometric (our)	500	0.474 ± 0.034	0.413 ± 0.016	0.514 ± 0.068	0.578 ± 0.022	0.687 ± 0.032	0.993 ± 0.037	
$\sigma = 0.50$								
GP	500	0.691 ± 0.029	0.916 ± 0.014	1.114 ± 0.15	1.272 ± 0.030	1.409 ± 0.019	1.542 ± 0.044	
SVISE	500	1.235 ± 0.083	0.9935 ± 0.015	0.7505 ± 0.052	0.736 ± 0.072	1.3565 ± 0.278	1.425 ± 0.086	
KM-basis	500	0.495 ± 0.010	0.727 ± 0.008	0.890 ± 0.024	1.683 ± 0.020	1.744 ± 0.038	1.732 ± 0.065	
LatentSDE	500	1.158 ± 0.036	1.151 ± 0.045	1.160 ± 0.032	1.151 ± 0.036	1.146 ± 0.033	1.176 ± 0.046	
LatentSDE+GP-pre	500	1.158 ± 0.045	1.159 ± 0.034	1.159 ± 0.027	1.151 ± 0.034	1.150 ± 0.028	1.191 ± 0.052	
GSBM	500	6.106 ± 2.988	4.818 ± 3.060	4.738 ± 3.304	4.875 ± 3.222	9.076 ± 1.451	26.187 ± 18.804	
[SF]2M	1500	1.869 ± 0.482	1.813 ± 0.286	1.484 ± 0.096	1.876 ± 0.247	1.753 ± 0.158	1.707 ± 0.233	
MFM _{RBF}	1500	1.516 ± 0.011	1.525 ± 0.006	1.538 ± 0.009	1.537 ± 0.017	1.528 ± 0.015	1.544 ± 0.019	
MFM _{LAND}	1500	1.517 ± 0.011	1.526 ± 0.006	1.536 ± 0.009	1.537 ± 0.017	1.528 ± 0.015	1.545 ± 0.019	
Geometric_{RBF} (our)	500	0.653 ± 0.014	0.690 ± 0.026	0.694 ± 0.026	0.761 ± 0.050	0.798 ± 0.047	0.933 ± 0.160	
Geometric (our)	500	0.462 ± 0.019	0.541 ± 0.023	0.621 ± 0.012	0.675 ± 0.030	0.750 ± 0.038	0.865 ± 0.057	

Table 1

Performance comparison in terms of weighted root mean square error (wRMSE) of considered frameworks for different noise conditions σ and inter-observation intervals τ for the Van der Pol system.

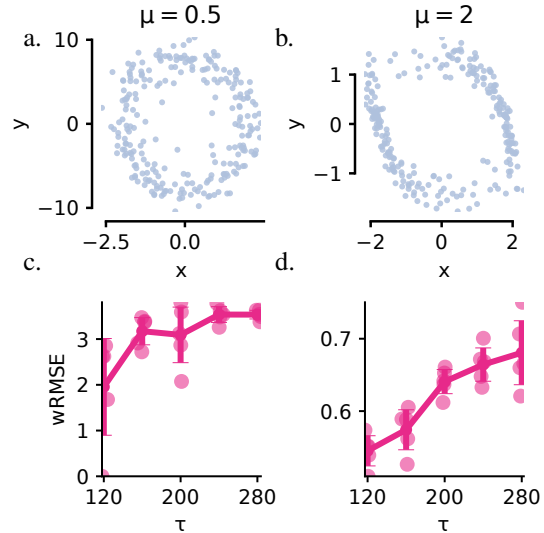


Figure 4

Geometry-aware inference provides accurate drift estimation for different empirical manifold geometries resulting from different parameter regimes of the Van der Pol system. (a.-b.) Empirical manifold for the Van der Pol system with different μ parameters. Notice the different scales on the axes. (c.-d.) Inference performance of the proposed framework against inter-observation interval τ . Error bars indicate one standard deviation over five independent runs.

378	379	Out of equilibrium system				Hopf			Selkov	
		wRMSE ↓	$\tau = 150$	$\tau = 200$	$\tau = 250 \times dt$	$\tau = 200$	$\tau = 300$	$\tau = 400 \times dt$	$\tau = 100$	$\tau = 200 \times dt$
380	380	GP	2.632 \pm 0.007	3.387 \pm 0.012	3.733 \pm 0.011	0.781 \pm 0.006	0.969 \pm 0.015	1.069 \pm 0.006	0.550 \pm 0.021	0.682 \pm 0.040
381	381	SVISE	35.204 \pm 39.888	3.462 \pm 0.129	7.540 \pm 7.602	2.113 \pm 0.658	4.960 \pm 2.687	3.936 \pm 1.063	5.793 \pm 0.028	2.028 \pm 0.045
382	382	LatentSDE	2.348 \pm 0.032	2.340 \pm 0.047	2.356 \pm 0.042	1.168 \pm 0.052	1.161 \pm 0.053	1.173 \pm 0.046	0.742 \pm 0.022	0.747 \pm 0.021
383	383	Geometric (ours)	2.762 \pm 0.132	3.034 \pm 0.143	2.693 \pm 0.992	0.210 \pm 0.013	0.237 \pm 0.010	0.255 \pm 0.028	0.414 \pm 0.245	0.682 \pm 0.071

Table 2

Performance comparison in terms of wRMSE for the considered frameworks for three different nonlinear dynamical systems and for increasing inter-observation interval τ . Numbers indicate mean wRMSE and standard deviation of five independent runs for each setting.

For a system with a drift function following Van der Pol dynamics, we found that only after two E.M. iterations, the estimated force field (red arrows) is well aligned to the true force field that generated the observations (grey arrows) (Fig. 2a.). For comparison we demonstrate also the result of the estimation with Gaussian likelihood (GP), which results in a flow field orthogonal to the ground truth one.

We performed systematic estimations for this system under different noise conditions σ , observed at different inter-observation intervals τ for different lengths of trajectories T (see Sec. J). For the examined noise amplitudes (Fig. 2 f.), the proposed path augmentation algorithm improves the naive estimation with Gaussian assumptions within two iterations (Fig. 2). For increasing noise the improvement contributed by our approach decreases (Fig. 2f.), as the invariant geometry is less well defined, but is still considerable.

Impact of the geometry of empirical manifold. We performed inference for different parameter values of the Van der Pol system ($\mu = 1$ (as above) and $\mu = 0.5$ and $\mu = 2$), that result in asymmetries of the invariant density (Fig. 4). We observed that the performance of all inference frameworks deteriorates for increasing asymmetry (larger dynamic range along one dimension), yet our method still delivered more accurate predictions compared to the other considered frameworks. Approximating the invariant geometry with a different metric learning method does not confer any considerable performance difference for our approach (c.f. Table 1 Geometric_{RBF} where we employed the metric introduced in Arvanitidis et al. (2021) and further developed in Kapusniak et al. (2024), where a positive linear combination of Gaussian RBFs centred at selected cluster centres is used to estimate a diagonal metric.)

Impact of noise amplitude. For systems with small dynamical noise (small σ), geodesics approximate the manifold structure better, however the path integral control is limited by the control costs proportional to inverse noise covariance. Our framework had comparable accuracy for all inter-observation lengths, but improvement was small for small lengths since in that setting the estimation with Gaussian likelihood already provides a good approximation of the ground truth drift.

We compared our method to the approach proposed in Batz et al. (2018). In this work, the authors perform augmentation with Ornstein-Uhlenbeck bridges, i.e. assuming linear underlying dynamics. We found that our approach delivered more accurate estimates for larger inter-observation intervals. For inter-observation intervals with only one observation per oscillation period (Fig. 3c.,d.), our approach delivered better results by considering additionally knowledge of the direction of movement in the state space (c.f. Sec. J). The variance of estimates of the proposed method was smaller compared to Batz et al. due to consistency imposed by conditioning on the invariant geometry of the system. Predictions improve with longer observation intervals T , and for decreasing noise amplitude σ . In both settings the invariant geometry is more well approximated by the empirical manifold.

State estimation with linear (Ornstein-Uhlenbeck) dynamics (Batz et al., 2018), is in general less capable of correctly estimating the latent system state and subsequently correctly approximating the unknown drift function especially as the length of the inter-observation interval τ increases.

Effects of noise miss-estimation. We further investigated the impact of noise misestimation on the accuracy of drift inference (S.I. Fig. 6). Our findings indicate that after two augmentations conditioned on the invariant geometry, small inaccuracies in the employed dynamical noise during the simulation of augmented paths have a negligible effect on the overall accuracy of the inferred drift. In particular, for small inter-observation intervals, the inference procedure remains highly

432 robust to misestimated noise amplitudes. As the inter-observation intervals increase, the effect of
433 noise deviations on performance remains minimal, provided the noise used in the augmentation
434 deviates by at most ± 0.1 from the true noise amplitude. Thus, stochastic dynamics may still be
435 identified even with inaccurate or misestimated diffusion constants.

436 Additional results are provided in the Supplement (see Sec. I).

439 5 DISCUSSION

440 Discovering unknown driving forces governing stochastic systems poses still a significant challenge,
441 despite extensive existing research on that frontier. Our work demonstrates the benefits of integrating
442 information from both the temporal and geometric structure of the observed data. Our findings
443 showed a substantial improvement in estimating the underlying stochastic dynamics, especially in
444 sparsely sampled, nonlinear systems driven by non-conservative forces.

445 We introduced **geometric inductive biases** into inference of stochastic systems by treating the deter-
446 ministic flow field as a scaffold upon which system states fluctuate. We approximated this scaffold
447 in terms of **distortions of a metric induced by the system's measurements**. This approach ef-
448 fectively approximates the low-dimensional invariant density (empirical manifold) without the need
449 to project to a lower dimensional space, whose dimensionality would be hard to estimate due to
450 the presence of fluctuations. The key insight is that **geodesics** computed on the empirical manifold
451 with respect to the approximated metric constitute the **most probable path** of the unknown system
452 between consecutive observations in the Onsager-Machlup sense. Using these **geodesics as con-**
453 **trol constraints**, we formulated a path-augmentation scheme that bridges sparse observations with
454 trajectories consistent with both the temporal order and the geometry of the data.

455 Widely used inference methods, predominantly developed within the statistics community, often
456 employ path (*data*) augmentation to approximate transition densities between successive observa-
457 tions. However, this approach suffers from several challenges: **1.)** First, the unobserved information
458 between successive observations is an infinite-dimensional object, requiring the solution of a com-
459 plex and computationally intensive problem (bridge sampling) (Gronau et al., 2017). We addressed
460 this challenging problem using the computationally efficient framework developed in Maoutsa and
461 Opper (2022). **2.)** Second, direct drift estimation from sparse observations results in estimated dy-
462 namics that significantly deviate from the ground truth. Thereby consecutive observations of the
463 system have small probability under the law of the estimated SDE. This discrepancy, in turn, leads
464 to several computational difficulties: **i)** Most bridge sampling schemes become too computationally
465 demanding, or even fail, when attempting to generate transition densities between atypical states for
466 the considered stochastic dynamics. For instance, the method of (Maoutsa and Opper, 2021) suc-
467 cessfully generates transition densities between atypical states only for conservative systems through
468 a reweighting with Brownian bridge dynamics. Alternatively, an exceedingly large number of sam-
469 ples would be required for accurate numerical approximation. **ii)** Second, iterative algorithms, such
470 as Expectation Maximisation, which exhibit only *local* convergence (Romero et al., 2019), may
471 converge to inaccurate solutions, when the initial estimation significantly deviates from the ground
472 truth.

473 To overcome these limitations, we proposed incorporating the information ingrained in the local
474 geometric structure of the observations into the state estimation (path augmentation). This approach
475 is motivated by the observation that commonly employed path augmentation methods often yield
476 transition densities that deviate substantially from the true underlying densities when observations
477 are sparse (Fig. 1E.). This discrepancy arises from the fact that these approaches rely on trivial
478 stochastic dynamics that fail to adequately capture the curvature of the ground truth transition den-
479 sities when the observed system is nonlinear (see also theoretical analysis in Sec. H.2). Our numerical
480 experiments demonstrate that, indeed, the proposed approach effectively recovers the underlying
481 drift function for systems with steady-state probability currents (Ding et al., 2020).

482 **Relation to Schrödinger bridge sampling.** The framework we employed for the augmentation re-
483 lies on a deterministic particle formulation of the path integral control formalism (Kappen, 2005b).
484 This framework can be connected to the dynamic Schrödinger bridge problem, if we consider trans-
485 ferring probability mass between two Dirac measures or very narrow Gaussians that sit on each
486 observation, considering additionally a potential that constraints the intermittent dynamics similar

486 to the one considered in Neklyudov et al. (2023a). Thus, in principle, one can employ one of the
487 recently developed alternative frameworks that solve the dynamic Schrödinger bridge problem for
488 path augmentation. The recent Bridge and Flow Matching frameworks (Lipman et al., 2022; Al-
489 berge et al., 2023; Shi et al., 2023; Liu et al., 2023) correspond to the control problem we formulate
490 in the SI Eq. 32, without the control constraints. In contrast, the Generalised Schrödinger Bridge
491 Matching (GSBM) framework proposed by Liu et al. (2023) uses a cost functional that is equiv-
492 alent to the controlled cost we employ to construct our augmentations. In this setting, the penalty
493 term corresponds to the geodesic proximity constraint used in our framework. The GSBM could, in
494 principle, replace the particle-based framework we use. However, here, we employed a framework
495 that relies on particle representations of the involved densities, which can be later easily employed
496 to formulate the Monte Carlo approximations of the integrals involved in the Gaussian process in-
497 ference for the drift (Eq. 42). Yet, the Gaussian variant of the GSBM framework that incorporates
498 time-dependent penalty constraints (analogous to our geodesic constraints), might be an interesting
499 avenue to explore for potential incorporation in our framework (Tong et al., 2023a).

500 Similarly, for approximating the metric induced by the observations, we employed the frame-
501 work of Arvanitidis et al. (2019), while we could have employed alternative metric learning ap-
502 proaches (Scarvelis and Solomon, 2022; Hauberg et al., 2012; Barua et al., 2025; Gruffaz and Sassen,
503 2025). However, the framework of Arvanitidis et al. (2019) perfectly fits the purposes of our work,
504 because it employs a non-parametric (kernel) estimation for approximating the metric and computes
505 the geodesics through GP regression. This allows to evaluate the geodesic equation at different in-
506 crements, that is necessary for imposing the time dependent geodesic constraint. A similar metric
507 approximation has been recently employed in Kapusniak et al. (2024) for metric flow matching, i.e.,
508 for augmentation that respects the geometry of the dataset. While our approach has a similar flavour
509 to this work, our framework additionally requires the augmented data to be temporary ordered and
510 to respect the stochastic flow of the estimated system. This results in learning a global drift that
511 approximates the underlying stochastic dynamics, instead of learning a local drift that transports a
512 snapshot of states from some initial to a final configuration.

513 **Limitations.** The proposed approach relies on the geometric characterisation of the invariant den-
514 sity of the system’s dynamics. This requires sufficiently long observation windows to accurately
515 characterise said density and correctly approximate the unobserved paths with geodesic curves.
516 Thus, our approach is limited to systems where the invariant density can be approximated by a
517 manifold where we can identify geodesics. An alternative method worth exploring would consider
518 the learned invariant metric directly in the dynamics of the augmented process. Moreover, we have
519 considered here inference of stochastic differential equations with known state independent diffu-
520 sion. While this approach might seem limited, several processes with state dependent diffusion
521 functions can be transformed into processes with state independent diffusions (Beskos et al., 2006a;
522 Roberts and Stramer, 2001) through the Lambert transform if they fulfil the appropriate conditions
523 for the drift function.

523
524
525
526
527
528
529
530
531
532
533
534
535
536
537
538
539

540 6 REPRODUCIBILITY STATEMENT 541

542 We have taken several steps to ensure the reproducibility of our results. A detailed description of
543 our methodology, including the inference framework and the geometry-aware path augmentation
544 procedure, is provided in Section 2 of the main text and further elaborated in Appendix A. All
545 theoretical aspects of our work, including the construction of the invariant metric, geodesics, and the
546 stochastic control formulation, are presented in full in the supplementary material (Appendix A.3,
547 A.3.2, and H). The implementation details of the Expectation–Maximisation scheme and Gaussian
548 process inference are also included in the appendix. Our numerical experiments, benchmarks, and
549 additional analyses (e.g., noise misestimation) are reported in the Supplement.

550 REFERENCES 551

553 Albert Einstein. Über die von der molekularkinetischen Theorie der wärme geforderte Bewegung
554 von in ruhenden Flüssigkeiten suspendierten Teilchen. *Annalen der Physik*, 4, 1905. (cited on
555 page: 1)

556 Tao Li. Chemical Langevin Equation for Complex Reactions. *The Journal of Physical Chemistry*
557 A, 124(5):810–816, 2020. (cited on page: 1)

559 L Silva-Dias and A López-Castillo. Spontaneous symmetry breaking of population: Stochastic
560 Lotka–Volterra model for competition among two similar preys and predators. *Mathematical
561 Biosciences*, 300:36–46, 2018. (cited on page: 1)

562 Charles K Fisher and Pankaj Mehta. The transition between the niche and neutral regimes in ecology.
563 *Proceedings of the National Academy of Sciences*, 111(36):13111–13116, 2014. (cited on page: 1)

565 Antonio A Alonso, Ignacio Molina, and Constantinos Theodoropoulos. Modeling bacterial popula-
566 tion growth from stochastic single-cell dynamics. *Applied and Environmental Microbiology*, 80
567 (17):5241–5253, 2014. (cited on page: 1)

568 J Cremers and A Hübner. Construction of differential equations from experimental data. *Zeitschrift
569 für Naturforschung A*, 42(8):797–802, 1987. (cited on page: 1)

571 Steven L Brunton, Joshua L Proctor, and J Nathan Kutz. Discovering governing equations from data
572 by sparse identification of nonlinear dynamical systems. *Proceedings of the National Academy of
573 Sciences*, 113(15):3932–3937, 2016. (cited on page: 1)

574 Bryan C Daniels and Ilya Nemenman. Automated adaptive inference of phenomenological dynam-
575 ical models. *Nature Communications*, 6(1):1–8, 2015. (cited on page: 1)

577 Kevin McGoff, Sayan Mukherjee, and Natesh Pillai. Statistical inference for dynamical systems: A
578 review. *Statistics Surveys*, 9:209–252, 2015. (cited on page: 1)

579 Holger Kantz and Thomas Schreiber. *Nonlinear time series analysis*, volume 7. Cambridge univer-
580 sity press, 2004. (cited on page: 1)

582 Michael Schmidt and Hod Lipson. Distilling free-form natural laws from experimental data. *Science*,
583 324(5923):81–85, 2009. (cited on page: 1)

584 Felipe Miguel Aparicio Acosta. Radial basis function and related models: an overview. *Signal
585 Processing*, 45(1):37–58, 1995. (cited on page: 1)

587 Michael Small and Chi Kong Tse. Minimum description length neural networks for time series
588 prediction. *Physical Review E*, 66(6):066701, 2002. (cited on page: 1)

589 Kevin Judd and Alistair Mees. On selecting models for nonlinear time series. *Physica D: Nonlinear
590 Phenomena*, 82(4):426–444, 1995. (cited on page: 1)

592 Michael Small and Kevin Judd. Comparisons of new nonlinear modeling techniques with applica-
593 tions to infant respiration. *Physica D: Nonlinear Phenomena*, 117(1-4):283–298, 1998. (cited on
page: 1)

594 David B Brückner, Pierre Ronceray, and Chase P Broedersz. **Inferring the dynamics of underdamped**
595 **stochastic systems**. *Physical Review Letters*, 125(5):058103, 2020. (cited on page: [1](#))
596

597 Anna Frishman and Pierre Ronceray. **Learning force fields from stochastic trajectories**. *Physical*
598 *Review X*, 10(2):021009, 2020. (cited on pages: [1](#), [7](#), and [48](#))

599 Eurika Kaiser, J Nathan Kutz, and Steven L Brunton. **Sparse identification of nonlinear dynamics**
600 **for model predictive control in the low-data limit**. *Proceedings of the Royal Society A*, 474(2219):
601 20180335, 2018. (cited on page: [1](#))

602 Josh Bongard and Hod Lipson. **Automated reverse engineering of nonlinear dynamical systems**.
603 *Proceedings of the National Academy of Sciences*, 104(24):9943–9948, 2007. (cited on page: [1](#))
604

605 Ioannis G Kevrekidis, C William Gear, James M Hyman, Panagiotis G Kevrekidis, Olof Runborg,
606 Constantinos Theodoropoulos, et al. **Equation-free, coarse-grained multiscale computation: en-**
607 **abling microscopic simulators to perform system-level analysis**. *Commun. Math. Sci*, 1(4):715–
608 762, 2003. (cited on page: [1](#))

609 Constantinos Theodoropoulos, Yue-Hong Qian, and Ioannis G Kevrekidis. **“Coarse” stability and**
610 **bifurcation analysis using time-steppers: A reaction-diffusion example**. *Proceedings of the Na-*
611 *tional Academy of Sciences*, 97(18):9840–9843, 2000. (cited on page: [1](#))

612 Mauricio Alvarez, David Luengo, and Neil D Lawrence. **Latent force models**. In *Artificial Intelli-*
613 *gence and Statistics*, pages 9–16. PMLR, 2009. (cited on page: [1](#))

614 Guido Sanguinetti, Neil D Lawrence, and Magnus Rattray. **Probabilistic inference of transcription**
615 **factor concentrations and gene-specific regulatory activities**. *Bioinformatics*, 22(22):2775–2781,
616 2006. (cited on page: [1](#))

617 Simo Särkkä. **The use of Gaussian processes in system identification**. *arXiv preprint*
618 *arXiv:1907.06066*, 2019. (cited on page: [1](#))
619

620 Peiyuan Teng. **Machine-learning quantum mechanics: Solving quantum mechanics problems using**
621 **radial basis function networks**. *Physical Review E*, 98(3):033305, 2018. (cited on page: [1](#))

622 Ravinder Bhattoo, Sayan Ranu, and NM Krishnan. **Learning the Dynamics of Particle-based Sys-**
623 **tems with Lagrangian Graph Neural Networks**. *arXiv preprint arXiv:2209.01476*, 2022. (cited
624 on page: [1](#))

625 Thomas Jüngling, Thomas Lymburn, Thomas Stemler, Débora Corrêa, David Walker, and Michael
626 Small. **Reconstruction of complex dynamical systems from time series using reservoir computing**.
627 In *2019 IEEE International Symposium on Circuits and Systems (ISCAS)*, pages 1–5. IEEE, 2019.
628 (cited on page: [1](#))

629 Philipp Batz, Andreas Ruttner, and Manfred Opper. **Approximate Bayes learning of stochastic dif-**
630 **ferential equations**. *Physical Review E*, 98(2):022109, 2018. (cited on pages: [2](#), [3](#), [6](#), [8](#), [22](#), [23](#),
631 [24](#), [33](#), and [49](#))

632 Rudolf Friedrich and Joachim Peinke. **Description of a turbulent cascade by a Fokker-Planck equa-**
633 **tion**. *Physical Review Letters*, 78(5):863, 1997. (cited on pages: [2](#), [3](#), [22](#), [24](#), [33](#), and [39](#))

634 Mario Ragwitz and Holger Kantz. **Indispensable finite time corrections for Fokker-Planck equations**
635 **from time series data**. *Physical Review Letters*, 87(25):254501, 2001. (cited on pages: [2](#), [22](#), [33](#),
636 and [39](#))

637 Philipp Batz, Andreas Ruttner, and Manfred Opper. **Variational estimation of the drift for stochastic**
638 **differential equations from the empirical density**. *Journal of Statistical Mechanics: Theory and*
639 *Experiment*, 2016(8):083404, 2016. (cited on pages: [2](#) and [33](#))

640 Yiqi Gu, John Harlim, Senwei Liang, and Haizhao Yang. **Stationary density estimation of Itô diffu-**
641 **sions using Deep Learning**, 2021. (cited on page: [2](#))

642 Amit Singer and Ronald R Coifman. **Non-linear independent component analysis with diffusion**
643 **maps**. *Applied and Computational Harmonic Analysis*, 25(2):226–239, 2008. (cited on pages: [2](#)
644 and [34](#))

648 Feliks Nüske, Péter Koltai, Lorenzo Boninsegna, and Cecilia Clementi. **Spectral properties of effec-
649 tive dynamics from conditional expectations.** *Entropy*, 23(2):134, 2021. (cited on page: 2)
650

651 Edward L Ionides, Carles Bretó, and Aaron A King. **Inference for nonlinear dynamical systems.**
652 *Proceedings of the National Academy of Sciences*, 103(49):18438–18443, 2006. (cited on page: 2)
653

654 Ronen Talmon and Ronald R Coifman. **Intrinsic modeling of stochastic dynamical systems using**
655 **empirical geometry.** *Applied and Computational Harmonic Analysis*, 39(1):138–160, 2015. (cited
656 on pages: 2 and 34)

657 Carmeline J Dsilva, Ronen Talmon, C William Gear, Ronald R Coifman, and Ioannis G Kevrekidis.
658 **Data-driven reduction for a class of multiscale fast-slow stochastic dynamical systems.** *SIAM*
659 *Journal on Applied Dynamical Systems*, 15(3):1327–1351, 2016. (cited on page: 2)

660 Tyrus Berry and John Harlim. **Iterated diffusion maps for feature identification.** *Applied and Com-
661 putational Harmonic Analysis*, 45(1):84–119, 2018. (cited on page: 2)

662 Tyrus Berry and John Harlim. **Nonparametric uncertainty quantification for stochastic gradient**
663 **flows.** *SIAM/ASA Journal on Uncertainty Quantification*, 3(1):484–508, 2015. (cited on page: 2)
664

665 Arthur P Dempster, Nan M Laird, and Donald B Rubin. **Maximum likelihood from incomplete data**
666 **via the EM algorithm.** *Journal of the Royal Statistical Society: Series B (Methodological)*, 39(1):
667 1–22, 1977. (cited on pages: 2 and 4)

668 Robert S Liptser and Albert N Shiryaev. **Statistics of random processes II: Applications**, volume 6.
669 Springer Science & Business Media, 2013. (cited on pages: 3 and 23)

670 Andreas Rutar, Philipp Batz, and Manfred Opper. **Approximate Gaussian process inference for**
671 **the drift function in stochastic differential equations.** *Advances in Neural Information Processing*
672 *Systems*, 26, 2013. (cited on pages: 3, 23, 24, 29, 30, 31, 33, and 39)

673 Roland Hostettler, Filip Tronarp, and Simo Särkkä. **Modeling the drift function in stochastic differ-
674 ential equations using reduced rank Gaussian processes.** *IFAC-PapersOnLine*, 51(15):778–783,
675 2018. (cited on pages: 3 and 33)

676 Zheng Zhao, Filip Tronarp, Roland Hostettler, and Simo Särkkä. **State-space Gaussian process for**
677 **drift estimation in stochastic differential equations.** In *ICASSP 2020-2020 IEEE International*
678 *Conference on Acoustics, Speech and Signal Processing (ICASSP)*, pages 5295–5299. IEEE,
679 2020. (cited on pages: 3 and 33)

680 Giorgos Sermaidis, Omiros Papaspiliopoulos, Gareth O Roberts, Alexandros Beskos, and Paul
681 Fearnhead. **Markov chain Monte Carlo for exact inference for diffusions.** *Scandinavian Jour-
682 nal of Statistics*, 40(2):294–321, 2013. (cited on pages: 3, 23, 24, and 33)

683 Christian Fröhlich, Alexandra Gessner, Philipp Hennig, Bernhard Schölkopf, and Georgios Arvan-
684 itidis. **Bayesian Quadrature on Riemannian Data Manifolds.** *International Conference on Ma-
685 chine Learning*, pages 3459–3468, 2021. doi: <https://doi.org/10.48550/arXiv.2102.06645>. (cited
686 on pages: 3 and 27)

687 Joshua B Tenenbaum, Vin de Silva, and John C Langford. **A global geometric framework for**
688 **nonlinear dimensionality reduction.** *Science*, 290(5500):2319–2323, 2000. (cited on page: 4)
689

690 Mukund Balasubramanian and Eric L Schwartz. **The isomap algorithm and topological stability.**
691 *Science*, 295(5552):7–7, 2002. (cited on page: 4)

692 AL Mead. **Review of the development of multidimensional scaling methods.** *Journal of the Royal*
693 *Statistical Society: Series D (The Statistician)*, 41(1):27–39, 1992. (cited on page: 4)

694 Sam T Roweis and Lawrence K Saul. **Nonlinear dimensionality reduction by locally linear embed-
695 ding.** *Science*, 290(5500):2323–2326, 2000. (cited on page: 4)

696 Georgios Arvanitidis, Soren Hauberg, Philipp Hennig, and Michael Schober. **Fast and robust short-
697 est paths on manifolds learned from data.** In *The 22nd International Conference on Artificial*
698 *Intelligence and Statistics*, pages 1506–1515. PMLR, 2019. (cited on pages: 4, 6, 10, 27, 28, 47,
699 48, and 50)

702 Manfredo Perdigao Do Carmo and J Flaherty Francis. *Riemannian geometry*, volume 6. Springer,
703 1992. (cited on pages: 4, 26, and 28)

704

705 Georgios Arvanitidis, Lars Kai Hansen, and Søren Hauberg. *Latent space oddity: on the curvature*
706 *of deep generative models*. *arXiv preprint arXiv:1710.11379*, 2017. (cited on pages: 4, 28, 35,
707 and 47)

708 Matthew James Beal. *Variational algorithms for approximate Bayesian inference*. University of
709 London, University College London (United Kingdom), 2003. (cited on pages: 4 and 25)

710

711 Raphaël Chetrite and Hugo Touchette. *Variational and optimal control representations of condi-*
712 *tioned and driven processes*. *Journal of Statistical Mechanics: Theory and Experiment*, 2015
713 (12):P12001, 2015. (cited on pages: 5 and 25)

714 Satya N Majumdar and Henri Orland. *Effective Langevin equations for constrained stochastic pro-*
715 *cesses*. *Journal of Statistical Mechanics: Theory and Experiment*, 2015(6):P06039, 2015. (cited
716 on pages: 5 and 25)

717 Manfred Opper. *Variational inference for stochastic differential equations*. *Annalen der Physik*, 531
718 (3):1800233, 2019. (cited on pages: 5, 25, 26, 28, and 33)

719

720 Hilbert J Kappen. *Path integrals and symmetry breaking for optimal control theory*. *Journal of*
721 *Statistical Mechanics: theory and experiment*, 2005(11):P11011, 2005a. (cited on page: 6)

722

723 Dimitra Maoutsas and Manfred Opper. *Deterministic particle flows for constraining stochastic non-*
724 *linear systems*. *Phys. Rev. Research*, 4:043035, Oct 2022. (cited on pages: 6, 9, 23, 28, 29,
725 and 48)

726 Kevin Course and Prasanth B Nair. *State estimation of a physical system with unknown governing*
727 *equations*. *Nature*, 622(7982):261–267, 2023a. (cited on pages: 6 and 49)

728

729 Arshed Nabeel, Ashwin Karichannavar, Shuaib Palathingal, Jitesh Jhawar, David B Brückner,
730 Danny Raj M, and Vishwesha Guttal. *Discovering stochastic dynamical equations from eco-*
731 *logical time series data*. *The American Naturalist*, 205(4):E100–E117, 2025. (cited on pages: 6,
732 33, and 49)

733 Kevin Course and Prasanth Nair. *Amortized reparametrization: efficient and scalable variational*
734 *inference for latent SDEs*. *Advances in Neural Information Processing Systems*, 36:78296–78318,
735 2023b. (cited on pages: 6, 34, and 49)

736

737 Kacper Kapusniak, Peter Potapchik, Teodora Reu, Leo Zhang, Alexander Tong, Michael Bronstein,
738 Joey Bose, and Francesco Di Giovanni. *Metric flow matching for smooth interpolations on the*
739 *data manifold*. *Advances in Neural Information Processing Systems*, 37:135011–135042, 2024.
(cited on pages: 6, 8, 10, 35, 47, and 49)

740

741 Georgios Arvanitidis, Soren Hauberg, and Bernhard Schölkopf. *Geometrically Enriched Latent*
742 *Spaces*. In *International Conference on Artificial Intelligence and Statistics*, pages 631–639.
743 PMLR, 2021. (cited on pages: 6 and 8)

744

745 Guan-Horng Liu, Yaron Lipman, Maximilian Nickel, Brian Karrer, Evangelos A Theodorou, and
746 Ricky TQ Chen. *Generalized Schrödinger Bridge Matching*. *arXiv preprint arXiv:2310.02233*,
2023. (cited on pages: 6, 10, 34, 35, and 49)

747

748 Alexander Tong, Nikolay Malkin, Kilian Fatras, Lazar Atanackovic, Yanlei Zhang, Guillaume
749 Huguet, Guy Wolf, and Yoshua Bengio. *Simulation-free Schrödinger bridges via score and flow*
750 *matching*. *arXiv preprint arXiv:2307.03672*, 2023a. (cited on pages: 7, 10, 34, and 49)

751

752 Evgeny Evgenievich Selkov. *Self-oscillations in glycolysis 1. a simple kinetic model*. *European*
753 *Journal of Biochemistry*, 4(1):79–86, 1968. (cited on pages: 7 and 48)

754

755 Quentin F Gronau, Alexandra Sarafoglou, Dora Matzke, Alexander Ly, Udo Boehm, Maarten Mars-
756 man, David S Leslie, Jonathan J Forster, Eric-Jan Wagenmakers, and Helen Steingroever. *A*
757 *tutorial on bridge sampling*. *Journal of Mathematical Psychology*, 81:80–97, 2017. (cited on
758 page: 9)

756 Dimitra Maoutsou and Manfred Opper. **Deterministic particle flows for constraining SDEs**. *Machine*
757 *Learning and the Physical Sciences, Workshop at the 35th Conference on Neural Information*
758 *Processing Systems (NeurIPS)*, arXiv preprint arXiv:2110.13020, 2021. (cited on pages: 9, 23,
759 and 50)

760 Orlando Romero, Sarthak Chatterjee, and Sérgio Pequito. **Convergence of the expectation-**
761 **maximization algorithm through discrete-time Lyapunov stability theory**. In *2019 American Con-*
762 *trol Conference (ACC)*, pages 163–168. IEEE, 2019. (cited on pages: 9 and 54)

764 Mingnan Ding, Zhanchun Tu, and Xiangjun Xing. **Covariant formulation of nonlinear Langevin**
765 **theory with multiplicative Gaussian white noises**. *Physical Review Research*, 2(3):033381, 2020.
766 (cited on page: 9)

767 Hilbert J Kappen. **Linear theory for control of nonlinear stochastic systems**. *Physical Review Letters*,
768 95(20):200201, 2005b. (cited on page: 9)

770 Kirill Neklyudov, Rob Brekelmans, Alexander Tong, Lazar Atanackovic, Qiang Liu, and Alireza
771 Makhzani. **A computational framework for solving Wasserstein Lagrangian flows**. arXiv preprint
772 arXiv:2310.10649, 2023a. (cited on page: 10)

774 Yaron Lipman, Ricky TQ Chen, Heli Ben-Hamu, Maximilian Nickel, and Matt Le. **Flow matching**
775 **for generative modeling**. arXiv preprint arXiv:2210.02747, 2022. (cited on pages: 10 and 34)

776 Michael S Albergo, Nicholas M Boffi, and Eric Vanden-Eijnden. **Stochastic interpolants: A unifying**
777 **framework for flows and diffusions**. arXiv preprint arXiv:2303.08797, 2023. (cited on pages: 10
778 and 34)

780 Yuyang Shi, Valentin De Bortoli, Andrew Campbell, and Arnaud Doucet. **Diffusion Schrödinger**
781 **bridge matching**. *Advances in Neural Information Processing Systems*, 36:62183–62223, 2023.
782 (cited on page: 10)

783 Christopher Scarvelis and Justin Solomon. **Riemannian metric learning via optimal transport**. arXiv
784 preprint arXiv:2205.09244, 2022. (cited on page: 10)

786 Søren Hauberg, Oren Freifeld, and Michael Black. **A geometric take on metric learning**. *Advances*
787 *in Neural Information Processing Systems*, 25, 2012. (cited on page: 10)

789 Arnab Barua, Haralampos Hatzikirou, and Sumiyoshi Abe. **Geodesic learning**. *Physica A: Statistical*
790 *Mechanics and its Applications*, 669:130539, 2025. (cited on page: 10)

791 Samuel Gruffaz and Josua Sassen. **Riemannian metric learning: Closer to you than you imagine**.
792 arXiv preprint arXiv:2503.05321, 2025. (cited on page: 10)

794 Alexandros Beskos, Omiros Papaspiliopoulos, Gareth O Roberts, and Paul Fearnhead. **Exact and**
795 **computationally efficient likelihood-based estimation for discretely observed diffusion processes**
796 **(with discussion)**. *Journal of the Royal Statistical Society: Series B (Statistical Methodology)*, 68
797 (3):333–382, 2006a. (cited on page: 10)

798 Gareth O Roberts and Osnat Stramer. **On inference for partially observed nonlinear diffusion models**
799 **using the Metropolis–Hastings algorithm**. *Biometrika*, 88(3):603–621, 2001. (cited on page: 10)

801 Andrew Golightly and Darren J Wilkinson. **Bayesian inference for nonlinear multivariate diffusion**
802 **models observed with error**. *Computational Statistics & Data Analysis*, 52(3):1674–1693, 2008.
803 (cited on pages: 23 and 24)

804 Omiros Papaspiliopoulos, Yvo Pokern, Gareth O Roberts, and Andrew M Stuart. **Nonparametric**
805 **estimation of diffusions: a differential equations approach**. *Biometrika*, 99(3):511–531, 2012.
806 (cited on pages: 23 and 24)

808 Alexandros Beskos, Omiros Papaspiliopoulos, and Gareth O Roberts. **Retrospective exact simula-**
809 **tion of diffusion sample paths with applications**. *Bernoulli*, 12(6):1077–1098, 2006b. (cited on
810 pages: 23 and 24)

810 Siddhartha Chib, Michael K Pitt, and Neil Shephard. [Likelihood based inference for diffusion driven](#)
811 [state space models](#). *Por Clasificar*, pages 1–33, 2006. (cited on pages: 23, 24, and 33)

812

813 Valentin De Bortoli, Arnaud Doucet, Jeremy Heng, and James Thornton. [Simulating Diffusion](#)
814 [Bridges with Score Matching](#). *arXiv preprint arXiv:2111.07243*, 2021. (cited on page: 23)

815

816 Ge Liu, Peter F Craigmile, and Radu Herbei. [A study of the data augmentation strategy for stochastic](#)
817 [differential equations](#). *Journal of Statistical Computation and Simulation*, 90(10):1753–1772,
818 2020. (cited on page: 23)

819

820 Carl Edward Rasmussen. [Gaussian processes in machine learning](#). In *Summer School on Machine*
821 *Learning*, pages 63–71. Springer-Verlag, 2003. (cited on pages: 24 and 30)

822

823 Steven J Lade. [Finite sampling interval effects in Kramers–Moyal analysis](#). *Physics Letters A*, 373
824 (41):3705–3709, 2009. (cited on pages: 24 and 36)

825

826 Christoph Honisch and Rudolf Friedrich. [Estimation of Kramers-Moyal coefficients at low sampling](#)
827 [rates](#). *Physical Review E*, 83(6):066701, 2011. (cited on page: 24)

828

829 John M Lee. *Introduction to Riemannian manifolds*, volume 176. Springer, 2018. (cited on page: 26)

830

831 Stephen Wiggins. *Normally hyperbolic invariant manifolds in dynamical systems*, volume 105.
832 Springer Science & Business Media, 1994. (cited on page: 27)

833

834 Salah-Eldin A Mohammed and Michael KR Scheutzow. [The stable manifold theorem for stochastic](#)
835 [differential equations](#). *Annals of Probability*, pages 615–652, 1999. (cited on page: 27)

836

837 TV Giry and Igor Dmitrievich Chueshov. [Inertial manifolds and stationary measures for stochasti-](#)
838 [cally perturbed dissipative dynamical systems](#). *Sbornik: Mathematics*, 186(1):29–45, 1995. (cited
839 on page: 27)

840

841 Neil Fenichel and JK Moser. [Persistence and smoothness of invariant manifolds for flows](#). *Indiana*
842 *University Mathematics Journal*, 21(3):193–226, 1971. (cited on page: 27)

843

844 Ludwig Arnold. [Stochastic differential equations as dynamical systems](#). In *Realization and Mod-*
845 *elling in System Theory*, pages 489–495. Springer, 1990. (cited on page: 27)

846

847 Andrew Carverhill. [Flows of stochastic dynamical systems: ergodic theory](#). *Stochastics: An In-*
848 *ternational Journal of Probability and Stochastic Processes*, 14(4):273–317, 1985. (cited on
849 page: 27)

850

851 Ofir Pele and Michael Werman. [Fast and robust earth mover’s distances](#). In *2009 IEEE 12th In-*
852 *ternational Conference on Computer Vision*, pages 460–467. IEEE, September 2009. (cited on
853 page: 29)

854

855 Sebastian Reich. [A nonparametric ensemble transform method for Bayesian inference](#). *SIAM Jour-*
856 *nal on Scientific Computing*, 35(4):A2013–A2024, 2013. (cited on page: 29)

857

858 Michalis Titsias. [Variational learning of inducing variables in sparse Gaussian processes](#). *Artificial*
859 *Intelligence and Statistics*, pages 567–574, 2009. (cited on page: 30)

860

861 Lehel Csató and Manfred Opper. [Sparse on-line Gaussian processes](#). *Neural computation*, 14(3):
862 641–668, 2002. (cited on page: 30)

863

864 Lars Onsager and Stefan Machlup. [Fluctuations and irreversible processes](#). *Physical Review*, 91(6):
865 1505, 1953. (cited on page: 31)

866

867 Tooru Taniguchi and EGD Cohen. [Onsager-Machlup theory for nonequilibrium steady states and](#)
868 [fluctuation theorems](#). *Journal of Statistical Physics*, 126(1):1–41, 2007. (cited on page: 32)

869

870 Artur B Adib. [Stochastic actions for diffusive dynamics: Reweighting, sampling, and minimization](#).
871 *The Journal of Physical Chemistry B*, 112(19):5910–5916, 2008. (cited on page: 32)

872

873 Robert Graham. [Path integral formulation of general diffusion processes](#). *Zeitschrift für Physik B*
874 *Condensed Matter*, 26(3):281–290, 1977. (cited on page: 32)

864 Ruslan Leontievich Stratonovich. **On the probability functional of diffusion processes.** *Selected*
865 *Translations in Mathematical Statistics and Probability*, 10:273–286, 1971. (cited on page: 32)
866

867 Detlef Dürr and Alexander Bach. **The Onsager-Machlup function as Lagrangian for the most proba-**
868 **ble path of a diffusion process.** *Communications in Mathematical Physics*, 60(2):153–170, 1978.
869 (cited on page: 32)

870 Y Takahashi and S Watanabe. **The probability functionals (Onsager-Machlup functions) of diffusion**
871 **processes.** In *Stochastic Integrals*, pages 433–463. Springer, 1981. (cited on page: 32)
872

873 Robert Graham. **Onsager-Machlup Function of Nonlinear Non-Equilibrium Thermodynamics.** In
874 *Functional Integration*, pages 263–280. Springer, 1980. (cited on page: 32)

875 Erlend Grong and Stefan Sommer. **Most probable flows for Kunita SDEs.** *arXiv preprint*
876 *arXiv:2209.03868*, 2022. (cited on page: 32)
877

878 Mireille Capitaine. **On the Onsager-Machlup functional for elliptic diffusion processes.** *Séminaire*
879 *de Probabilités XXXIV*, pages 313–328, 2000. (cited on page: 32)

880 Bernt Øksendal. **Stochastic differential equations.** In *Stochastic differential equations*, pages 65–84.
881 Springer, 2003. (cited on page: 32)
882

883 Cagatay Yildiz, Markus Heinonen, Jukka Intosalmi, Henrik Mannerstrom, and Harri Lahdesmaki.
884 **Learning stochastic differential equations with Gaussian processes without gradient matching.** In
885 *2018 IEEE 28th International Workshop on Machine Learning for Signal Processing (MLSP)*,
886 pages 1–6. IEEE, 2018. (cited on page: 33)

887 J Peinke, R Friedrich, and Antoon Naert. **A new approach to characterize disordered structures.**
888 *Zeitschrift für Naturforschung A*, 52(8-9):588–592, 1997. (cited on page: 33)
889

890 Rudolf Friedrich, Silke Siegert, Joachim Peinke, Marcus Siefert, Michael Lindemann, Jan Raethjen,
891 Güntner Deuschl, Gerhard Pfister, et al. **Extracting model equations from experimental data.**
892 *Physics Letters A*, 271(3):217–222, 2000. (cited on page: 33)

893 Federica Ferretti, Victor Chardès, Thierry Mora, Aleksandra M Walczak, and Irene Giardina. **Build-**
894 **ing general Langevin models from discrete datasets.** *Physical Review X*, 10(3):031018, 2020.
895 (cited on page: 33)

896 Lorenzo Boninsegna, Feliks Nüske, and Cecilia Clementi. **Sparse learning of stochastic dynamical**
897 **equations.** *The Journal of chemical physics*, 148(24):241723, 2018. (cited on page: 33)
898

899 Yunfei Huang, Youssef Mabrouk, Gerhard Gompper, and Benedikt Sabass. **Sparse inference and**
900 **active learning of stochastic differential equations from data.** *arXiv preprint arXiv:2203.11010*,
901 2022. (cited on page: 33)

902 David Lamouroux and Klaus Lehnertz. **Kernel-based regression of drift and diffusion coefficients**
903 **of stochastic processes.** *Physics Letters A*, 373(39):3507–3512, 2009. (cited on page: 33)
904

905 George J Jiang and John L Knight. **A nonparametric approach to the estimation of diffusion pro-**
906 **cesses, with an application to a short-term interest rate model.** *Econometric Theory*, 13(5):615–
907 645, 1997. (cited on page: 33)

908 Stefan Klus, Feliks Nüske, Sebastian Peitz, Jan-Hendrik Niemann, Cecilia Clementi, and Christof
909 Schütte. **Data-driven approximation of the Koopman generator: Model reduction, system identi-**
910 **fication, and control.** *Physica D: Nonlinear Phenomena*, 406:132416, 2020. (cited on page: 33)
911

912 Richard Stanton. **A nonparametric model of term structure dynamics and the market price of interest**
913 **rate risk.** *The Journal of Finance*, 52(5):1973–2002, 1997. (cited on page: 33)

914 Lars P Hansen and Jose A Scheinkman. **Back to the future: Generating moment implications for**
915 **continuous-time Markov processes**, 1993. (cited on page: 33)
916

917 Mario Ragwitz and Holger Kantz. **Ragwitz and Kantz reply.** *Physical Review Letters*, 89(14):
149402, 2002. (cited on page: 33)

918 D Kleinhans, R Friedrich, A Nawroth, and J Peinke. **An iterative procedure for the estimation of**
919 **drift and diffusion coefficients of Langevin processes.** *Physics Letters A*, 346(1-3):42–46, 2005.
920 *(cited on page: 33)*
921

922 David Kleinhans and Rudolf Friedrich. **Maximum likelihood estimation of drift and diffusion func-**
923 **tions.** *Physics Letters A*, 368(3-4):194–198, 2007. *(cited on page: 33)*
924

925 Bjørn Eraker. **MCMC analysis of diffusion models with application to finance.** *Journal of Business*
926 *& Economic Statistics*, 19(2):177–191, 2001. *(cited on page: 33)*
927

928 Monica Billio, Alain Monfort, and Christian Robert. **The simulated likelihood ratio method.** *Institut*
929 *National de la Statistique et des Etudes Economiques*, 1998. *(cited on page: 33)*
930

931 Lea Duncker, Gergo Bohner, Julien Boussard, and Maneesh Sahani. **Learning interpretable**
932 **continuous-time models of latent stochastic dynamical systems.** In *International conference on*
933 *machine learning*, pages 1726–1734. PMLR, 2019. *(cited on page: 33)*
934

935 Prakhar Verma, Vincent Adam, and Arno Solin. **Variational Gaussian process diffusion processes.**
936 In *International Conference on Artificial Intelligence and Statistics*, pages 1909–1917. PMLR,
937 2024. *(cited on page: 33)*
938

939 Cédric Archambeau, Manfred Opper, Yuan Shen, Dan Cornford, and John Shawe-Taylor. **Variational**
940 **inference for diffusion processes.** *Advances in Neural Information Processing Systems*, 20:17–24,
941 2007. *(cited on page: 33)*
942

943 Xuechen Li, Ting-Kam Leonard Wong, Ricky T. Q. Chen, and David Duvenaud. **Scalable gradients**
944 **for Stochastic Differential Equations**, 2020. *(cited on page: 33)*
945

946 Yury A Kutoyants and Jurij A Kutojanc. **Statistical inference for ergodic diffusion processes.**
947 Springer Science & Business Media, 2004. *(cited on page: 34)*
948

949 Ronald R Coifman, Stephane Lafon, Ann B Lee, Mauro Maggioni, Boaz Nadler, Frederick Warner,
950 and Steven W Zucker. **Geometric diffusions as a tool for harmonic analysis and structure defi-**
951 **nition of data: Diffusion maps.** *Proceedings of the National Academy of Sciences of the United*
952 *States of America*, 102(21):7426–7431, 2005. *(cited on page: 34)*
953

954 Boaz Nadler, Stéphane Lafon, Ronald R Coifman, and Ioannis G Kevrekidis. **Diffusion maps,**
955 **spectral clustering and reaction coordinates of dynamical systems.** *Applied and Computational*
956 *Harmonic Analysis*, 21(1):113–127, 2006. *(cited on page: 34)*
957

958 Dimitrios Giannakis. **Data-driven spectral decomposition and forecasting of ergodic dynamical sys-**
959 **tems.** *Applied and Computational Harmonic Analysis*, 47(2):338–396, 2019. *(cited on pages: 34*
960 *and 36)*
961

962 Andrew L Ferguson, Athanassios Z Panagiotopoulos, Ioannis G Kevrekidis, and Pablo G
963 Debenedetti. **Nonlinear dimensionality reduction in molecular simulation: The diffusion map**
964 **approach.** *Chemical Physics Letters*, 509(1-3):1–11, 2011. *(cited on page: 34)*
965

966 Aram-Alexandre Pooladian, Heli Ben-Hamu, Carles Domingo-Enrich, Brandon Amos, Yaron Lip-
967 man, and Ricky TQ Chen. **Multisample flow matching: Straightening flows with minibatch cou-**
968 **plings.** *arXiv preprint arXiv:2304.14772*, 2023. *(cited on page: 34)*
969

970 Michael S Albergo and Eric Vanden-Eijnden. **Building normalizing flows with stochastic inter-**
971 **polants.** *arXiv preprint arXiv:2209.15571*, 2022. *(cited on page: 34)*
972

973 Alexander Tong, Kilian Fatras, Nikolay Malkin, Guillaume Huguet, Yanlei Zhang, Jarrid Rector-
974 Brooks, Guy Wolf, and Yoshua Bengio. **Improving and generalizing flow-based generative models**
975 **with minibatch optimal transport.** *arXiv preprint arXiv:2302.00482*, 2023b. *(cited on page: 34)*
976

977 Kirill Neklyudov, Rob Brekelmans, Daniel Severo, and Alireza Makhzani. **Action matching: Learn-**
978 **ing stochastic dynamics from samples.** In *International Conference on Machine Learning*, pages
979 25858–25889. PMLR, 2023b. *(cited on pages: 34 and 49)*

972 Andres F Duque, Sacha Morin, Guy Wolf, and Kevin R Moon. **Geometry regularized autoencoders.**
973 *IEEE transactions on pattern analysis and machine intelligence*, 45(6):7381–7394, 2022. (cited
974 on page: 35)

975 Dimitris Kalatzis, David Eklund, Georgios Arvanitidis, and Søren Hauberg. **Variational autoen-**
976 **coders with Riemannian Brownian motion priors.** *arXiv preprint arXiv:2002.05227*, 2020. (cited
977 on page: 35)

978 Emile Mathieu and Maximilian Nickel. **Riemannian continuous normalizing flows.** *Advances in*
979 *neural information processing systems*, 33:2503–2515, 2020. (cited on page: 35)

980 Valentin De Bortoli, Emile Mathieu, Michael Hutchinson, James Thornton, Yee Whye Teh, and
981 Arnaud Doucet. **Riemannian score-based generative modelling.** *Advances in neural information*
982 *processing systems*, 35:2406–2422, 2022. (cited on page: 35)

983 Yunyi Shen, Renato Berlinghieri, and Tamara Broderick. **Multi-marginal Schrödinger bridges with**
984 **iterative reference refinement.** *arXiv preprint arXiv:2408.06277*, 2024. (cited on page: 35)

985 Nina Miolane, Nicolas Guigui, Alice Le Brigant, Johan Mathe, Benjamin Hou, Yann Thanwerdas,
986 Stefan Heyder, Olivier Peltre, Niklas Koep, Hadi Zaatiti, et al. **Geomstats: a Python package for**
987 **Riemannian geometry in machine learning.** *Journal of Machine Learning Research*, 21(223):1–9,
988 2020. (cited on page: 35)

989 Stefan Sommer. **Probabilistic approaches to geometric statistics: Stochastic processes, transition**
990 **distributions, and fiber bundle geometry.** In *Riemannian Geometric Statistics in Medical Image*
991 *Analysis*, pages 377–416. Elsevier, 2020. (cited on page: 35)

992 Charles Fefferman, Sanjoy Mitter, and Hariharan Narayanan. **Testing the manifold hypothesis.**
993 *Journal of the American Mathematical Society*, 29(4):983–1049, 2016. (cited on page: 35)

994 Tal Shnitzer, Ronen Talmon, and Jean-Jacques Slotine. **Manifold Learning for Data-Driven Dy-**
995 **namical System Analysis.** In *The Koopman Operator in Systems and Control*, pages 359–382.
996 Springer, 2020. (cited on pages: 35 and 36)

997 Jared L Callaham, J-C Loiseau, Georgios Rigas, and Steven L Brunton. **Nonlinear stochastic mod-**
998 **elling with Langevin regression.** *Proceedings of the Royal Society A*, 477(2250):20210092, 2021.
999 (cited on page: 36)

1000 Alexander Tong, Jessie Huang, Guy Wolf, David Van Dijk, and Smita Krishnaswamy. **Trajecto-**
1001 **ryNet: A dynamic optimal transport network for modeling cellular dynamics.** In *International*
1002 *conference on Machine Learning*, pages 9526–9536. PMLR, 2020. (cited on page: 36)

1003 Tal Shnitzer, Ronen Talmon, and Jean-Jacques Slotine. **Manifold learning with contracting observers**
1004 **for data-driven time-series analysis.** *IEEE Transactions on Signal Processing*, 65(4):904–918,
1005 2016. doi: <https://doi.org/10.1109/TSP.2016.2616334>. (cited on page: 36)

1006 Nelida Črnjarić-Žic, Senka Maćešić, and Igor Mezić. **Koopman operator spectrum for random**
1007 **dynamical systems.** *Journal of Nonlinear Science*, 30(5):2007–2056, 2020. (cited on page: 36)

1008 Dorothy Maharam. **Invariant measures and Radon-Nikodym derivatives.** *Transactions of the Amer-*
1009 *ican Mathematical Society*, 135:223–248, 1969. (cited on page: 36)

1010 David Ruelle. **Ergodic theory of differentiable dynamical systems.** *Publications Mathématiques de*
1011 *l’Institut des Hautes Études Scientifiques*, 50(1):27–58, 1979. (cited on page: 36)

1012 David Ruelle. **Chaotic evolution and strange attractors**, volume 1. Cambridge University Press,
1013 1989. (cited on page: 37)

1014 Lai-Sang Young. **What are SRB measures, and which dynamical systems have them?** *Journal of*
1015 *Statistical Physics*, 108(5):733–754, 2002. (cited on page: 37)

1016 Edward Ott. **Chaos in dynamical systems.** Cambridge university press, 2002. (cited on page: 37)

1026 Lai-Sang Young. **Dimension, entropy and Lyapunov exponents.** *Ergodic theory and dynamical
1027 systems*, 2(1):109–124, 1982. (cited on page: 37)

1028

1029 François Ledrappier and Lai-Sang Young. **The metric entropy of diffeomorphisms: part II: relations
1030 between entropy, exponents and dimension.** *Annals of Mathematics*, 122(3):540–574, 1985. (cited
1031 on page: 37)

1032

1033 Valery Iustinovich Oseledets. **A multiplicative ergodic theorem. Characteristic Ljapunov, exponents
1034 of dynamical systems.** *Trudy Moskovskogo Matematicheskogo Obshchestva*, 19:179–210, 1968.
(cited on page: 37)

1035

1036 Balázs Bárány and Antti Käenmäki. **Ledrappier–Young formula and exact dimensionality of self-
1037 affine measures.** *Advances in Mathematics*, 318:88–129, 2017. (cited on page: 37)

1038

1039 David Ruelle. **An inequality for the entropy of differentiable maps.** *Boletim da Sociedade Brasileira
1040 de Matemática-Bulletin/Brazilian Mathematical Society*, 9(1):83–87, 1978. (cited on page: 37)

1041

1042 Hannes Risken. **The Fokker-Planck Equation: Methods of Solution and Applications.** Springer-
1043 Verlag, 2nd edition, 1996. (cited on page: 37)

1044

1045 Lars Hörmander. **Hypoelliptic second order differential equations.** 1967. (cited on page: 38)

1046

1047 Yuri Kifer. **Random perturbations of dynamical systems.** *Nonlinear Problems in Future Particle
1048 Accelerators*, 189, 1988. (cited on page: 38)

1049

1050 Ludwig Arnold. **Random dynamical systems.** In *Dynamical Systems: Lectures Given at the 2nd
1051 Session of the Centro Internazionale Matematico Estivo (CIME) held in Montecatini Terme, Italy,
1052 June 13–22, 1994*, pages 1–43. Springer, 2006. (cited on page: 38)

1053

1054 Arnulf Jentzen and Peter E Kloeden. **Taylor approximations for stochastic partial differential equa-
1055 tions.** SIAM, 2011. (cited on page: 41)

1056

1057 Wolfgang Kühnel. **Differential geometry: Curves - Surfaces - Manifolds**, Second edition. American
1058 Mathematical Society, Providence, RI, 2, 2002. (cited on page: 43)

1059

1060 Evelyn Fix. **Discriminatory analysis: nonparametric discrimination, consistency properties**, vol-
1061 ume 1. USAF School of Aviation Medicine, 1985. (cited on page: 49)

1062

1063 Thomas Cover and Peter Hart. **Nearest neighbor pattern classification.** *IEEE transactions on infor-
1064 mation theory*, 13(1):21–27, 1967. (cited on page: 49)

1065

1066 Dimitra Maoutsou, Sebastian Reich, and Manfred Opper. **Interacting particle solutions of Fokker-
1067 Planck equations through gradient–log–density estimation.** *Entropy*, 22(8):802, 2020. (cited on
1068 page: 50)

1069

1070

1071

1072

1073

1074

1075

1076

1077

1078

1079

1080	SUPPLEMENTARY INFORMATION	
1081		
1082		
1083	A Drift inference for high and low frequency observations	22
1084	A.1 High frequency observations	23
1085	A.2 Low frequency observations	24
1086	A.3 Approximate posterior over paths.	25
1087	A.3.1 Approximate posterior over paths <u>without</u> geometric constraints	25
1088	A.3.2 Approximate posterior over paths with geometric constraints	26
1089	Riemannian geometry.	26
1090	Riemannian geometry of observations.	27
1091	Extended free energy functional.	28
1092	A.4 Approximate posterior over drift functions.	29
1093		
1094		
1095		
1096	B Sparse Gaussian process estimation	30
1097		
1098		
1099	C Theoretical evidence that may support the use of geodesics as geometric constraints	31
1100		
1101		
1102	D Does the proposed approach invalidate the Markovian property of the diffusion process?	32
1103		
1104		
1105		
1106	E Related work and positioning of the present work	33
1107	▷ Modelling general SDEs from state observations.	33
1108	▷ Modelling SDEs from population level snapshots/boundary conditions.	34
1109	Geometry aware generative methods.	34
1110	Approximating observation geometry in the ambient space.	34
1111	Positioning of the present work.	35
1112		
1113		
1114		
1115	F Geometric constraints on inference	35
1116		
1117		
1118	G Theoretical justification for Riemannian manifold approximation of the invariant density	36
1119		
1120	G.1 Dimensionality of invariant measures induced by deterministic dynamics	36
1121	G.2 Dimensionality of invariant measures induced by stochastic dynamics	37
1122		
1123	H Theoretical justification of geometric augmentation for large inter-observation intervals	39
1124		
1125		
1126	H.1 Inference performance deteriorates with increasing inter-observation interval for existing frameworks	39
1127		
1128	H.2 Inference based on Euler-Maruyama discretisation does not account for the curvature of the trajectories in the state space	40
1129		
1130	H.2.1 First remainder term $R_{1,a}$	41
1131	First component $R_{1,a}^1$ of remainder term $R_{1,a}$: Flow curvature term.	42
1132	Second component $R_{1,a}^2$ of remainder term $R_{1,a}$	44
1133		

1134	Third component $R_{1,a}^3$ of remainder term $R_{1,a}$	45
1135		
1136	H.2.2 Second remainder term $R_{1,b}$	45
1137	H.2.3 Third remainder term $R_{1,c}$	46
1138	H.2.4 Fourth remainder term $R_{1,d}$	46
1139		
1140		
1141	I Additional numerical results	47
1142	I.1 Inference with noise miss-estimation	47
1143		
1144	I.2 Ablations with respect to metric learning algorithm	47
1145		
1146	J Details on numerical experiments	47
1147	J.1 On computation of geodesic curves	48
1148		
1149	J.2 Details on baseline methods	48
1150		
1151	K Algorithmic details	50
1152		
1153	L Impact Statement	54
1154		
1155	M LLMs usage statement	54
1156		

A DRIFT INFERENCE FOR HIGH AND LOW FREQUENCY OBSERVATIONS

Effective dynamics of systems with many degrees of freedom or inherently stochastic are often described in terms of a stochastic differential equation (SDE)

$$d\mathbf{X}_t = \mathbf{f}(\mathbf{X}_t)dt + \boldsymbol{\eta}(t)dt = \mathbf{f}(\mathbf{X}_t)dt + \boldsymbol{\sigma}d\mathbf{W}_t, \quad (13)$$

where the drift $\mathbf{f}(\cdot) : \mathcal{R}^d \rightarrow \mathcal{R}^d$ describes the deterministic forces acting on the system, while the delta-correlated Gaussian white noise term $\boldsymbol{\eta}(t)$, $\langle \boldsymbol{\eta}(t)\boldsymbol{\eta}(t') \rangle = \boldsymbol{\sigma}\delta(t-t')$ describes the effect of stochastic forces as a product of a diffusion matrix (or constant) $\boldsymbol{\sigma} : \mathcal{R}^{d \times d}$ that accounts for the magnitude of the stochastic forces acting on the system, and a d -dimensional Wiener process \mathbf{W}_t that contributes random influences.

Often the detailed equation that governs the evolution of the state of the system is unknown. Therefore, understanding a system of interest often requires identification from time series observations of its state. In more practical terms, given some **prior probability** for the drift function, we want to compute the **posterior probability** $P(\mathbf{f}|\{\mathcal{O}_k\}_{k=1}^K)$ that identifies the unknown drift function of Eq. 13 that most likely gave rise to the observations of the system state $\{\mathcal{O}_k\}_{k=1}^K$. The exact relationship between the observations and the system state will be defined more precisely in the following.

When a system is observed nearly continuously (inter-observation interval length τ much smaller than the characteristic time scale of the system $\tau \ll \tau_{\text{char}}$), temporal methods regress the system state \mathbf{X}_t against the state increments $\mathbf{Y}_t = \frac{\mathbf{X}_{t+\tau} - \mathbf{X}_t}{\tau}$ to identify the drift function (Friedrich and Peinke, 1997; Ragwitz and Kantz, 2001). In a Bayesian framework, this corresponds to Gaussian process regression with a Gaussian likelihood (SI A.1). However, for large inter-observation intervals τ , these methods fail (Batz et al., 2018), as the Gaussian likelihood assumption is invalid for general nonlinear systems with sparse observations (Fig. 1C.). In such cases, the likelihood is a *path integral* over continuous trajectories of the unobserved process (SI A.2), making Gaussian-based estimates inaccurate (Fig. 1C.).

This underwhelming performance has motivated the development of methods that combine state estimation (or **path augmentation**) and dynamical inference. These methods reconstruct continuous paths to approximate transition densities between observations, enabling inference by estimating the system's state between observations. However, for large time intervals, transition densities are usually analytically intractable, except in a few trivial cases of scalar or linear processes. As a result,

the prevailing strategy is to approximate transition densities by sampling marginal distributions of **diffusion bridges**, which are diffusion processes constrained by their initial and terminal states (Golightly and Wilkinson, 2008; Papaspiliopoulos et al., 2012; Sermaidis et al., 2013; Beskos et al., 2006b; Chib et al., 2006). Yet, existing methods employ path augmentation with simplified bridge dynamics (e.g., Brownian (Chib et al., 2006; Golightly and Wilkinson, 2008) or Ornstein-Uhlenbeck bridges (Batz et al., 2018)) that do not accurately reflect the underlying transition densities for non-linear systems (Fig. 1E.).

An alternative path augmentation strategy would obtain a coarse drift estimate, typically achieved by assuming a Gaussian likelihood between observations (see SI Eq. 16), and would subsequently employ a stochastic bridge sampler (De Bortoli et al., 2021; Maoutsa and Opper, 2022; 2021) to construct stochastic bridges using the coarsely estimated nonlinear drift. However, for large inter-observation intervals, the coarsely estimated drift function often deviates significantly from the true function that generated the observations. Consequently, the observations frequently fall into low-probability regions of the estimated diffusion dynamics (Fig. 1 E.), rendering the construction of diffusion bridges either too computationally demanding or impossible (Liu et al., 2020).

A.1 HIGH FREQUENCY OBSERVATIONS

In an optimal but rather practically unrealistic scenario, we would observe the system (path) $\mathbf{X}_{0:T}$ in (nearly) continuous time, and thus we would try to identify the drift from $P(\mathbf{f}|\mathbf{X}_{0:T})$. In such a case, the infinitesimal transition probabilities of the diffusion process between consecutive time-points are Gaussian, i.e.,

$$P_f(\mathbf{X}_{0:T} | \mathbf{f}) \propto \exp \left(-\frac{1}{2dt} \sum_t \|\mathbf{X}_{t+dt} - \mathbf{X}_t - \mathbf{f}(\mathbf{X}_t)dt\|_D^2 \right). \quad (14)$$

Here we have introduced the weighted norm $\|\mathbf{u}\|_D \doteq \mathbf{u}^\top \cdot \mathbf{D}^{-1} \cdot \mathbf{u}$, with $\mathbf{D} \doteq \sigma \sigma^\top$ indicating the noise covariance.

In turn, the transition probabilities of a discretised drift-less process (a Wiener path) $P_W(\mathbf{X}_{0:T})$ with same diffusion σ is

$$P_W(\mathbf{X}_{0:T}) = \exp \left(-\frac{1}{2dt} \sum_t \|\mathbf{X}_{t+dt} - \mathbf{X}_t\|_D^2 \right). \quad (15)$$

We can thus express the likelihood for the drift f as the likelihood ratio between the transition probabilities of Eq. 14 and Eq. 15, which for diffusion processes is expressed by the Radon-Nykodym derivative between $P_f(\mathbf{X}_{0:T}|f)$ and $P_W(\mathbf{X}_{0:T})$ for paths $\mathbf{X}_{0:T}$ within the time interval $[0, T]$ (Liptser and Shiryaev, 2013)

$$\mathcal{L}(\mathbf{X}_{0:T} | \mathbf{f}) = \exp \left(-\frac{1}{2} \sum_t \|\mathbf{f}(\mathbf{X}_t)\|_D^2 dt + \sum_t \langle \mathbf{f}(\mathbf{X}_t), \mathbf{X}_{t+dt} - \mathbf{X}_t \rangle_D \right), \quad (16)$$

where for brevity we have introduced the notation $\langle \mathbf{u}, \mathbf{v} \rangle_D \doteq \mathbf{u}^\top \cdot \mathbf{D}^{-1} \cdot \mathbf{v}$ for the weighted inner product with respect to the inverse noise covariance \mathbf{D}^{-1} . This expression results from applying the Girsanov theorem on the path measures induced by a process with drift \mathbf{f} and a Wiener process, with same diffusion σ , and employing an Euler-Maruyama discretisation on the continuous path $\mathbf{X}_{0:T}$.

The likelihood of a continuously observed path of the SDE (Eq. 16) has a quadratic form in terms of the drift function. Therefore a Gaussian measure over function values (Gaussian process) is a natural conjugate prior for this likelihood. Thus, to identify the drift in a non-parametric form, we assume a Gaussian process prior for the function values $\mathbf{f} \sim P_0(\mathbf{f}) = \mathcal{GP}(\mathbf{m}^f, k^f)$, where \mathbf{m}^f and k^f denote the mean and covariance function of the Gaussian process (Ruttor et al., 2013). The prior measure can be written as

$$P_0(\mathbf{f}) = \exp \left(-\frac{1}{2} \int \int \mathbf{f}(\mathbf{x}) (k^f(\mathbf{X}, \mathbf{X}'))^{-1} \mathbf{f}(\mathbf{X}') d\mathbf{X} d\mathbf{X}' \right), \quad (17)$$

if we consider a zero mean Gaussian process $\mathbf{m}^f = \mathbf{0}$.

1242 Bayesian inference for the drift function \mathbf{f} requires the computation of a probability distribution in
 1243 the function space, the posterior probability distribution $P_f(\mathbf{f} \mid \mathbf{X}_{0:T})$. From the Bayes' rule the
 1244 posterior can be written as

1245

$$P_f(\mathbf{f} \mid \mathbf{X}_{0:T}) = \frac{P_0(\mathbf{f})\mathcal{L}(\mathbf{X}_{0:T} \mid \mathbf{f})}{Z} \propto P_0(\mathbf{f})\mathcal{L}(\mathbf{X}_{0:T} \mid \mathbf{f}), \quad (18)$$

1246

1247 where Z denotes a normalising factor defined as

1248

$$Z = \int P_0(\mathbf{f})\mathcal{L}(\mathbf{X}_{0:T} \mid \mathbf{f})\mathcal{D}\mathbf{f}, \quad (19)$$

1249

1250 where $\mathcal{D}\mathbf{f}$ denotes integration over the Hilbert space $\mathbf{f} : H_0[\mathbf{f}] < \infty$. Here we have expressed
 1251 the prior probability over functions as $P_0(\mathbf{f}) = e^{-H_0[\mathbf{f}]}$. In Ruttor et al. (2013) the authors show
 1252 that in this continuous-time setting, nonparametric estimation of the drift can be attained through
 1253 a Gaussian process regression (Rasmussen, 2003) with the objective to identify the mapping from
 1254 the system state \mathbf{X}_t to state increments $d\mathbf{X}_t$. More precisely, we consider as the regressor the N
 1255 observations of the system state \mathbf{X}_t and as the associated response variables the state increments
 1256

1257

$$\mathbf{Y}_t = \frac{\mathbf{X}_{t+dt} - \mathbf{X}_t}{dt}, \quad (20)$$

1258

1259 and select the kernel function of the Gaussian process as $k^f(\mathbf{X}, \mathbf{X}')$.

1260

1261 If we denote with $\mathcal{X} = \{\mathbf{X}_t\}_{t=0}^{T-dt}$ and $\mathcal{Y} = \{\mathbf{Y}_t\}_{t=0}^{T-dt}$ the set of state observations and observation
 1262 increments, the mean of the posterior process over drift functions \mathbf{f} can be expressed as

1263

$$\bar{\mathbf{f}}(\mathbf{x}) = k^f(\mathbf{x}, \mathcal{X})^\top \left(\mathcal{K} + \frac{\mathbf{D}}{dt} I_N \right)^{-1} \mathcal{Y}, \quad (21)$$

1264

1265 where we abused the notation and denoted with $k^f(\mathbf{x}, \mathcal{X})$ the vector resulting from evaluating the
 1266 kernel k^f at points \mathbf{x} and $\{\mathcal{O}_k\}_{k=1}^{K-1}$. Similarly $\mathcal{K} = k^f(\mathcal{X}, \mathcal{X})$ stands for the $(K-1) \times (K-1)$
 1267 matrix resulting from evaluation of the kernel on all observation pairs. In a similar vein, the posterior
 1268 variance can be written as

1269

$$\Sigma^2(\mathbf{x}) = k^f(\mathbf{x}, \mathbf{x}) - k^f(\mathbf{x}, \mathcal{X})^\top \left(\mathcal{K} + \frac{\mathbf{D}}{dt} \right)^{-1} k^f(\mathbf{x}, \mathcal{X}), \quad (22)$$

1270

1271 where the term \mathbf{D}/dt plays the role of observation noise.

1272

1273 **A.2 LOW FREQUENCY OBSERVATIONS**

1274

1275 As the inter-observation interval increases (*low frequency observations*), the validity of the Gaussian
 1276 likelihood used in drift estimation diminishes as the transition density is no longer Gaussian.
 1277 Consequently, methods for drift estimation with Gaussian assumptions (Friedrich and Peinke, 1997;
 1278 Ruttor et al., 2013) become increasingly inaccurate. To discount the effects of low frequency sam-
 1279 pling, Lade (Lade, 2009) proposed a method to compute finite-time corrections for drift estimates,
 1280 which has been mainly applied to one-dimensional problems (Honisch and Friedrich, 2011). In
 1281 parallel, the statistics community has proposed path augmentation techniques that involve sampling
 1282 with a simplified system's dynamics between time-consecutive observations to augment the ob-
 1283 served trajectory to a nearly continuous-time path (Golightly and Wilkinson, 2008; Papaspiliopoulos
 1284 et al., 2012; Sermaidis et al., 2013; Beskos et al., 2006b; Chib et al., 2006). However, for large
 1285 inter-observation intervals and nonlinear systems, the augmented trajectories match poorly the un-
 1286 derlying path statistics and these methods often exhibit poor convergence rates or fail to identify the
 1287 correct dynamics (Figure 1 c. and d.). We note that path augmentation using Ornstein-Uhlenbeck
 1288 bridges and local linearisation of the **ground truth** dynamics provides a reasonable approximation
 1289 of the underlying transition density up to a certain inter-observation interval. Nevertheless, during
 1290 inference, the ground truth dynamics is unknown, and the proposed local linearisations based on
 1291 inaccurate drift estimates (Batz et al., 2018) perform poorly in this sparsely sampled regime.

1292

1296 As the inter-observation interval τ increases, if the system is nonlinear, the likelihood assumed be-
 1297 tween two consecutive observations is no longer Gaussian, but is rather expressed as a *path integral*
 1298

$$1299 \quad P(\mathcal{O}_{1:K} | \mathbf{f}) = \int P(\mathcal{O}_{1:K} | \mathbf{X}_{0:T}) P(\mathbf{X}_{0:T} | \mathbf{f}) \mathcal{D}(\mathbf{X}_{0:T}), \quad (23)$$

1300 where $\mathcal{O}_{1:K} \doteq \{\mathcal{O}_k\}_{k=1}^K$ identifies the set of K observations collected within the interval $[0, T]$,
 1301 $P(\mathbf{X}_{0:T} | \mathbf{f})$ the prior path probability resulting from a diffusion process with drift $\mathbf{f}(\mathbf{x})$, $\mathcal{D}(\mathbf{X}_{0:T})$
 1302 identifies the formal volume element on the path space, and $P(\mathcal{O}_{1:K} | \mathbf{X}_{0:T})$ stands for the likeli-
 1303 hood of observations given the latent path $\mathbf{X}_{0:T}$.
 1304

1305 However, the path integral of Eq. 23 is in general intractable for nonlinear systems.
 1306 thus we need to simultaneously estimate the drift and latent state of the diffusion pro-
 1307 cess, i.e., to approximate the joint posterior measure of latent paths and drift functions
 1308 $P(\mathbf{X}_{0:T}, \mathbf{f} | \mathcal{O}_{1:K})$. Therefore we consider the unobserved continuous path $\mathbf{X}_{0:T}$ as la-
 1309 tent random variables and employ an Expectation Maximisation (EM) algorithm to identify
 1310 a maximum a posteriori estimate for the drift function. More precisely, we follow an it-
 1311 erative algorithm, where at each iteration n we alternate between the two following steps:
 1312 An **Expectation** step, where given a drift estimate $\hat{\mathbf{f}}^n(\mathbf{x})$ we construct an approximate posterior
 1313 over the latent variables $Q(\mathbf{X}_{0:T}) \approx P(\mathbf{X}_{0:T} | \mathcal{O}_{1:K}, \hat{\mathbf{f}}^n(\mathbf{x}))$, and compute the expected log-
 1314 likelihood of the augmented path
 1315

$$1316 \quad \mathcal{L}(\hat{\mathbf{f}}^n(\mathbf{x}), Q) = \mathbb{E}_Q \left[\ln \mathcal{L}(\mathbf{X}_{0:T}, \mathcal{O}_{1:K} | \hat{\mathbf{f}}^n(\mathbf{x})) \right]. \quad (24)$$

1317 A **Maximisation** step, where we update the drift estimation by maximising the expected log likeli-
 1318 hood
 1319

$$1320 \quad \mathbf{f}^{n+1}(\mathbf{x}) = \arg \max_f \left[\mathcal{L}(\mathbf{f}^n(\mathbf{x}), Q) - \ln P_0(\mathbf{f}^n(\mathbf{x})) \right]. \quad (25)$$

1321 In Eq. 25, P_0 denotes the Gaussian process prior over function values.
 1322

1323 A.3 APPROXIMATE POSTERIOR OVER PATHS.

1324 To obtain an approximate posterior over the latent paths we perform **variational inference** (Beal,
 1325 2003). In this section, we first formulate the approximate posterior over paths (conditional distri-
 1326 bution for the path given the observations) by considering only individual observations as constraints
 1327 (Section A.3.1). However, this approach results computationally taxing calculations during path
 1328 augmentation, since the observations are atypical states of the initially estimated drift. To over-
 1329 come this issue, we subsequently extend the formalism (Section A.3.2) to incorporate constraints
 1330 that consider also the local geometry of the observations.
 1331

1332 A.3.1 APPROXIMATE POSTERIOR OVER PATHS WITHOUT GEOMETRIC CONSTRAINTS

1333 Given a drift function (or a drift estimate) $\hat{\mathbf{f}}(\mathbf{x})$ we can apply variational techniques to approximate
 1334 the posterior measure over the latent path conditioned on the observations $\mathcal{O}_{1:K}$. We consider
 1335 that the **prior process** (the process without considering the observations $\mathcal{O}_{1:K}$) is described by the
 1336 equation

$$1337 \quad P(\mathbf{X}_{0:T} | \hat{\mathbf{f}}) : \quad d\mathbf{X}_t = \hat{\mathbf{f}}(\mathbf{X}_t) dt + \sigma d\mathbf{W}_t. \quad (26)$$

1338 We will define an approximating (posterior) process that is conditioned on the observations. The
 1339 conditioned process is also a diffusion process with the same diffusion as Eq. 26 but with a modi-
 1340 fied, time-dependent drift $g(x, t)$ that accounts for the observations (Chetrite and Touchette, 2015;
 1341 Majumdar and Orland, 2015). We identify the approximate posterior measure Q with the posterior
 1342 measure induced by an approximating process that is conditioned by the observations $\mathcal{O}_{1:K}$ (Opper,
 1343 2019), with governing equation
 1344

$$1345 \quad Q(\mathbf{X}_{0:T}) : \quad d\mathbf{X}_t = \mathbf{g}(\mathbf{X}_t, t) dt + \sigma d\mathbf{W}_t = \left(\hat{\mathbf{f}}(\mathbf{X}_t) + \mathbf{u}(\mathbf{X}_t, t) \right) dt + \sigma d\mathbf{W}_t. \quad (27)$$

1350 The effective drift $\mathbf{g}(\mathbf{X}_t, t)$ of Eq. 27 may be obtained from the solution of the variational problem
 1351 of minimising the free energy
 1352

$$1353 \mathcal{F}[Q] = \mathcal{KL}\left(Q(\mathbf{X}_{0:T}) \parallel P(\mathbf{X}_{0:T} \mid \hat{\mathbf{f}})\right) - \sum_{k=1}^K \left\langle \ln P(\mathcal{O}_k \mid \mathbf{X}_{t_k}) \right\rangle_Q. \quad (28)$$

1356 By applying the Cameron-Girsanov-Martin theorem we can express the Kullback-Leibler divergence
 1357 between the two path measures induced by the diffusions with drift $\hat{\mathbf{f}}(\mathbf{x})$ and $\mathbf{g}(\mathbf{x}, t)$ as
 1358

$$1359 \mathcal{KL}\left(Q(\mathbf{X}_{0:T}) \parallel P(\mathbf{X}_{0:T} \mid \hat{\mathbf{f}})\right) = \left\langle \ln \left(\frac{dQ(\mathbf{X}_{0:T})}{dP(\mathbf{X}_{0:T} \mid \hat{\mathbf{f}})} \right) \right\rangle_Q \quad (29)$$

$$1360 = \left\langle \left(-\frac{1}{2} \int_0^T \|\hat{\mathbf{f}}(\mathbf{X}_t) - \mathbf{g}(\mathbf{X}_t, t)\|_{\mathbf{D}}^2 dt + \int_0^T \frac{\hat{\mathbf{f}}(\mathbf{X}_t) - \mathbf{g}(\mathbf{X}_t, t)}{\mathbf{D}} d\mathbf{W}_t \right) \right\rangle_Q$$

$$1361 = \left\langle \left(-\frac{1}{2} \int_0^T \|\hat{\mathbf{f}}(\mathbf{X}_t) - \mathbf{g}(\mathbf{X}_t, t)\|_{\mathbf{D}}^2 dt + V_T \right) \right\rangle_Q \quad (30)$$

$$1362 = \frac{1}{2} \int_0^T \int \|\mathbf{g}(\mathbf{x}, t) - \hat{\mathbf{f}}(\mathbf{x})\|_{\mathbf{D}}^2 q_t(\mathbf{x}) d\mathbf{x} dt + \mathfrak{C}, \quad (31)$$

1363 where $q_t(\mathbf{x})$ stands for the marginal density for \mathbf{X}_t of the approximate process. In the third line
 1364 we have introduced the random variable $V_T = \int_0^T \frac{\hat{\mathbf{f}}(\mathbf{X}_t) - \mathbf{g}(\mathbf{X}_t, t)}{\mathbf{D}} d\mathbf{W}_t$. Under the assumption that
 1365 the function $\ell(\mathbf{X}_t) = \hat{\mathbf{f}}(\mathbf{X}_t) - \mathbf{g}(\mathbf{X}_t, t)$ is bounded, piece-wise continuous, and in $L^2[0, \infty)$, V_T
 1366 follows the distribution $\mathcal{N}\left(V_T \mid 0, \int_0^T \ell^2(s) ds\right)$, which for a given T will result into a constant \mathfrak{C} .
 1367 Thus the second term in Eq. 31 is not relevant for the minimisation of the free energy and will be
 1368 omitted.

1369 We can thus express the free energy of Eq. 28 as (Opper, 2019)
 1370

$$1371 \mathcal{F}[Q] = \frac{1}{2} \int_0^T \int \left[\|\mathbf{g}(\mathbf{x}, t) - \hat{\mathbf{f}}(\mathbf{x})\|_{\mathbf{D}}^2 + U(\mathbf{x}, t) \right] q_t(\mathbf{x}) d\mathbf{x} dt, \quad (32)$$

1372 where the term $U(\mathbf{x}, t)$ accounts for the observations $U(\mathbf{x}, t) = -\sum_{t_k} \ln P(\mathcal{O}_k \mid \mathbf{x}) \delta(t - t_k)$.
 1373

1374 The minimisation of the functional of the free energy can be construed as a stochastic control
 1375 problem (Opper, 2019) with the objective to identify a time-dependent drift adjustment $\mathbf{u}(\mathbf{x}, t) :=$
 1376 $\mathbf{g}(\mathbf{x}, t) - \hat{\mathbf{f}}(\mathbf{x})$ for the system with drift $\hat{\mathbf{f}}(\mathbf{x})$ so that the controlled dynamics fulfil the constraints
 1377 imposed by the observations.

1378 A.3.2 APPROXIMATE POSTERIOR OVER PATHS WITH GEOMETRIC CONSTRAINTS

1379 The previously described construction of the approximate measure in terms of stochastic bridges is
 1380 relevant when the observations have non vanishing probability under the law of the prior diffusion
 1381 process of Eq. 26. However, when the prior process (with the estimated drift \hat{f}) differs consider-
 1382 ably from the process that generated the observations, such a construction might either provide a
 1383 bad approximation of the underlying path measure, or show slow numerical convergence in the
 1384 construction of the diffusion bridges. To overcome this issue, we consider here additional constraints
 1385 for the posterior process that force the paths of the posterior measure to respect the local geometry
 1386 of the observations. In the following we provide a brief introduction on the basics of Riemannian
 1387 geometry and consequently continue with the geometric considerations of the proposed method.

1388 **Riemannian geometry.** A d -dimensional **Riemannian manifold** (Do Carmo and Flaherty Fran-
 1389 cis, 1992; Lee, 2018) $(\mathcal{M}, \mathfrak{h})$ embedded in a d -dimensional ambient space $\mathcal{X} = \mathcal{R}^d$ is a smooth

1404 curved d -dimensional surface endowed with a smoothly varying inner product (Riemannian) **metric**
 1405 $\mathfrak{h} : \mathbf{x} \rightarrow \langle \cdot | \cdot \rangle_{\mathbf{x}}$ on $\mathcal{T}_{\mathbf{x}}\mathcal{M}$. A tangent space $\mathcal{T}_{\mathbf{x}}\mathcal{M}$ is defined at each point $\mathbf{x} \in \mathcal{M}$. The Riemannian metric \mathfrak{h} defines a canonical volume measure on the manifold \mathcal{M} . Intuitively this characterises
 1406 how to compute inner products locally between points on the tangent space of the manifold \mathcal{M} , and
 1407 therefore determines also how to compute norms and thus distances between points on \mathcal{M} .
 1408

1409 A **coordinate chart** (G, ϕ) provides the mapping from an open set G on \mathcal{M} to an open set V in
 1410 the Euclidean space. The dimensionality of the manifold is d if for each point $\mathbf{x} \in \mathcal{M}$ there exists
 1411 a local neighborhood $G \subset \mathcal{R}^d$. We can represent the metric \mathfrak{h} on the local chart (G, ϕ) by the
 1412 positive definite matrix (**metric tensor**) $H(\mathbf{x}) = (\mathfrak{h}_{i,j})_{\mathbf{x}, 0 \leq i,j \leq d} = \left(\langle \frac{\partial}{\partial x_i} | \frac{\partial}{\partial x_j} \rangle_{\mathbf{x}} \right)_{0 \leq i,j \leq d}$ at each
 1413 point $\mathbf{x} \in G$.
 1414

1415 For $\mathbf{v}, \mathbf{w} \in \mathcal{T}_{\mathbf{x}}\mathcal{M}$ and $\mathbf{x} \in G$, their inner product can be expressed in terms of the matrix representation
 1416 of the metric \mathfrak{h} on the tangent space $\mathcal{T}_{\mathbf{x}}\mathcal{M}$ as $\langle \mathbf{v} | \mathbf{w} \rangle_{\mathbf{x}} = \mathbf{v}^{\top} H(\mathbf{x}) \mathbf{w}$, where $H(\mathbf{x}) \in \mathcal{R}^{d \times d}$
 1417 .

1418 The **length of a curve** $\gamma : [0, 1] \rightarrow \mathcal{M}$ on the manifold is defined as the integral of the norm of the
 1419 tangent vector
 1420

$$1421 \ell(\gamma_{t'}) = \int_0^1 \|\dot{\gamma}_{t'}\|_{\mathfrak{g}} dt' = \int_0^1 \sqrt{\dot{\gamma}_{t'}^{\top} H(\gamma_{t'}) \dot{\gamma}_{t'}} dt', \quad (33)$$

1423 where the dotted letter indicates the velocity of the curve $\dot{\gamma}_{t'} = \partial_{t'} \gamma_{t'}$. A **geodesic curve** is a locally
 1424 length minimising smooth curve that connects two given points on the manifold.
 1425

1426 **Riemannian geometry of observations.** For approximating the posterior over paths we take into
 1427 account the geometry of the invariant density as it is represented by the observations. To that end,
 1428 we consider systems whose dynamics induce invariant (inertial) manifolds that contain the global at-
 1429 tractor of the system and on which system trajectories concentrate (Wiggins, 1994; Mohammed and
 1430 Scheutzow, 1999; Giry and Chueshov, 1995; Fenichel and Moser, 1971; Arnold, 1990; Carverhill,
 1431 1985). We assume thus that the continuous-time trajectories $\mathbf{X}_{0:T} \in \mathcal{R}^d$ of the underlying system
 1432 concentrates on an invariant manifold $\mathcal{M} \in \mathcal{R}^{m \leq d}$ of dimensionality m (possibly) smaller than d .
 1433 The discrete-time observations \mathcal{O}_k are thus samples of the manifold \mathcal{M} . The central premise of our
 1434 approach is that **unobserved paths between successive observations will be lying either on or**
 1435 **in the vicinity of the manifold \mathcal{M}** . In particular, we postulate that unobserved paths should lie **in**
 1436 **the vicinity of geodesics that connect consecutive observations** on \mathcal{M} . To that end we propose a
 1437 path augmentation framework that constraints the augmented paths to lie in the vicinity of identified
 1438 geodesics between consecutive observations.

1439 However, while this view of a lower dimensional manifold embedded in a higher dimensional am-
 1440 bient space helps to build our intuition for the proposed method, for computational purposes we
 1441 adopt a complementary view inspired by the discussion in (Fröhlich et al., 2021). According to
 1442 this view, we consider the entire observation space \mathcal{R}^d as a smooth Riemannian manifold, $\mathcal{M} \doteq \mathcal{R}^d$,
 1443 characterised by a Riemannian metric \mathfrak{h} . The effect of the nonlinear geometry of the observations is
 1444 then captured by the metric \mathfrak{h} . Thus to approximate the geometric structure of the system's invari-
 1445 ant density, we learn the Riemannian metric tensor $H : \mathcal{R}^d \rightarrow \mathcal{R}^{d \times d}$ and compute the geodesics
 1446 between consecutive observations according to the learned metric. Intuitively according to this view
 1447 the observations $\{\mathcal{O}_k\}_{k=1}^K$ introduce distortions in the way we compute distances on the state space.
 1448

1449 In effect this approach does not reduce the dimensionality of the space we operate, but changes
 1450 the way we compute inner products and thus distances, lengths, and geodesic curves on \mathcal{M} . The
 1451 alternative perspective of working on a lower dimensional manifold would strongly depend on the
 1452 correct assessment of the dimensionality of said manifold. For example, one could use a Variational
 1453 Autoencoder to approximate the observation manifold and subsequently obtain the Riemannian met-
 1454 ric from the embedding of the manifold mediated by the decoder. However, our preliminary results
 1455 of such an approach revealed that such a method requires considerable fine tuning to adapt to the
 1456 characteristics of each dynamical system and is sensitive to the estimation of the dimensionality of
 1457 the approximated manifold.

1458 To learn the Riemannian metric and compute the geodesics we follow the framework proposed by
 1459 Arvanitidis et al. in (Arvanitidis et al., 2019). In particular, we approximate the local metric induced
 1460 by the observations at location \mathbf{x} of the state space, in a non-parametric form by the inverse of the

1458 weighted local diagonal covariance computed on the observations as (Arvanitidis et al., 2019)
 1459

$$1460 \quad 1461 \quad 1462 \quad H_{dd}(\mathbf{x}) = \left(\sum_{i=1}^K w_i(\mathbf{x}) (x_i^{(d)} - \bar{x}^{(d)})^2 + \epsilon \right)^{-1}, \quad (34)$$

1463 with weights $w_i(\mathbf{x}) = \exp\left(-\frac{\|\mathbf{x}_i - \mathbf{x}\|_2^2}{2\sigma_{\mathcal{M}}^2}\right)$, and $x^{(d)}$ denoting the d -th dimensional component of the
 1464 vector \mathbf{x} . The parameter $\epsilon > 0$ ensures non-zero diagonals of the weighted covariance matrix, while
 1465 $\sigma_{\mathcal{M}}$ characterises the curvature of the manifold.
 1466

1467 Between consecutive observations for each interval $[\mathcal{O}_k, \mathcal{O}_{k+1}]$, we identify the geodesic
 1468 $\gamma_{t'}^k$ as the energy minimising curve, i.e., as the minimiser of the kinetic energy functional
 1469 $\mathcal{E}(\gamma_{t'}^k) = \int_0^1 L_{\mathcal{M}}(\gamma_{t'}^k, \dot{\gamma}_{t'}^k) dt'$
 1470

$$1471 \quad 1472 \quad 1473 \quad \gamma_{t'}^{k*} = \arg \min_{\gamma_{t'}^k, \gamma_0^k = \mathcal{O}_k, \gamma_1^k = \mathcal{O}_{k+1}} \int_0^1 L_{\mathcal{M}}(\gamma_{t'}^k, \dot{\gamma}_{t'}^k) dt',$$

$$1474 \quad 1475 \quad 1476 \quad \text{with } \int_0^1 L_{\mathcal{M}}(\gamma_{t'}^k, \dot{\gamma}_{t'}^k) dt' = \frac{1}{2} \int_0^1 \|\dot{\gamma}_{t'}^k\|_{\mathbf{h}}^2, \quad (35)$$

1477 where $L_{\mathcal{M}}(\gamma_{t'}^k, \dot{\gamma}_{t'}^k)$ denotes the Lagrangian. The minimising curve of this functional is the same
 1478 as the minimiser of the curve length functional $\ell(\gamma_{t'})$ (Eq. 33), i.e., the geodesic (Do Carmo and
 1479 Flaherty Francis, 1992).

1480 By applying calculus of variations, the minimising curve of the functional $\mathcal{E}(\gamma_{t'}^k)$ can be obtained
 1481 from the Euler-Lagrange equations, resulting in the following system of second order differential
 1482 equations (Arvanitidis et al., 2017; Do Carmo and Flaherty Francis, 1992)

$$1483 \quad 1484 \quad 1485 \quad \ddot{\gamma}_t^k = -\frac{1}{2} H(\gamma_t^k)^{-1} \left(2 \left(I \otimes (\dot{\gamma}_t^k)^\top \right) \frac{\partial \text{vec}[H(\gamma_t^k)]}{\partial \gamma_t^k} \dot{\gamma}_t^k - \frac{\partial \text{vec}[H(\gamma_t^k)^\top]}{\partial \gamma_t^k} (\dot{\gamma}_t^k \otimes \dot{\gamma}_t^k) \right), \quad (36)$$

1486 with boundary conditions $\gamma_0^k = \mathcal{O}_k$ and $\gamma_1^k = \mathcal{O}_{k+1}$, where \otimes stands for the Kroenecker product,
 1487 and $\text{vec}[A]$ denotes the vectorisation operation of matrix A through stacking the columns of A into
 1488 a vector. We follow Arvanitidis et al. (2019) and obtain the geodesics by approximating the solution
 1489 of the boundary value problem of Eq. 36 with a probabilistic differential equation solver.
 1490

1491 **Extended free energy functional.** We denote the collection of individual geodesics by
 1492 $\Gamma_t \doteq \{\gamma_{t'}^k\}_{t=(k-1)\tau+t'\tau}$, where $\gamma_{t'}^k$ is the geodesic connecting \mathcal{O}_k and \mathcal{O}_{k+1} , and $t' \in [0, 1]$ de-
 1493 notes a rescaled time variable. Additional to the constraints imposed in the previously explained
 1494 setting (Sec A.3.1), here we add an extra term in the free energy $\bar{U}_{\mathcal{G}}(\mathbf{x}, t) \doteq \|\Gamma_t - \mathbf{x}\|^2$ that accounts
 1495 for the local geometry of the invariant density, and guides the latent path towards the geodesic curves
 1496 $\gamma_{t'}^k$ that connect consecutive observations

$$1497 \quad 1498 \quad 1499 \quad \mathcal{F}[Q] = \frac{1}{2} \int_0^T \int \left[\|g(\mathbf{x}, t) - \hat{f}(\mathbf{x})\|_D + U_{\mathcal{O}}(\mathbf{x}, t) + \beta U_{\mathcal{G}}(\mathbf{x}, t) \right] q_t(\mathbf{x}) d\mathbf{x} dt. \quad (37)$$

1500 Here we denote the observation term by $U_{\mathcal{O}}(\mathbf{x}, t) \doteq -\sum_{t_k} \ln P(\mathcal{O}_k | \mathbf{x}) \delta(t - t_k)$, while β stands for a
 1501 weighting constant that determines the relative weight of the geometric term in the control objective.
 1502

1503 Following (Opper, 2019), for each inter-observation interval $[\mathcal{O}_k, \mathcal{O}_{k+1}]$ we identify the poste-
 1504 rior path measure (minimiser of Eq. 37) by the solution of a stochastic optimal control prob-
 1505 lem (Maoutsou and Opper, 2022) with the objective to obtain a time-dependent drift adjustment
 1506 $\mathbf{u}(\mathbf{x}, t) := \mathbf{g}(\mathbf{x}, t) - \hat{\mathbf{f}}(\mathbf{x})$ for the system with drift $\hat{\mathbf{f}}(\mathbf{x})$ with initial and terminal constraints defined
 1507 by $U_{\mathcal{O}}(\mathbf{x}, t)$, and additional path constraints $U_{\mathcal{G}}(\mathbf{x}, t)$.

1508 For the case of exact observations, i.e., for an observation process $\psi(\mathbf{x}) = \mathbf{x}$, we can compute the
 1509 drift adjustment for each of the $K - 1$ inter-observation intervals independently. Thus for each inter-
 1510 val between consecutive observations, we identify the optimal control $\mathbf{u}(\mathbf{x}, t)$ required to construct
 1511 a stochastic bridge following the dynamics of Eq. 26 with initial and terminal states the respective
 observations \mathcal{O}_k and \mathcal{O}_{k+1} .

1512 The optimal drift adjustment for such a stochastic control problem for the inter-observation interval
 1513 between \mathcal{O}_k and \mathcal{O}_{k+1} can be obtained from the solution of the backward equation (see (Maoutsu
 1514 and Opper, 2022))

$$1515 \quad 1516 \quad \frac{\partial \phi_t(\mathbf{x})}{\partial t} = -\mathcal{L}_{\hat{f}}^\dagger \phi_t(\mathbf{x}) + U_{\mathcal{G}}(\mathbf{x}, t) \phi_t(\mathbf{x}), \quad (38)$$

1517 with terminal condition $\phi_T(\mathbf{x}) = \chi(\mathbf{x}) = \delta(\mathbf{x} - \mathcal{O}_{k+1})$ and with $\mathcal{L}_{\hat{f}}^\dagger$ denoting the adjoint Fokker-
 1518 Planck operator for the process of Eq. 26. As shown in (Maoutsu and Opper, 2022) the optimal drift
 1519 adjustment $\mathbf{u}(\mathbf{x}, t)$ can be expressed in terms of the difference of the logarithmic gradients of two
 1520 probability flows

$$1522 \quad \mathbf{u}^*(\mathbf{x}, t) = D \left(\nabla \ln q_{T-t}(\mathbf{x}) - \nabla \ln \rho_t(\mathbf{x}) \right), \quad (39)$$

1523 where ρ_t fulfils the forward (filtering) partial differential equation (PDE)

$$1525 \quad 1526 \quad \frac{\partial \rho_t(\mathbf{x})}{\partial t} = \mathcal{L}_{\hat{f}} \rho_t(\mathbf{x}) - U_{\mathcal{G}}(\mathbf{x}, t) \rho_t(\mathbf{x}), \quad (40)$$

1527 while q_t is the solution of a time-reversed PDE that depends on the logarithmic gradient of $\rho_t(\mathbf{x})$

$$1529 \quad 1530 \quad \frac{\partial q_t(\mathbf{x})}{\partial t} = -\nabla \cdot \left[\left(\sigma^2 \nabla \ln \rho_{T-t}(\mathbf{x}) - \mathbf{f}(\mathbf{x}, T-t) \right) q_t(\mathbf{x}) \right] + \frac{\sigma^2}{2} \nabla^2 q_t(\mathbf{x}), \quad (41)$$

1532 with initial condition $q_0(\mathbf{x}) \propto \rho_T(\mathbf{x}) \chi(\mathbf{x})$.

1533 For the numerical solution of the control problem we use the numerical framework accompanying
 1534 Maoutsu and Opper (2022), where the path constraints associated with the geodesic curves are
 1535 imposed through the two staged process for particle propagation described in the paper for path
 1536 constraints, with the particle reweighting being performed through optimal transport implemented
 1537 using the PyEMD python toolbox (Pele and Werman, 2009).

1538 More precisely, according to this framework we propagate a particle representation of the proba-
 1539 bility density $\rho_t(\mathbf{x})$ according to the filtering equation of Eq. 40. This follows the dynamics of
 1540 the uncontrolled process with drift $\hat{\mathbf{f}}$ and particle reweighting at each time step as determined by
 1541 the path constrained (potential) $U_{\mathcal{G}}(\mathbf{x}, t)$, that quantifies the proximity to the geodesic at each time
 1542 point. In the particle representation we apply this reweighting in the form of a deterministic optimal
 1543 transportation of the particles (Reich, 2013).

1544 A.4 APPROXIMATE POSTERIOR OVER DRIFT FUNCTIONS.

1545 For a fixed path measure Q , the optimal measure for the drift Q_f is a Gaussian process given by

$$1549 \quad 1550 \quad Q_f \propto P_f \exp \left(-\frac{1}{2} \int \|\mathbf{f}(\mathbf{x})\|_D^2 A(\mathbf{x}) - 2 \langle \mathbf{f}(\mathbf{x}), B(\mathbf{x}) \rangle_D d\mathbf{x} \right), \quad (42)$$

1552 with

$$1553 \quad 1554 \quad A(\mathbf{x}) \doteq \int_0^T q_t(\mathbf{x}) dt,$$

1555 and

$$1556 \quad 1557 \quad B(\mathbf{x}) \doteq \int_0^T q_t(\mathbf{x}) g(\mathbf{x}, t) dt,$$

1558 where $q_t(\mathbf{x})$ denotes the marginal constrained density of the state \mathbf{X}_t . The function $g(\mathbf{x}, t)$ denotes
 1559 the effective drift.

1560 We assume a Gaussian process prior for the unknown function \mathbf{f} , i.e., $\mathbf{f} \sim P_0(\mathbf{f}) = \mathcal{GP}(\mathbf{m}^f, k^f)$
 1561 where \mathbf{m}^f and k^f denote the mean and covariance function of the Gaussian process. Following Rut-
 1562 tor *et al.* (Ruttor *et al.*, 2013), we employ a sparse kernel approximation for the drift f by optimising
 1563 the function values over a sparse set of S inducing points $\{Z_i\}_{i=1}^S$. We obtain the resulting drift
 1564 from

$$1565 \quad \hat{\mathbf{f}}_S(\mathbf{x}) = k^f(\mathbf{x}, \mathcal{Z}) (I + \Lambda \mathcal{K}_S)^{-1} \mathbf{d}, \quad (43)$$

1566 where we have defined introduced the notation $\mathcal{K}_S \doteq k^f(\mathcal{Z}, \mathcal{Z})$
1567

$$1568 \quad \Lambda = \frac{1}{\sigma^2} \mathcal{K}_S^{-1} \left(\int k^f(\mathcal{Z}, \mathbf{x}) A(\mathbf{x}) k^f(\mathbf{x}, \mathcal{Z}) d\mathbf{x} \right) \mathcal{K}_S^{-1}. \quad (44)$$

$$1571 \quad \mathbf{d} = \frac{1}{\sigma^2} \mathcal{K}_S^{-1} \left(\int k^f(\mathcal{Z}, \mathbf{x}) B(\mathbf{x}) d\mathbf{x} \right) \mathcal{K}_S^{-1}, \quad (45)$$

1574 The associated variance results similarly from the equation

$$1575 \quad \Sigma_S^2(\mathbf{x}) = k^f(\mathbf{x}, \mathbf{x}) - k^f(\mathbf{x}, \mathcal{Z}) (I + \Lambda \mathcal{K}_S)^{-1} \Lambda k^f(\mathcal{Z}, \mathbf{x}). \quad (46)$$

1577 We employ a sample based approximation of the densities in Eq. 42 resulting from the particle
1578 sampling of the path measure Q resulting from the geometric augmentation, i.e. the integrals over
1579 $\int q_t(\mathbf{x})$ are over the samples of the augmented paths. Thus by representing the densities by samples,
1580 we can rewrite the density $p_t(x)$ in terms of a sum of Dirac delta functions centered around the
1581 particles positions

$$1582 \quad p_t(\mathbf{x}) \approx \frac{1}{N} \sum_{j=1}^N \delta(\mathbf{x} - \mathbf{X}_j(t)),$$

1585 and replace the Riemannian integrals with summation over particles, i.e. perform a Monte Carlo
1586 integration. Here $\mathbf{X}_j(t)$ represents the position of the j -th particle at time point t .
1587

1588 B SPARSE GAUSSIAN PROCESS ESTIMATION

1590 Since the amount of required observations for accurate drift estimation is generally large for systems
1591 with nonlinear dynamics, regular Gaussian process regression becomes computationally intensive.
1592 Its computational complexity scales as $\mathcal{O}(N^3)$ with the number of observations N due to the $N \times N$
1593 kernel matrix inversions required for inference (c.f. Eq. 22 and Rasmussen (2003)). Therefore,
1594 Ruttor et al. (2013) employ the sparse (low dimensional approximation) counterpart of Gaussian
1595 process regression (Titsias, 2009; Csató and Opper, 2002) that reduces significantly the computation
1596 time by reducing the computational complexity to $\mathcal{O}(NM^2)$, where $M \ll N$ denotes the number
1597 of selected sparse (inducing) points. Here we present briefly the derivation.

1598 For sparse Gaussian process drift inference, we augment the distributions with M inducing points
1599 $\mathbf{z} = [z_1, \dots, z_M]$ with inducing values $\mathbf{u} = [\mathbf{f}(z_m)]_{m=1}^M$ that are jointly Gaussian distributed with
1600 the latent function values $\{\mathbf{f}(\mathbf{X}_t)\}_{t=0}^T$.

1602 As demonstrated previously the true posterior for function values \mathbf{f} is expressed as a product

$$1603 \quad P_f(\mathbf{f}) = \frac{1}{Z} P_o(\mathbf{f}) e^{-\mathcal{A}(\mathbf{f})}, \quad (47)$$

1606 where Z a normalisation constant, $\mathcal{A}(\mathbf{f}) = \frac{1}{2} \mathbf{f}^T \Lambda \mathbf{f} - \mathbf{a}^T \mathbf{f}$ a quadratic form of \mathbf{f} (see Eq. 16), while
1607 $P_o(\mathbf{f})$ denotes a prior Gaussian measure. Thus the posterior $P_f(\mathbf{f})$ is also Gaussian.

1608 To employ sparse Gaussian process inference, we approximate P_f with $Q_f = \mathcal{GP}(m^q(\cdot), k^q(\cdot, \cdot))$,
1609 with mean and variance functions to be calculated, depending only on the *smaller* subset ($M \ll N$)
1610 of inducing function values \mathbf{u} ,

$$1611 \quad Q_f(\mathbf{f}) \propto R(\mathbf{u}) P_o(\mathbf{f}). \quad (48)$$

1612 The effective likelihood $R(\mathbf{u})$ is chosen as the minimiser of the Kullback-Leibler divergence
1613 $\mathcal{KL}(Q_f || P_f)$.

1614 We may now express the prior $P_o(\mathbf{f})$ and the approximate marginal $Q_f(\mathbf{f})$ in terms of the inducing
1615 points

$$1616 \quad P_o(\mathbf{f}) = P_o(\mathbf{f} | \mathbf{u}) P_o(\mathbf{u}), \quad (49)$$

1617 and

$$1618 \quad Q_f(\mathbf{f}) = Q_f(\mathbf{f} | \mathbf{u}) Q_f(\mathbf{u}) = P_o(\mathbf{f} | \mathbf{u}) Q_f(\mathbf{u}), \quad (50)$$

1619 under the assumption that the posterior conditional $Q_f(\mathbf{f} | \mathbf{u})$ matches the prior conditional $P_o(\mathbf{f} | \mathbf{u})$.

1620 We select the effective likelihood $R(u)$ as the minimiser of the relative entropy between Q_f and P_f
1621

$$\begin{aligned}
1622 \quad \mathcal{KL}(Q_f || P_f) &= \int Q_f(\mathbf{f}) \ln \frac{Q_f(\mathbf{f})}{P_f(\mathbf{f})} d\mathbf{f} \\
1623 &= \int P_o(\mathbf{f}|\mathbf{u}) Q_f(\mathbf{u}) \ln \frac{P_o(\mathbf{f}) R(\mathbf{u})}{\frac{1}{Z} P_o(\mathbf{f}) e^{-\mathcal{A}(\mathbf{f})}} d\mathbf{f} d\mathbf{u} \\
1624 &= \int P_o(\mathbf{f}|\mathbf{u}) Q_f(\mathbf{u}) \ln \frac{P_o(\mathbf{f}) R(\mathbf{u})}{\frac{1}{Z} P_o(\mathbf{f}|\mathbf{u}) e^{-\mathcal{A}(\mathbf{f}|\mathbf{u})} P_o(\mathbf{u})} d\mathbf{f} d\mathbf{u} \\
1625 &= \int P_o(\mathbf{f}|\mathbf{u}) Q_f(\mathbf{u}) \ln \frac{P_o(\mathbf{u}) R(\mathbf{u})}{\frac{1}{Z} e^{-\mathcal{A}(\mathbf{f}|\mathbf{u})} P_o(\mathbf{u})} d\mathbf{f} d\mathbf{u} \\
1626 &= \int P_o(\mathbf{f}|\mathbf{u}) Q_f(\mathbf{u}) \ln \frac{R(\mathbf{u})}{\frac{1}{Z} e^{-\mathcal{A}(\mathbf{f}|\mathbf{u})}} d\mathbf{f} d\mathbf{u} \\
1627 &= \ln Z + \int Q_f(\mathbf{u}) \ln \left(\frac{e^{\ln R(\mathbf{u})}}{e^{-\mathbb{E}_o[\mathcal{A}(\mathbf{f}|\mathbf{u})]}} \right) d\mathbf{u}.
\end{aligned} \tag{51}$$

1637 In Eq. 51 in the second line, we have introduced Eq. 47-Eq. 50. In the third line we have introduced
1638 $\frac{P_o(\mathbf{f})}{P_o(\mathbf{f}|\mathbf{u})} = P_0(\mathbf{u})$ from Eq. 49. In the final line we rearranged the terms that do not depend on
1639 \mathbf{f} outside of the integral over \mathbf{f} , moved the $\ln Z$ term out of the integration over \mathbf{u} , and denoted
1640 $\langle \cdot \rangle_0 = \int P_0(\mathbf{f}|\mathbf{u}) d\mathbf{f}$.

1641 To minimise the relative entropy $\mathcal{KL}[Q_f || P_f]$ we conclude that the optimal choice for the effective
1642 likelihood $R(\mathbf{u})$ is

$$R(\mathbf{u}) \propto e^{-\langle \mathcal{A}(\mathbf{f}|\mathbf{u}) \rangle_o}. \tag{52}$$

1643 Given the quadratic form of $\mathcal{A}(\mathbf{f})$ we may write the conditional expectation in Eq. 52 as a quadratic
1644 form too

$$\begin{aligned}
1645 \quad \langle \mathcal{A}(\mathbf{f}|\mathbf{u}) \rangle_o &= \frac{1}{2} \langle \mathbf{f}|\mathbf{u} \rangle_o^\top \Lambda \langle \mathbf{f}|\mathbf{u} \rangle_o + \frac{1}{2} \text{Tr}(\text{Cov}_o[\mathbf{f}|\mathbf{u}]\Lambda) - a^\top \langle \mathbf{f}|\mathbf{u} \rangle_o \\
1646 &= \frac{1}{2} \langle \mathbf{f}|\mathbf{u} \rangle_o^\top \Lambda \langle \mathbf{f}|\mathbf{u} \rangle_o - a^\top \langle \mathbf{f}|\mathbf{u} \rangle_o + \text{const.},
\end{aligned} \tag{53}$$

1647 where in the last line we take into account that the term $\text{Tr}(\text{Cov}_o[\mathbf{f}|\mathbf{u}]\Lambda)$ is independent of the sparse
1648 function values \mathbf{u} (c.f. Ruttor et al. (2013)). In Eq. 53 $\Lambda \doteq \text{diag}[\Delta t D^{-1}, \dots, \Delta t D^{-1}]$.

1649 In particular, the conditional expectation of function values f conditioned on the inducing point
1650 function values $\mathbf{u} \equiv \mathcal{U}$ at inducing point locations $\mathbf{z} \equiv \mathcal{Z}$ equals

$$\bar{f}^s(\mathbf{x}) = \langle f|\mathbf{u} \rangle_o = k(\mathbf{x}, \mathcal{Z}) k(\mathcal{Z}, \mathcal{Z})^{-1} \mathcal{U}, \tag{54}$$

1651 while the covariance equals

$$(\Sigma^s)^2(\mathbf{x}) = k(\mathbf{x}, \mathbf{x}) - k(\mathbf{x}, \mathcal{Z}) k(\mathcal{Z}, \mathcal{Z})^{-1} k(\mathcal{Z}, \mathbf{x}), \tag{55}$$

1652 where we have employed similar notation for the kernel functions as in Eqs. 21-22.

C THEORETICAL EVIDENCE THAT MAY SUPPORT THE USE OF GEODESICS AS GEOMETRIC CONSTRAINTS

1653 The Onsager-Machlup functional for diffusion processes has been known in theoretical physics as
1654 a characteriser of the most probable path (MPP) between two pre-defined states of the process.
1655 In (Onsager and Machlup, 1953), Onsager and Machlup used the thermal fluctuations of a diffusion
1656 process to show that the probability density of a path $\gamma \in C^1([0, T], \mathcal{R}^d)$ in \mathcal{R}^d over finite interval
1657 can be expressed as a Boltzmann factor

$$P(\gamma) \sim \exp \left[- \int_0^T L(\gamma(t), \dot{\gamma}(t)) dt \right], \tag{56}$$

1674 where

$$1675 \quad 1676 \quad 1677 \quad 1678 \quad 1679 \quad 1680 \quad 1681 \quad 1682 \quad 1683 \quad 1684 \quad 1685 \quad 1686 \quad 1687 \quad 1688 \quad 1689 \quad 1690 \quad 1691 \quad 1692 \quad 1693 \quad 1694 \quad 1695 \quad 1696 \quad 1697 \quad 1698 \quad 1699 \quad 1700 \quad 1701 \quad 1702 \quad 1703 \quad 1704 \quad 1705 \quad 1706 \quad 1707 \quad 1708 \quad 1709 \quad 1710 \quad 1711 \quad 1712 \quad 1713 \quad 1714 \quad 1715 \quad 1716 \quad 1717 \quad 1718 \quad 1719 \quad 1720 \quad 1721 \quad 1722 \quad 1723 \quad 1724 \quad 1725 \quad 1726 \quad 1727$$

$$L(\gamma(t), \dot{\gamma}(t)) = \frac{1}{2} \left\| \frac{\dot{\gamma}(t) - \mathbf{f}(\gamma(t))}{\mathbf{D}} \right\|^2 + \frac{1}{2} \nabla \cdot \mathbf{f}(\gamma(t)).^1 \quad (57)$$

The function $L(\gamma(t), \dot{\gamma}(t))$ is known as the **Onsager-Machlup** function (action), while its integral over time is known as Onsager-Machlup action functional. It has been used as Lagrangian in Euler-Lagrange minimisation schemes to identify the **most probable path (MPP)** of a diffusion process between two given points in the state space (Graham, 1977; Stratonovich, 1971).

Stratonovich (Stratonovich, 1971) considered the probability that a sample of a multidimensional diffusion process will lie in the vicinity of (within a tube of infinitesimal thickness around) an idealised smooth path in the state space. To compute this probability he constructed a probability functional which is identical to the Onsager-Machlup functional considered as Lagrangian for the diffusion process. Duerr et al. (Dürr and Bach, 1978) considered scalar diffusion processes and constructed the Onsager-Machlup function from the asymptotic limit of the transition probability between the starting and end state of the path using a Girsanov transformation.

Considering Brownian motions defined on a Riemannian manifold $(\mathcal{M}, \mathbf{g})$ with associated Riemannian metric \mathbf{g} , the Onsager-Machlup functional can be expressed as the integral over the Lagrangian (Takahashi and Watanabe, 1981; Graham, 1980; Grong and Sommer, 2022)

$$L(\gamma, \dot{\gamma}) = \frac{1}{2} \|\dot{\gamma}(t)\|_{\mathbf{g}}^2 - \frac{1}{12} S(\gamma(t)), \quad (58)$$

where $\|\cdot\|_{\mathbf{g}}$ denotes the Riemannian norm on the tangent space $\mathcal{T}_X \mathcal{M}$ of the manifold with respect to the metric \mathbf{g} , and $S(\cdot)$ stands for the scalar curvature of the manifold at each point. The first term is the Lagrangian used to identify geodesic curves on manifolds (c.f. A.3.2)

In our proposed formalism, for computational purposes we have assumed the entire \mathcal{R}^d as smooth manifold. We can identify the first term of Eq. 58 with the Lagrangian we optimised for computing the geodesics on the manifold $(\mathcal{R}^d, \mathbf{g})$, where \mathbf{g} is the metric learned from the observations.

However the system we observed was a diffusion process defined in \mathcal{R}^d with an Euclidean metric. Constructing a path augmentation scheme that guides the augmented paths towards the geodesics of a diffusion defined with respect to a different metric raises questions about the validity of our approach. Here we should note that diffusions with a general state dependent diffusion coefficient $\sigma \in \mathcal{R}^{d \times m}$, and m -dimensional Brownian motion, can be considered as evolving on the manifold $(\mathcal{R}^d, \mathbf{g})$, with the associated metric $\mathbf{g} = (\sigma \sigma^\top)^{-1}$ (Capitaine, 2000). Thus it may be possible to associate the metric learned from the data with the metric arising from a state dependent diffusion by applying a transformation akin to an inverse Lamperti transform (Øksendal, 2003) to transform our learned SDE to one that would have induced the learned metric due to the state dependent diffusion. The existence of such a transformation would justify the proposed method. Our empirical results demonstrate that such a transformation may be possible.

D DOES THE PROPOSED APPROACH INVALIDATE THE MARKOVIAN PROPERTY OF THE DIFFUSION PROCESS?

The proposed path augmentation seemingly invalidates the Markovian property of the diffusion process. According to the Markov property of the diffusion of Eq. 1, the system state $\mathbf{X}_{k\tau+\delta t}$ should depend only the state $\mathbf{X}_{k\tau}$, i.e., the observation \mathcal{O}_k . The proposed augmentation makes the state $\mathbf{X}_{k\tau+\delta t}$ depending not only on the next observation $\mathcal{O}_{k+1} = \mathbf{X}_{(k+1)\tau}$, but also on past and future states that lie in the vicinity of these observations.

We effectively construct the augmented paths to compute the likelihood of a drift estimate. To compute this likelihood we require to evaluate the transition probabilities between consecutive observations. Since for general nonlinear systems the transition probabilities are in general intractable, we have to resort to numerical approximations. Ideally we would approximate the transition density

¹Onsager and Machlup's initial work concentrated around linear processes and therefore the functional initially introduced by the did not include the second term with the divergence of \mathbf{f} as this is a constant for linear \mathbf{f} . It was later added to the OM function to account for trajectory entropy corrections (Taniguchi and Cohen, 2007; Adib, 2008)

1728 with a bridge sampler that would consider the nonlinear estimated SDE conditioned to pass through
1729 consecutive observations. However for coarse drift estimates, the observations have zero probability
1730 under the law of the estimated SDE, and construction of those bridges would result either in very
1731 taxing computations or would fail altogether. Instead, here, we compute the likelihood of a "cor-
1732 rected" estimate (the correction resulting from the invariant density) under which the observations
1733 have non-zero probability, and subsequently re-estimate the drift on the augmented path with this
1734 "corrected" estimate. By taking into account the local geometry of the observations, we provide
1735 systematic corrections for the misestimated drift function to generate the augmented paths. This ef-
1736 fectively nudges the augmentation process towards the second observation of each inter-observation
1737 interval through the path constraint that forces the augmented paths towards the geodesics.
1738

1739 E RELATED WORK AND POSITIONING OF THE PRESENT WORK 1740

1741 Here, we briefly review further related work on inference or modelling of SDEs and position our
1742 work further with respect to the existing literature.
1743

1744 **Modelling general SDEs from state observations.** As already mentioned in the Introduction
1745 and in Sec. A existing inference methods for SDEs can be broadly clustered in temporal and geo-
1746 metric methods, where the former accounts for the temporal order of the observations, while the
1747 latter approximate the invariant system density and discard any time information.
1748

1749 **Temporal methods** rely on the Euler-Maruyama discretisation of the SDE paths approximating
1750 conditional expectations of state increments (i.e. the Krammers Moyal coefficients). They model
1751 the drift either in terms of Gaussian processes (Ruttor et al., 2013; Batz et al., 2018; Hostettler et al.,
1752 2018; Zhao et al., 2020; Yildiz et al., 2018), basis functions (Nabeel et al., 2025; Ragwitz and Kantz,
1753 2001; Friedrich and Peinke, 1997; Peinke et al., 1997; Friedrich et al., 2000; Ferretti et al., 2020) or
1754 libraries of functions (Boninsegna et al., 2018; Huang et al., 2022), kernel regression (Lamouroux
1755 and Lehnertz, 2009; Jiang and Knight, 1997), dynamic mode decomposition to learn the eigenfunc-
1756 tions of the Koopman operator (Klus et al., 2020), by approximating the central moments of the
1757 transition densities (Stanton, 1997), or by applying generalised methods of moments (Hansen and
1758 Scheinkman, 1993).

1759 As explicitly detailed in Sec. A, most temporal methods do not provide accurate drift estimates when
1760 the interval between observations is large. The two prevailing approaches to mitigate this finite-
1761 sampling rate effects is to either account for the systematic bias introduced by the finite sampling
1762 rate by estimating an explicit correction term for the inferred drift (Ragwitz and Kantz, 2001; 2002;
1763 Kleinhans et al., 2005; Kleinhans and Friedrich, 2007), or by performing state estimation for the
1764 unobserved paths (also known as path or data augmentation) and then estimating the drift from the
1765 continuous paths.

1766 The former approach works only for scalar systems, while the latter employs simplified bridge dy-
1767 namics (e.g., Brownian (Chib et al., 2006; Eraker, 2001; Sermaidis et al., 2013) or Ornstein Uhlen-
1768 beck (Batz et al., 2018; Billio et al., 1998) bridges) that are analytically tractable or computationally
1769 non-demanding. However, for large τ and for nonlinear systems, these simplified bridge dynamics
1770 match poorly the underlying path statistics. (Fig. 1 D.). It is important to mention here, that path
1771 augmentation with Ornstein Uhlenbeck bridges similar to Batz et al. (2018) provides a good ap-
1772 proximation of the underlying transition density, when the underlying linear process employed for
1773 each bridge has a drift that comes from the local linearisation of the **ground truth** drift function.
1774 However, during inference the true dynamics are unknown and the local linearisations on inaccurate
1775 drift estimates employed in Batz et al. (2018) provide imprecise approximations for large τ .
1776

1777 Alternative methods, employ variational inference (Batz et al., 2016; Opper, 2019; Duncker et al.,
1778 2019; Verma et al., 2024) and approximate the posterior path measure with a tractable Gaussian
1779 process induced by a time-varying linear SDE. This results in ODEs for the posterior mean and
covariance matrix and an ELBO that is optimized directly (Archambeau et al., 2007; Duncker et al.,
2019).

1780 Building on the building on a prolific line of work on neural ODEs, neural SDEs (Li et al., 2020)
1781 employ gradient-based stochastic variational inference and the stochastic adjoint sensitivity method
to compute gradients of solutions of stochastic equations with respect to their parameters. Building

1782 on these methods, Course and Nair (2023b) remove the need for adjoint-based gradient computations by combining amortized inference with a reparametrization of the ELBO by assuming a latent
1783 linear process that generates the latent path.
1784

1785 **Geometric approaches** on the other hand, discard the temporal structure of the observations, and
1786 treat them as samples of the invariant density. Thereby these methods either employ density estimation
1787 to identify the drift as the gradient of a potential Kutoyants and Kutojanc (2004), or resort to
1788 spectral approximations of the generator of the diffusion process through manifold learning.
1789

1790 Manifold learning methods employ often the *diffusion maps* algorithm, introduced by Coiffman and
1791 colleagues Singer and Coifman (2008), to learn the dominant part of the spectrum of the transfer
1792 operator of the observed diffusion process Coifman et al. (2005); Nadler et al. (2006); Giannakis
1793 (2019); Ferguson et al. (2011); Talmor and Coifman (2015). In essence, these methods, learn
1794 from the data the few leading eigenfunctions of the Laplace–Beltrami operator that captures the
1795 Riemannian geometry of the observations, and consider them as a parametrisation of the manifold
1796 representing the invariant density.
1797

1798 **▷ Modelling SDEs from population level snapshots/boundary conditions.** With recent
1799 computational advances in optimal transport, a growing body of work focuses on the implementation
1800 of Schrödinger bridge sampling methods, including formulations with additional path constraints.
1801 These mostly generative methods aim to transport the data distribution from some initial boundary
1802 condition to a terminal one, typically by learning the underlying stochastic equation to perform this
1803 transport through Schrödinger bridge sampling (Lipman et al., 2022; Pooladian et al., 2023; Albergo
1804 et al., 2023; Albergo and Vanden-Eijnden, 2022). Flow matching (Lipman et al., 2022) identifies
1805 the probability flow ODE that pushes forward an initial Gaussian density to a target one by solving
1806 a regression problem. The method relies on analytically tractable probability paths that provide
1807 closed-form regression targets for learning the velocity field, resulting in simulation-free training of
1808 deterministic flows. However, the framework is restricted to Gaussian distributions since the em-
1809 ployed objective becomes intractable for general source distributions. Conditional flow matching
1810 (CFM) (Tong et al., 2023b) generalizes flow matching by introducing conditional probability paths
1811 between paired samples, allowing the marginal velocity field to be learned with regression without
1812 requiring explicit evaluation of the marginal densities or restrictive assumptions on the source distri-
1813 bution. Generalized Schrödinger Bridge Matching (GSBM) (Liu et al., 2023) follows an alternating
1814 optimisation scheme that learns both drift and marginals. Given prescribed boundary conditions
1815 for initial and terminal densities, the framework minimises a kinetic energy term, and formulates the
1816 resulting problem in terms of a stochastic optimal control problem conditioned on the boundary con-
1817 ditions and a path cost that accounts for additional constraints. Action matching (Neklyudov et al.,
1818 2023b) introduces a simulation-free variational objective that identifies a time-dependent scalar po-
1819 tential (entropic action) s_t , whose gradient ∇s_t transports the densities from the initial to the bound-
1820 ary condition through the continuity equation. In its entropic formulation the ∇s_t can be considered
1821 as the drift of the underlying SDE, whose marginals match the boundary conditions. However, by
1822 construction, the framework can recover only gradient drifts and is therefore not suitable for iden-
1823 tifying general stochastic systems with stationary probability currents. In contrast, simulation-free
1824 score and flow matching ([SF]² M) (Tong et al., 2023a) jointly learns the probability-flow ODE and
1825 the score function by regressing against closed-form quantities derived from conditional Brownian
1826 bridge paths, facilitating simulation-free identification of general Schrödinger bridge dynamics with
1827 non-gradient drifts.
1828

1829 **Geometry aware generative methods.** Metric flow matching (MFM) generalizes CFM by learn-
1830 ing interpolants that account for the geometry of the data. However, MFM does not assume a
1831 stochastic underlying process, as our framework does, only a deterministic interpolation (transport)
1832 that respects the data manifold. However, by assuming a specific noise amplitude for the underlying
1833 SDE, one can consider the flow field as generated by the effective drift of a probability flow ODE
1834 associated with the considered SDE and make inferences about the underlying drift function. This is
1835 the approach we followed when comparing the performance of MFM to our framework in Table 1.
1836

1837 **Approximating observation geometry in the ambient space.** In our work, we approximate the
1838 geometry induced by the observations by endowing the ambient space \mathcal{R}^d with an observation-
1839 dependent Riemannian metric $H(\mathbf{x})$ (Eq. 4) that encodes the local anisotropy of the data distribution.
1840

1836 In our framework this metric acts as a constraint for data-augmentation and as a geometric inductive
1837 bias for drift function inference: augmented paths are encouraged to remain in regions where the
1838 metric $H(\mathbf{x})$ induces smaller distances, i.e. in the vicinity of geodesics computed with respect to
1839 this metric, thereby aligning the augmented paths with the empirical observation geometry.

1840 This perspective connects to a growing body of work that **approximates Riemannian metrics di-**
1841 **rectly in the ambient space** as a proxy for the unknown curved low-dimensional data manifold,
1842 instead of first estimating its intrinsic dimensionality and then constructing explicit low-dimensional
1843 embeddings.

1844 In parallel, an increasing body of literature focuses on endowing generative models with geometric
1845 constraints or inductive biases. While most methods function in an autoencoder-like setting, by
1846 learning an embedding function for projecting to a lower dimensional space that respects prescribed
1847 or learned geometric constraints (Duque et al., 2022; Kalatzis et al., 2020; Arvanitidis et al., 2017)
1848 geometry, "Riemannian" methods, similar to our proposed method, operate in the ambient space by
1849 directly a Riemannian geometry embedded there and define normalizing flows or other generative
1850 processes directly on the manifold of interest. Mathieu and Nickel (2020) introduce a framework
1851 for continuous normalizing flows defined in the ambient space, respecting a prescribed Riemannian
1852 geometry. Similarly, De Bortoli et al. (2022) proposed a score-based generative model that models
1853 target densities with support on prescribed Riemannian manifolds in terms of a time-reversal of
1854 Langevin dynamics.

1855 Metric flow matching (Kapusniak et al., 2024) interpolates data distributions that respect the
1856 geodesic interpolants computed according to the metric induced by the observations. The method
1857 employs a data-adapted metric in the ambient space to design interpolants (geodesic curves) with low
1858 kinetic energy under the approximated geometry, and constrains the generative paths to respect man-
1859 ifold induced by the data samples. Our construction is conceptually similar with these approaches,
1860 in that we also avoid explicit low-dimensional embeddings and instead approximate the observa-
1861 tion manifold through a Riemannian metric living in the ambient space. However, in contrast to
1862 methods focused on deterministic transport or simulation-free matching, we use the learned metric
1863 to regularise continuous-time diffusion bridges and drift inference, through the stochastic controlled
1864 geometric augmentation, so that the recovered stochastic dynamics are geometrically consistent with
1865 the geometry of the observation-induced invariant measure.

1866 **Positioning of the present work.** Our approach combines the nonparametric flexibility of
1867 Gaussian-process-based drift inference from time-series data with recent geometric ideas for
1868 population-level SDE modelling. Similar to Metric Flow Matching (Kapusniak et al., 2024), we
1869 posit that augmented trajectories should remain on the manifold induced by the observations: both
1870 frameworks estimate a data-adapted Riemannian metric and construct interpolants (geodesics and
1871 bridges) that respect this geometry. MFM learns the underlying ODE necessary to transport an
1872 initial distribution to a target one under the data-adapted metric, while our framework assumes un-
1873 derlying stochastic dynamics. Nevertheless, once the diffusion is known or coarsely estimated, one
1874 can interpret the inferred ODE as a probability flow ODE and make inferences about the underlying
1875 drift function of a stochastic system. The GSBM framework (Liu et al., 2023) employs a stochastic
1876 control objective that is similar to the objective we consider for constructing the augmented paths.
1877 However, unlike our framework, GSBM does not introduce geometric constraints for the augmented
1878 paths. However, the path constraint they consider can be formulated with geometric consider-
1879 ations as we did in our comparisons here. Finally, whereas these methods typically learn a drift that
1880 transports a single source distribution to a single terminal snapshot, yielding thus a **locally valid**
1881 **dynamics**, our method, akin to multi-marginal bridge sampling (Shen et al., 2024), fits a sequence
1882 of bridges across multiple time points to recover a **single global drift** consistent with the underlying
1883 drift dynamics.

1884 F GEOMETRIC CONSTRAINTS ON INFERENCE

1885 Our method bridges the gap between approaches that rely only on the temporal structure of observa-
1886 tions and those that approximate the invariant density, while ignoring temporal order. Motivated by
1887 advances in geometric statistics (Miolane et al., 2020; Sommer, 2020), and the growing interest on
1888 the concept of manifold hypothesis (Fefferman et al., 2016; Shnitzer et al., 2020), i.e., the considera-

tion that the state of multi-dimensional dynamical systems often resides in low-dimensional regions of the state space, several recent methods integrate geometric and temporal constraints in stochastic system identification. In *Langevin regression* framework (Callaham et al., 2021), the Kramers-Moyal (KM) coefficients are estimated and low sampling effects are accounted for by solving an adjoint Fokker-Planck equation, with regularisation via moment matching (Lade, 2009). Tong et al. (2020) consider the manifold of the observations for inference of cellular dynamics. Their method employs dynamic optimal transport to interpolate between measured distributions constrained to lie in the vicinity of the observations. While sharing similar intuitions with our method, Tong et al. do not employ SDE modelling for inherently stochastic cellular dynamics and do not consider the underlying geometry of the observations, relying solely on constraints penalizing pairwise distances between them. Shnitzer et al. (Shnitzer et al., 2020; 2016) employ diffusion maps to approximate the eigenfunctions of the backward Kolmogorov operator (the generator of the stochastic Koopman operator (Giannakis, 2019; Črnjarić-Žic et al., 2020)). By evolving the dominant operator eigen-spectrum with a Kalman filter, they account for the temporal order of observations. However, their approach is limited to conservative systems and requires the presence of a spectral gap in the approximated operator's spectrum.

G THEORETICAL JUSTIFICATION FOR RIEMANNIAN MANIFOLD APPROXIMATION OF THE INVARIANT DENSITY

Our method is based on the argument that the invariant density² of the observed system imposes a low-dimensional structure on the state space, within which the observations are confined. We propose that this low-dimensional structure is well approximated by a Riemannian manifold $\mathcal{M}_\infty \in \mathcal{R}^{m \leq d}$ and that the observations $\{\mathcal{O}_k\}_{k=1}^K$ offer a reliable discrete approximation to \mathcal{M}_∞ .

We employ the notion of a "low-dimensional structure" as a concise way to refer to the fact that for many dissipative dynamical systems, the invariant measure has support on a subset of the state space with dimension smaller than the ambient space dimension. This phenomenon arises due to the dissipative nature of these systems, which causes volume contraction in the state space, resulting in trajectories concentrating asymptotically on attractors of lower dimension than the state space dimension. To provide further justification on this, in the following section, we start by building intuition from deterministic dynamical systems and then generalise to stochastic dynamics.

G.1 DIMENSIONALITY OF INVARIANT MEASURES INDUCED BY DETERMINISTIC DYNAMICS

We consider a dissipative deterministic dynamical system of the form

$$\dot{\mathbf{x}}_t = \mathbf{f}(\mathbf{x}_t), \quad \mathbf{x}_t \in \mathcal{R}^d, \quad (59)$$

generating a semiflow $(\Phi^t)_{t \geq 0}$. Under standard assumptions, the dynamics admit an invariant probability measure μ describing the distribution of states along long-term typical trajectories. From an ergodic perspective, μ is the natural object characterising the asymptotic behaviour of the system. For almost every initial condition in μ , the empirical measure

$$\frac{1}{T} \int_0^T \delta_{\mathbf{x}_t} dt \quad (60)$$

converges (in the weak sense) to μ .

For dissipative systems, phase-space volumes contract along typical trajectories, so the Lebesgue measure is not invariant under the dynamics, i.e. state space volume is not preserved when pushed forward through the flow (Ruelle, 1979). This implies that the system state does not explore the ambient space uniformly. Instead, trajectories concentrate asymptotically on subsets of state space of vanishing Lebesgue measure. In fact, this concentration phenomenon persists even in chaotic systems, where, although trajectories separate exponentially along unstable directions, contraction along stable directions dominates the evolution of infinitesimal volumes in the state space.

²In the following the discussion concentrates around invariant measures. We point out here that the invariant density is the Radon-Nikodym derivative of the invariant measure with respect to some reference measure, often the Lebesgue measure if it exists (Maharam, 1969).

1944 The resulting invariant measure μ typically has an **effective dimension** smaller than the ambient
 1945 space dimension. To quantify this, we require a notion of dimensionality that remains meaningful
 1946 when the Lebesgue measure vanishes. The Hausdorff dimension (Ruelle, 1989; Young, 2002;
 1947 Ott, 2002) lends itself for such a purpose since it naturally extends from sets to probability
 1948 measures (Young, 1982). More precisely, the Hausdorff dimension of an invariant measure μ is defined
 1949 as the smallest Hausdorff dimension among all measurable sets containing μ

$$\dim_H(\mu) = \inf \{ \dim_H(\mathcal{A}) : \mu(\mathcal{A}) = 1 \}. \quad (61)$$

1952 A useful aspect of this formulation is its local interpretation. Under mild regularity assumptions,
 1953 $\dim_H(\mu)$ can be characterised by the scaling of probability mass around typical points under μ . If,
 1954 for almost every \mathbf{x} ,

$$\mu(B_\varepsilon(\mathbf{x})) \sim \varepsilon^{d_\mu} \quad \text{as } \varepsilon \rightarrow 0, \quad (62)$$

1955 then $d_\mu = \dim_H(\mu)$. Thus, this dimension reflects how probability mass concentrates across scales.

1956 In (smooth) deterministic dynamical systems, the interplay between expansion and contraction along
 1957 different directions governs this local scaling behaviour. This is well characterised by Lyapunov exponents
 1958 that quantify the exponential deformation of infinitesimal neighbourhoods, while the metric
 1959 (Kolmogorov-Sinai) entropy h_μ quantifies the rate at which trajectories generate information. Well
 1960 known results in ergodic theory (Ledrappier and Young, 1985) show that the Hausdorff dimension
 1961 of an invariant measure can be expressed directly in terms of these quantities, and **is strictly smaller**
 1962 **than the ambient space dimension d in dissipative systems** with non-trivial Lyapunov exponents,
 1963 i.e. both positive and negative exponents.

1964 More precisely, according to the Oseledets' theorem (Oseledets, 1968), the system has a Lyapunov
 1965 spectrum $\lambda_1 \geq \dots \geq \lambda_d$, and dissipativity implies on average volume contraction, i.e.

$$\sum_{i=1}^d \lambda_i < 0. \quad (63)$$

1968 Ledrappier and Young (1985) formulate an expression for the Hausdorff dimension of the invariant
 1969 measure μ in terms of the Lyapunov exponents $\{\lambda_i\}_{i=1}^d$ and the Kolmogorov-Sinai entropy
 1970 h_μ (Bárány and Käenmäki, 2017)

$$\dim_H(\mu) = k + \frac{h_\mu - \sum_{i=1}^k \lambda_i}{|\lambda_{k+1}|}, \quad (64)$$

1971 where k is the largest integer for which $\sum_{i=1}^k \lambda_i \geq h_\mu$. This relation holds under standard smoothness
 1972 and hyperbolicity assumptions (for instance for $C^{1+\alpha}$ systems with non-zero Lyapunov exponents
 1973 almost everywhere). Intuitively, k here quantifies the number of expanding dimensions needed
 1974 to characterise the system's entropy.

1975 Since the sum of all Lyapunov exponents is negative (Eq. 63), and the metric entropy is bounded by
 1976 the sum of positive Lyapunov exponents (Ruelle, 1978)

$$0 \leq h_\mu \leq \sum_{\lambda_i > 0} \lambda_i, \quad (65)$$

1977 the equality of Eq. 64 implies

$$\dim_H(\mu) < d, \quad (66)$$

1978 indicating that the invariant measure concentrates on a subset of the state space, whose Hausdorff
 1979 dimension is strictly smaller than the ambient space dimension d .

1980 G.2 DIMENSIONALITY OF INVARIANT MEASURES INDUCED BY STOCHASTIC DYNAMICS

1981 We now consider stochastic dynamical systems of the form

$$d\mathbf{X}_t = \mathbf{f}(\mathbf{X}_t)dt + \sigma d\mathbf{W}_t, \quad (67)$$

1982 similar to the systems we discuss in the main text. Under mild conditions on \mathbf{f} and σ , the corresponding
 1983 Markov semigroup admits a unique invariant probability measure μ_σ , which coincides with the
 1984 stationary solution of the associated Fokker-Planck equation (Risken, 1996).

1998 The additive noise regularises the deterministic invariant measure, yet its density concentrates ex-
1999ponentially around \mathcal{A} as $\sigma \rightarrow 0$. For non-degenerate noise σ , the Hörmander condition ensures
2000 that μ_σ is absolutely continuous with respect to the Lebesgue measure, and thus possesses a *smooth*
2001 invariant density (Hörmander, 1967). However, the invariant measure μ_σ of the stochastic system of
2002 Eq. 67 satisfies the following exponential concentration inequality around the deterministic attractor
2003 **\mathcal{A} for sufficiently small noise amplitude σ**

2004

$$\mu_\sigma(\{x \in \mathcal{R}^d : \text{dist}(x, \mathcal{A}) > \delta\}) \leq C(\delta) \exp\left(-\frac{c(\delta)}{\sigma^2}\right), \quad (68)$$

2005

2006 for all $\delta > 0$, where $C(\delta), c(\delta) > 0$ denote δ -dependent constants, that are nevertheless independent
2007 of noise amplitude σ (see Theorem 4.2.1 (Kifer, 1988)). This exponential concentration indicates
2008 that, although μ_σ is absolutely continuous with respect to the Lebesgue measure for $\sigma > 0$, it
2009 becomes increasingly confined near \mathcal{A} as $\sigma \rightarrow 0$. The effective dimension of μ_σ approaches that
2010 of the invariant measure of the deterministic system μ_0 , while remaining bounded above by the
2011 ambient dimension d . (Kifer, 1988; Arnold, 2006).

2012 In this sense, stochasticity does not destroy the low-dimensional structure induced by the deter-
2013 ministic dynamics, but thickens the invariant measure around the deterministic attractor geometry.
2014 Thus even though μ_σ is smooth, its effective dimension can still be low-dimensional in the sense
2015 of mass being tightly concentrated near a lower-dimensional skeleton determined by the underlying
2016 stochastic dynamics.

2018
2019
2020
2021
2022
2023
2024
2025
2026
2027
2028
2029
2030
2031
2032
2033
2034
2035
2036
2037
2038
2039
2040
2041
2042
2043
2044
2045
2046
2047
2048
2049
2050
2051

2052
2053 **H THEORETICAL JUSTIFICATION OF GEOMETRIC AUGMENTATION FOR**
2054 **LARGE INTER-OBSERVATION INTERVALS**

2055
2056 In the following sections we provide a theoretical analysis justifying our choice to employ geometric
2057 path augmentation to improve inference in the large inter-observation limit. In particular, in Sec H.1,
2058 we revisit the fact that inference starting from the Euler-Maruyama discretisation deteriorates for
2059 increasing inter-observation interval. Then we study the terms in the remainder of the discretisation
2060 that become important when the time step (or inter-observation interval) is large, and connect these
2061 terms with the geometry of the unknown vector field. We show that for non-linear systems the
2062 remainder contains terms related to the curvature of the flow, and that neglecting these terms amounts
2063 to assuming a vector field with straight flow-lines in-between observations. This introduces a bias
2064 in inference that is linear in the step size. By approximating the curvature by means of controlled
2065 path augmentation with reference the geodesic curves of the invariant manifold, our method partially
2066 accounts for these remainder terms.

2067
2068 **H.1 INFERENCE PERFORMANCE DETERIORATES WITH INCREASING INTER-OBSERVATION**
2069 **INTERVAL FOR EXISTING FRAMEWORKS**

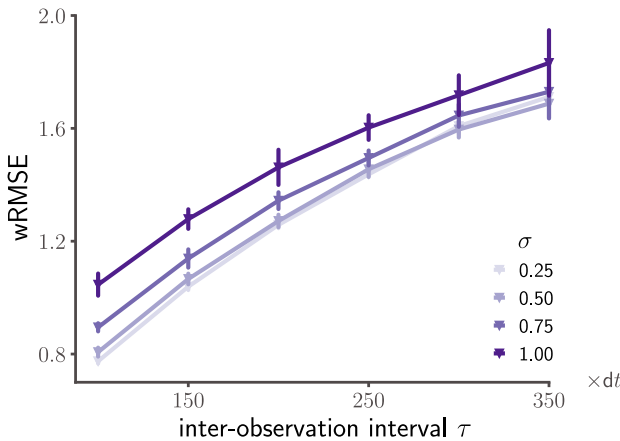


Figure 5

Increasing observation interval between successive observations τ deteriorates performance quantified by increasing weighted root mean squared error (wRMSE) for Gaussian process-based inference. Weighted root mean square error between estimated and ground truth drift vector fields for increasing observation interval τ between subsequent observations for different noise conditions (indicated by different hues). Observations were collected from a Van der Pol oscillator system simulated with $dt = 0.01$ for $T = 500$ time units. Error bars indicate one standard deviation over ten independent realizations.

2090
2091 We computed the weighted root mean square error (wRMSE) between ground truth flow fields
2092 and estimated ones for several commonly applied inference frameworks. We observed that the
2093 performance of all of them deteriorates once the inter-observation interval becomes large.

2094 We started with the method that motivated our research, approximating drift functions through Gaussian
2095 processes, the method outlined in Ruttor et al. (2013). The method approximates the drift
2096 functions with Gaussian process regression, using the system state \mathbf{X}_t as the regressor and state
2097 increments as the response variable $\mathbf{Y}_t \doteq \frac{\mathbf{x}_{t+\tau} - \mathbf{x}_t}{\tau}$. This is the Bayesian counterpart of earlier methods
2098 encountered in physics literature (Friedrich and Peinke, 1997; Ragwitz and Kantz, 2001), providing
2099 additionally uncertainty estimation through the Gaussian process approximation.

2100 As is evident from Figure 5 the discrepancy between ground truth and estimated vector fields
2101 increases for increasing temporal distance between successive observations. This should be under-
2102 stood, under the consideration that inference of the drift based on regression on state increments
2103 results from an approximation relying on a truncated Ito-Taylor expansion. This is also the starting
2104 point of the Euler Maruyama discretisation. As the time interval between successive steps of this
2105 approximation increases, the truncated approximation does not longer hold, and higher order terms
2106 should be considered.

2106 H.2 INference BASED ON EULER-MARUYAMA DISCRETISATION DOES NOT ACCOUNT FOR
 2107 THE CURVATURE OF THE TRAJECTORIES IN THE STATE SPACE
 2108

2109 To be more precise, a general SDE of the form

$$2110 \quad d\mathbf{X}_t = \mathbf{f}(\mathbf{X}_t, t)dt + \boldsymbol{\sigma}(\mathbf{X}_t, t)d\mathbf{W}_t. \quad (69)$$

2111 is a shorthand for the integral equation

$$2112 \quad \mathbf{X}_t = \mathbf{X}_{t_0} + \int_{t_0}^t \mathbf{f}(\mathbf{X}_s, s) ds + \int_{t_0}^t \boldsymbol{\sigma}(\mathbf{X}_s, s) d\mathbf{W}_s, \quad (70)$$

2115 where as previously in this manuscript, we consider the stochastic integrals in the **Itô sense**. (Here
 2116 we start from a more general formulation of the stochastic equation with both diffusion and drift
 2117 terms being state- and time-dependent to highlight that also for more general SDEs our geometric
 2118 argument is valid.)

2119 Applying the Itô formula on each integrand, and integrating from t_0 to t , we obtain the Itô-Taylor
 2120 expansion of Eq. 69

$$2121 \quad \mathbf{f}(\mathbf{X}_t, t) = \mathbf{f}(\mathbf{X}_{t_0}, t_0) + \int_{t_0}^t \frac{\partial \mathbf{f}(\mathbf{X}_s, s)}{\partial s} ds + \int_{t_0}^t \sum_u \frac{\partial \mathbf{f}(\mathbf{X}_s, s)}{\partial X^{(u)}} f_u(\mathbf{X}_s, s) ds \\ 2122 \quad + \int_{t_0}^t \sum_u \frac{\partial \mathbf{f}(\mathbf{X}_s, s)}{\partial X^{(u)}} [\boldsymbol{\sigma}(\mathbf{X}_s, s) d\mathbf{W}_s]_u + \int_{t_0}^t \frac{1}{2} \sum_{u,v} \frac{\partial^2 \mathbf{f}(\mathbf{X}_s, s)}{\partial X^{(u)} \partial X^{(v)}} [\boldsymbol{\sigma}(\mathbf{X}_s, s) \boldsymbol{\sigma}^\top(\mathbf{X}_s, s)]_{uv} ds \\ 2123 \quad = \mathbf{f}(\mathbf{X}_{t_0}, t_0) + \int_{t_0}^t \mathcal{L}_s^\dagger \mathbf{f}(\mathbf{X}_s, s) ds + \sum_\nu \int_{t_0}^t \mathcal{L}_{W,\nu} \mathbf{f}(\mathbf{X}_s, s) dW_s^{(\nu)}, \quad (71)$$

2126 and

$$2130 \quad \boldsymbol{\sigma}(\mathbf{X}_t, t) = \boldsymbol{\sigma}(\mathbf{X}_{t_0}, t_0) + \int_{t_0}^t \frac{\partial \boldsymbol{\sigma}(\mathbf{X}_s, s)}{\partial s} ds + \int_{t_0}^t \sum_u \frac{\partial \boldsymbol{\sigma}(\mathbf{X}_s, s)}{\partial X^{(u)}} f_u(\mathbf{X}_s, s) ds \\ 2132 \quad + \int_{t_0}^t \sum_u \frac{\partial \boldsymbol{\sigma}(\mathbf{X}_s, s)}{\partial X^{(u)}} [\boldsymbol{\sigma}(\mathbf{X}_s, s) d\mathbf{W}_s]_u + \int_{t_0}^t \frac{1}{2} \sum_{u,v} \frac{\partial^2 \boldsymbol{\sigma}(\mathbf{X}_s, s)}{\partial X^{(u)} \partial X^{(v)}} [\boldsymbol{\sigma}(\mathbf{X}_s, s) \boldsymbol{\sigma}^\top(\mathbf{X}_s, s)]_{uv} ds \\ 2134 \quad = \boldsymbol{\sigma}(\mathbf{X}_{t_0}, t_0) + \int_{t_0}^t \mathcal{L}_s^\dagger \boldsymbol{\sigma}(\mathbf{X}_s, s) ds + \sum_\nu \int_{t_0}^t \mathcal{L}_{W,\nu} \boldsymbol{\sigma}(\mathbf{X}_s, s) dW_s^{(\nu)}, \quad (72)$$

2138 where we have used the fact that the product of stochastic differentials due to the Ito isometry and
 2139 multiplication rules equals the noise covariance times the time step

$$2140 \quad dX_t^{(u)} dX_t^{(v)} = [\boldsymbol{\sigma} \boldsymbol{\sigma}^\top]_{uv} dt,$$

2141 where

$$2142 \quad dX_s^{(u)} = f_u ds + \sum_{j=1}^m \sigma_{uj} dW_s^{(j)},$$

2144 while the superscripts/subscripts u, v indicate dimensional components.

2145 In the above equations, we have introduced the operators acting on test-functions $\mathbf{h} : \mathcal{R}^D \rightarrow \mathcal{R}^D$

$$2147 \quad \mathcal{L}_t^\dagger \mathbf{h} = \frac{\partial \mathbf{h}}{\partial t} + \sum_u \frac{\partial \mathbf{h}}{\partial X^{(u)}} f_u + \frac{1}{2} \sum_{u,v} \frac{\partial^2 \mathbf{h}}{\partial X^{(u)} \partial X^{(v)}} [\boldsymbol{\sigma}(\mathbf{X}_s, s) \boldsymbol{\sigma}^\top(\mathbf{X}_s, s)]_{uv} \quad (73)$$

2149 and

$$2151 \quad \mathcal{L}_{W,v} \mathbf{h} = \sum_u \frac{\partial \mathbf{h}}{\partial X^{(u)}} \boldsymbol{\sigma}_{uv}, \quad \text{for } v = 1, \dots, n. \quad (74)$$

2153 With these expressions, the original integral equation for \mathbf{X}_t can be written as

$$2154 \quad \mathbf{X}_t = \mathbf{X}_{t_0} + \mathbf{f}(\mathbf{X}_{t_0}, t_0)(t - t_0) + \boldsymbol{\sigma}(\mathbf{X}_{t_0}, t_0)(\mathbf{W}_t - \mathbf{W}_{t_0}) + \quad (75)$$

$$2155 \quad R_1 = \begin{cases} + \int_{t_0}^t \int_{t_0}^s \mathcal{L}_u^\dagger \mathbf{f}(\mathbf{X}_u, u) du ds + \sum_\nu \int_{t_0}^t \int_{t_0}^s \mathcal{L}_{W,\nu} \mathbf{f}(\mathbf{X}_u, u) dW_u^{(\nu)} ds \\ + \int_{t_0}^t \int_{t_0}^s \mathcal{L}_u^\dagger \boldsymbol{\sigma}(\mathbf{X}_u, u) du d\mathbf{W}_s + \sum_\nu \int_{t_0}^t \int_{t_0}^s \mathcal{L}_{W,\nu} \boldsymbol{\sigma}(\mathbf{X}_u, u) dW_u^{(\nu)} d\mathbf{W}_s. \end{cases}$$

In the last equation, dropping the terms in the remainder R_1 results in the Euler–Maruyama integration scheme (Jentzen and Kloeden, 2011). Introducing the discrete time and noise increments

$$\Delta t_n = t_{n+1} - t_n = \int_{t_n}^{t_{n+1}} ds, \quad \Delta \mathbf{W}_n = \mathbf{W}_{t_{n+1}} - \mathbf{W}_{t_n} = \int_{t_n}^{t_{n+1}} d\mathbf{W}_s, \quad (76)$$

we result in the discrete time equation commonly used for numerical integration of SDEs

$$\mathbf{X}_{n+1} = \mathbf{X}_n + \mathbf{f}(\mathbf{X}_n, t_n) \Delta t_n + \boldsymbol{\sigma} \Delta \mathbf{W}_n. \quad (77)$$

This is also the starting point of most inference methods that employ the regression scheme mentioned above by approximating the drift as

$$\hat{\mathbf{f}}(\mathbf{X}_n, t_n) \approx \frac{\mathbf{X}_{n+1} - \mathbf{X}_n}{\Delta t} \sim \mathcal{N}\left(\mathbf{0}, \frac{\boldsymbol{\sigma} \boldsymbol{\sigma}^\top}{\Delta t}\right). \quad (78)$$

This discretisation is a zero-order approximation of the true dynamics, and assumes that $\mathbf{f}(\cdot)$ remains constant throughout the interval Δt , i.e. throughout the inter-observation interval τ in the inference setting. However as τ increases, higher-order terms in the remainder R_1 of the Itô–Taylor expansion become significant, since the assumption that the drift is approximately constant over τ does not hold.

We can glean onto the terms that become important once the inter-observation interval becomes large, by applying the Itô formula onto each one of the integrands in R_1 separately **for the specific setting we consider in this manuscript**, i.e. that of time-independent drift function $\mathbf{f}(\mathbf{x})$ and constant diffusion matrix $\boldsymbol{\sigma}$. In the following, we demonstrate that the leading-order error of this approximation is governed by the intrinsic geometry of the drift vector field. This provides further insight and a geometric explanation for the deterioration of inference methods for increasing inter-observation interval τ .

In short we show that, inference methods based on the Euler–Maruyama discretisation-based inference effectively assume that the vector field between consecutive observations \mathbf{X}_n and \mathbf{X}_{n+1} does not change. Our analysis shows this is equivalent to assuming trajectories are straight lines ($\mathbf{J}_f \mathbf{f} \parallel \mathbf{f}$) and the Itô correction is constant. In reality, trajectories curve ($\mathbf{J}_f \mathbf{f}$ has also a perpendicular component), and this curvature itself changes along the vector field. The Euler–Maruyama discretisation-based inference scheme systematically misses these higher-order geometric features, leading to biased drift estimates.

H.2.1 FIRST REMAINDER TERM $R_{1,a}$

We denote the first term of the reminder by $R_{1,a}$

$$R_{1,a} = \int_{t_0}^t \int_{t_0}^s \mathcal{L}_u^\dagger \mathbf{f}(\mathbf{X}_u) du ds. \quad (79)$$

Applying Itô’s formula to the integrand $\mathcal{L}_t^\dagger \mathbf{f}(\mathbf{X}_u, u)$, we get

$$d\mathcal{L}_u^\dagger \mathbf{f}(\mathbf{X}_u) = \frac{\partial}{\partial u} \mathcal{L}_u^\dagger \mathbf{f}(\mathbf{X}_u) du + \sum_{j=1}^d \frac{\partial \mathcal{L}_u^\dagger \mathbf{f}}{\partial X^{(j)}}(\mathbf{X}_u) dX_u^{(j)} + \frac{1}{2} \sum_{j,k=1}^d \frac{\partial^2 \mathcal{L}_u^\dagger \mathbf{f}}{\partial X^{(j)} \partial X^{(k)}}(\mathbf{X}_u) [\boldsymbol{\sigma} \boldsymbol{\sigma}^\top]_{jk} du. \quad (80)$$

Plugging in the original equation $dX_u^{(j)} = f_j du + \sum_{\nu=1}^m \sigma_{j\nu} dW_u^{(\nu)}$, and integrating over the time from t_0 to u

$$\begin{aligned} \mathcal{L}_u^\dagger \mathbf{f}(\mathbf{X}_u) &= \mathcal{L}_{t_0}^\dagger \mathbf{f}(\mathbf{X}_{t_0}) + \int_{t_0}^u \left(\frac{\partial}{\partial w} (\mathcal{L}_w^\dagger \mathbf{f}(\mathbf{X}_w)) + \sum_j \frac{\partial (\mathcal{L}_w^\dagger \mathbf{f})}{\partial X^{(j)}} f_j + \frac{1}{2} \sum_{j,k} \frac{\partial^2 (\mathcal{L}_w^\dagger \mathbf{f})}{\partial X^{(j)} \partial X^{(k)}} [\boldsymbol{\sigma} \boldsymbol{\sigma}^\top]_{jk} \right) dw \\ &\quad + \int_{t_0}^u \sum_j \frac{\partial (\mathcal{L}_w^\dagger \mathbf{f})}{\partial X^{(j)}} [\boldsymbol{\sigma} d\mathbf{W}_w]_j dw. \end{aligned} \quad (81)$$

2214 Applying Fubini's theorem in the original double integral, we change the order of integration
2215

$$2216 \int_{t_0}^t \int_{t_0}^s \phi(u) \, du \, ds = \int_{t_0}^t (t-u) \phi(u) \, du, \quad (82)$$

2217 and we obtain
2218

$$2219 \begin{aligned} 2220 R_{1,a} &= \int_{t_0}^t \int_{t_0}^s \mathcal{L}_u^\dagger \mathbf{f}(\mathbf{X}_u) \, du \, ds = \int_{t_0}^t (t-u) \left[\underbrace{\sum_j \frac{\partial \mathcal{L}_u^\dagger \mathbf{f}}{\partial X^{(j)}} f_j}_{R_{1,a}^1} + \underbrace{\frac{1}{2} \sum_{j,k} \frac{\partial^2 \mathcal{L}_u^\dagger \mathbf{f}}{\partial X^{(j)} \partial X^{(k)}} [\boldsymbol{\sigma} \boldsymbol{\sigma}^\top]_{jk}}_{R_{1,a}^2} \right] du \\ 2221 &\quad + \int_{t_0}^t (t-u) \underbrace{\sum_j \frac{\partial \mathcal{L}_u^\dagger \mathbf{f}}{\partial X^{(j)}} [\boldsymbol{\sigma} \, d\mathbf{W}_u]_j}_{R_{1,a}^3} + \frac{\tau^2}{2} \mathcal{L}_t^\dagger \mathbf{f}(\mathbf{X}_{t_0}). \end{aligned} \quad (83)$$

2230 In the previous equation we have dropped the term $\frac{\partial}{\partial w} (\mathcal{L}_w^\dagger \mathbf{f}(\mathbf{X}_w))$ that is equal to zero and that
2231 would require the drift \mathbf{f} to be time-dependent to be non-negligible.
2232

2233 **First component $R_{1,a}^1$ of remainder term $R_{1,a}$: Flow curvature term.** The Backward Kol-
2234 mogorov generator applied to a vector field \mathbf{f} can be written as

$$2235 \mathcal{L}^\dagger \mathbf{f} = \mathbf{J}_f \mathbf{f} + \frac{1}{2} \Delta_D \mathbf{f}. \quad (84)$$

2237 In Eq. 84, $\mathbf{J}_f \doteq \nabla \mathbf{f}$ denotes the Jacobian of \mathbf{f} , $\mathbf{D} \doteq \boldsymbol{\sigma} \boldsymbol{\sigma}^\top$ the noise covariance, and
2238 $\Delta_D \doteq \sum_{j,k} \mathbf{D}_{jk} \frac{\partial^2}{\partial X^{(j)} \partial X^{(k)}}$ is the noise-covariance weighted Laplacian operator. Thus each component
2239 of $\mathcal{L}^\dagger \mathbf{f}$ comprises the directional derivative of the drift $\mathbf{J}_f \mathbf{f}$ plus an anisotropic/noise-covariance
2240 weighted Laplacian of \mathbf{f} , which in component-wise form is expressed as
2241

$$2242 [\mathcal{L}^\dagger \mathbf{f}]_i = \sum_k \frac{\partial f_i}{\partial X^{(k)}} f_k + \frac{1}{2} \sum_{k,\ell} \mathbf{D}_{k\ell} \frac{\partial^2 f_i}{\partial X^{(k)} \partial X^{(\ell)}}. \quad (85)$$

2245 Differentiating wrt to $X^{(j)}$ yields
2246

$$2247 \frac{\partial}{\partial X^{(j)}} [\mathcal{L}^\dagger \mathbf{f}]_i = \sum_k \frac{\partial^2 f_i}{\partial X^{(j)} \partial X^{(k)}} f_k + \sum_k \frac{\partial f_i}{\partial X^{(k)}} \frac{\partial f_k}{\partial X^{(j)}} + \frac{1}{2} \sum_{k,\ell} \mathbf{D}_{k\ell} \frac{\partial^3 f_i}{\partial X^{(j)} \partial X^{(k)} \partial X^{(\ell)}}, \quad (86)$$

2250 and thus we rewrite the i -th component of the term $R_{1,a}^1$ as
2251

$$2252 [R_{1,a}^1]_i = \int_{t_0}^t (t-u) \left[\sum_{j,k} \frac{\partial^2 f_i}{\partial X^{(j)} \partial X^{(k)}} f_k f_j + \sum_{j,k} \frac{\partial f_i}{\partial X^{(k)}} \frac{\partial f_k}{\partial X^{(j)}} f_j + \frac{1}{2} \sum_{j,k,\ell} \mathbf{D}_{k\ell} \frac{\partial^3 f_i}{\partial X^{(j)} \partial X^{(k)} \partial X^{(\ell)}} f_j \right] du. \quad (87)$$

2256 The third-order state-derivative in the last summand of Eq. 87, indicates that this last term is inactive
2257 for linear or quadratic drift functions \mathbf{f} .
2258

2259 We re-write again this part of the remainder in a more compact vector notation in terms of the
2260 directional derivative of $(\mathbf{J}_f \mathbf{f})$ and $\frac{1}{2} \Delta_D \mathbf{f}$ along the vector field as
2261

$$2262 R_{1,a}^1 = \int_{t_0}^t (t-u) \left[\underbrace{\nabla(\mathbf{J}_f \mathbf{f}) \cdot \mathbf{f}}_{\text{flow curvature}} + \underbrace{\nabla\left(\frac{1}{2} \Delta_D \mathbf{f}\right) \cdot \mathbf{f}}_{\text{diffusive term along the flow}} \right] du. \quad (88)$$

2264 This part of the remainder captures two geometric effects that standard inference methods neglect:
2265 the **intrinsic curvature of deterministic flow trajectories in state space**, and the **systematic bias**
2266 **introduced by the spatial variation of both drift and diffusion** along these trajectories, when both
2267 drift and diffusion are assumed as constant between inter-observation intervals.

2268 • To understand the **first term**, $\nabla(\mathbf{J}_f \mathbf{f}) \cdot \mathbf{f}$, from a geometric perspective, let us consider a
 2269 deterministic dynamical system with dynamics $\dot{\mathbf{x}}_t = \mathbf{f}(\mathbf{x}_t)$. A trajectory initiated from an
 2270 initial condition \mathbf{x}_0 traces a streamline in the state space \mathcal{R}^d . We express the acceleration
 2271 of this trajectory in terms of the directional derivative

2272
$$\ddot{\mathbf{x}}_t = \frac{d}{dt} \mathbf{f}(\mathbf{x}_t) = \mathbf{J}_f(\mathbf{x}_t) \cdot \mathbf{f}(\mathbf{x}_t) = \mathbf{J}_f \cdot \mathbf{f}. \quad (89)$$

2273 The acceleration vector admits a natural orthogonal decomposition comprising a component
 2274 parallel to the vector field \mathbf{f} and an orthogonal component to \mathbf{f}

2275
$$\mathbf{J}_f \cdot \mathbf{f} = P_{\parallel}(\mathbf{f}) \mathbf{J}_f \cdot \mathbf{f} + P_{\perp}(\mathbf{f}) \mathbf{J}_f \cdot \mathbf{f}. \quad (90)$$

2276 Here $P_{\parallel}(\mathbf{f}(\mathbf{x})) = \frac{\mathbf{f}(\mathbf{x})\mathbf{f}^T(\mathbf{x})}{\|\mathbf{f}(\mathbf{x})\|^2}$ and $P_{\perp}(\mathbf{f}(\mathbf{x})) = \mathbb{I} - P_{\parallel}(\mathbf{f}(\mathbf{x}))$ stand for the parallel and orthogonal
 2277 projectors. The parallel component quantifies the rate of change of speed along the
 2278 trajectory (tangential acceleration), whilst the perpendicular component defines the **curva-**
 2279 **ture vector** $\kappa_{\text{flow}}(\mathbf{x})$ (Kühnel, 2002), which quantifies the bending of the trajectories

2280
$$\kappa_{\text{flow}}(\mathbf{x}) = \frac{P_{\perp}(\mathbf{f}(\mathbf{x}))\mathbf{J}_f(\mathbf{x})\mathbf{f}(\mathbf{x})}{\|\mathbf{f}(\mathbf{x})\|^2}. \quad (91)$$

2281 When $\kappa_{\text{flow}} = 0$, the trajectories are straight lines in the state space, while when
 2282 $\|\kappa_{\text{flow}}\| > 0$ they are curved.

2283 The term $\nabla(\mathbf{J}_f \mathbf{f}) \cdot \mathbf{f}$ quantifies the **evolution of the trajectory curvature**³ as the system
 2284 moves along the flow field. From Eq. 87 we have for each dimensional component i of this
 2285 term

2286
$$\begin{aligned} [\nabla(\mathbf{J}_f \mathbf{f}) \cdot \mathbf{f}]_i &= \sum_{j,k} \frac{\partial^2 f_i}{\partial X^{(j)} \partial X^{(k)}} f_k f_j + \sum_{j,k} \frac{\partial f_i}{\partial X^{(k)}} \frac{\partial f_k}{\partial X^{(j)}} f_j \\ &= [\mathbf{f}^T(\nabla^2 f_i)\mathbf{f}] + [\mathbf{J}_f^2 \mathbf{f}]_i. \end{aligned} \quad (92)$$

2287 We observe that this term captures the effects of how both second-order spatial variation of
 2288 the flow field (the Hessian $\nabla^2 f_i$) and the Jacobian of the acceleration ($\mathbf{J}_f^2 \mathbf{f}$) influence the
 2289 evolution of trajectories.

2290 – In Eq. 92, the **first sub-term**, $\mathbf{f}^T(\nabla^2 f_i)\mathbf{f}$, represents the **second directional derivative**
 2291 (or quadratic variation) of f_i along the flow direction \mathbf{f} . It measures the curvature
 2292 or second-order spatial variation of the i -th component of \mathbf{f} in the direction \mathbf{f} . In re-
 2293 gions where the Hessian $\nabla^2 \mathbf{f}$ is large (as is for the case of a highly nonlinear drift
 2294 with curving or bending behaviour), this term becomes significant, and it vanishes for
 2295 linear or constant drift \mathbf{f} . Neglecting this term corresponds to approximating the flow
 2296 by its linearisation.

2297 – The **second sub-term**, $\mathbf{J}_f^2 \mathbf{f} = \mathbf{J}_f(\mathbf{J}_f \mathbf{f})$, of Eq. 92 represents the action of the Ja-
 2298 cobian operator on the acceleration vector. Geometrically, it describes how the local
 2299 linearised field acts on the acceleration as we move an infinitesimal step along the flow
 2300 field, or in other words how the linear approximation changes when following the flow
 2301 direction \mathbf{f} .

2302 By temporal integration we have

2303
$$R_{1,a}^1 = \int_{t_0}^t (t-u) \left(\nabla(\mathbf{J}_f \mathbf{f}) \cdot \mathbf{f} + \nabla\left(\frac{1}{2} \Delta_D \mathbf{f}\right) \cdot \mathbf{f} \right) du \sim \frac{\tau^2}{2} \left(\nabla(\mathbf{J}_f \mathbf{f}) \cdot \mathbf{f} + \nabla\left(\frac{1}{2} \Delta_D \mathbf{f}\right) \cdot \mathbf{f} \right), \quad (93)$$

2304 indicating that the evolution of trajectory curvature introduces an $O(\tau^2)$ correction to the
 2305 transition density.

2306 Drift inference based on Euler–Maruyama–type discretisation ignores between others the
 2307 term $R_{1,a}^1$ introducing thereby a mean bias at each point \mathbf{x} in the state space,

2308
$$\beta_{1,a}^1(\mathbf{x}) = \frac{1}{\tau} R_{1,a}^1 \approx \frac{\tau}{2} [\nabla(\mathbf{J}_f \mathbf{f}) \cdot \mathbf{f} + \nabla\left(\frac{1}{2} \Delta_D \mathbf{f}\right) \cdot \mathbf{f}](\mathbf{x}). \quad (94)$$

2309 ³More precisely the directional derivative of the acceleration, $\mathbf{J}_f(\mathbf{x}) \cdot \mathbf{f}$ along the flow direction, or the **rate**
 2310 **at which the acceleration changes along the flow, or a measure of how the local curvature of \mathbf{f} as a vector**
 2311 **field influences trajectory evolution.**

This bias induces a mean error in drift estimate, when using Euler–Maruyama-based inference, leading to under- or over-estimation of the true drift at state \mathbf{x} . This error scales linearly with the interval τ .

Let us now consider the temporal rate of change experienced by a particle travelling along the flow field. The instantaneous speed of the particle at location \mathbf{x} is $\|\mathbf{f}(\mathbf{x})\|$. The quantity in the brackets in Eq. 94, $\nabla(\mathbf{J}_f \mathbf{f}) \cdot \mathbf{f} + \nabla(\frac{1}{2} \Delta_D \mathbf{f}) \cdot \mathbf{f}$, is a spatial derivative measuring how quickly the curvature and diffusion variation change as the particle moves in space. The rate of change of this variation per unit of time is expressed as

$$\frac{\|\nabla(\mathbf{J}_f \mathbf{f}) \cdot \mathbf{f} + \nabla(\frac{1}{2} \Delta_D \mathbf{f}) \cdot \mathbf{f}\|(\mathbf{x})}{\|\mathbf{f}(\mathbf{x})\|} \doteq \tau_{\text{curv}}^{-1}(\mathbf{x}). \quad (95)$$

In the last equation we have introduced the time scale of change τ_{curv} as the inverse of the rate of change, which captures the characteristic time it takes for the curvature/diffusion variation to change significantly along the particles trajectory. Then the relative magnitude error in the Euler–Maruyama-based drift estimate satisfies

$$\frac{\|\beta_{1,a}^1(\mathbf{x})\|}{\|\mathbf{f}(\mathbf{x})\|} = \frac{\tau}{2 \tau_{\text{curv}}(\mathbf{x})}, \quad (96)$$

implying that the estimate is reliable only when the inter-observation interval $\tau \ll 2 \tau_{\text{curv}}(\mathbf{x})$.

- The **second term** in Eq. 88, $\nabla(\frac{1}{2} \Delta_D \mathbf{f}) \cdot \mathbf{f}$, accounts for the diffusion part of the backward generator acting on the vector field \mathbf{f} . The anisotropic Laplacian $\Delta_D \mathbf{f}$ quantifies the **diffusion–weighted second-order spatial variation of the vector field**

$$[\Delta_D \mathbf{f}]_i = \sum_{j,k} D_{jk} \frac{\partial^2 f_i}{\partial X^{(j)} \partial X^{(k)}} = \nabla \cdot (\mathbf{D} \nabla f_i). \quad (97)$$

The directional derivative quantifies how this term evolves along the flow field

$$[\nabla(\frac{1}{2} \Delta_D \mathbf{f}) \cdot \mathbf{f}]_i = \frac{1}{2} \sum_{j,k,\ell} D_{k\ell} \frac{\partial^3 f_i}{\partial X^{(j)} \partial X^{(k)} \partial X^{(\ell)}} f_j. \quad (98)$$

This term captures how the diffusion-weighted spatial variation of the flow field varies across the state space. As trajectories traverse regions of varying drift curvature, the effective Itô correction itself changes, introducing systematic bias in inference methods that assume that drift is piece-wise constant in-between observations.

Second component $R_{1,a}^2$ of remainder term $R_{1,a}$. The second component of the remainder term $R_{1,a}$ reads

$$R_{1,a}^2 = \int_{t_0}^t (t-u) \frac{1}{2} \sum_{j,k} \frac{\partial^2 (\mathcal{L}_u^\dagger \mathbf{f})}{\partial X^{(j)} \partial X^{(k)}} [\boldsymbol{\sigma} \boldsymbol{\sigma}^\top]_{jk} du. \quad (99)$$

For the i -th dimensional component we have

$$\begin{aligned} \frac{\partial^2}{\partial X^{(h)} \partial X^{(j)}} [\mathcal{L}_u^\dagger f]_i &= \sum_k \frac{\partial^3 f_i}{\partial X^{(h)} \partial X^{(j)} \partial X^{(k)}} f_k + \sum_k \frac{\partial^2 f_i}{\partial X^{(j)} \partial X^{(k)}} \frac{\partial f_k}{\partial X^{(h)}} \\ &\quad + \sum_k \frac{\partial^2 f_i}{\partial X^{(h)} \partial X^{(k)}} \frac{\partial f_k}{\partial X^{(j)}} + \sum_k \frac{\partial f_i}{\partial X^{(k)}} \frac{\partial^2 f_k}{\partial X^{(h)} \partial X^{(j)}} \\ &\quad + \frac{1}{2} \sum_{k,\ell} \mathbf{D}_{k\ell} \frac{\partial^4 f_i}{\partial X^{(h)} \partial X^{(j)} \partial X^{(k)} \partial X^{(\ell)}}. \end{aligned} \quad (100)$$

For this remainder term, we have for each dimensional component i

$$[R_{1,a}^2]_i = \int_{t_0}^t (t-u) \frac{1}{2} \sum_{j,k} \mathbf{D}_{jk} \left[\frac{\partial^2}{\partial X^{(k)} \partial X^{(j)}} [\mathcal{L}_u^\dagger \mathbf{f}]_i \right] du. \quad (101)$$

2376 Geometrically, $R_{1,a}^2$ captures the **diffusion-weighted second-order spatial variation** of the gen-
 2377 erator $\mathcal{L}_u^\dagger \mathbf{f}$ across the $\sqrt{\tau}$ -sized ellipsoid set by \mathbf{D} , i.e. the anisotropic Laplacian $\Delta_D(\mathcal{L}_u^\dagger \mathbf{f})$,
 2378 the diffusion-weighted second spatial variation of the drift along the flow. Dropping this term
 2379 in inference amounts to assuming $\mathcal{L}_u^\dagger \mathbf{f}$ is locally flat and results in an $O(\tau)$ drift bias of size
 2380 $\beta_{1,a}^2 \approx (\tau/4) \Delta_D(\mathcal{L}_u^\dagger \mathbf{f})$, underestimating anisotropy and the evolution of curvature of the flow
 2381 field, so inferred flow-lines appear too straight.

2382
 2383 **Third component $R_{1,a}^3$ of remainder term $R_{1,a}$.**
 2384

2385
$$R_{1,a}^3 = \int_{t_0}^t (t-u) \sum_j \frac{\partial \mathcal{L}_u^\dagger \mathbf{f}}{\partial X^{(j)}} [\sigma \, d\mathbf{W}_u]_j, \quad (102)$$

 2386
 2387

2388
 2389
$$[R_{1,a}^3]_i = \int_{t_0}^t (t-u) \sum_{j,m} \frac{\partial}{\partial X^{(j)}} [\mathcal{L}_u^\dagger \mathbf{f}]_i \sigma_{jm} d\mathbf{W}_u^{(m)}, \quad (103)$$

 2390
 2391

2392 This is a martingale term capturing the stochastic coupling between diffusion and the spatial inhomoge-
 2393 neity of the generator. In inference, this term doesn't introduce bias, since $\langle R_{1,a}^3 \rangle = 0$. However,
 2394 neglecting this term, ignores a second-order variance contribution with $\text{Var}(R_{1,a}^3/\tau) = O(\tau)$.
 2395
 2396

2397 H.2.2 SECOND REMAINDER TERM $R_{1,b}$

2398 We denote the second term of the reminder by $R_{1,b}$

2399
 2400
$$R_{1,b} = \sum_{\nu=1}^n \int_{t_0}^t \int_{t_0}^s \mathcal{L}_{W,\nu} \mathbf{f} dW_u^{(\nu)} ds. \quad (104)$$

 2401
 2402

2403 Applying Fubini's theorem again to change the order of integration, we re-write $R_{1,b}$ in the form of
 2404 a stochastic integral

2405
$$R_{1,b} = \sum_{\nu=1}^n \int_{t_0}^t (t-u) \mathcal{L}_{W,\nu} \mathbf{f} dW_u^{(\nu)}. \quad (105)$$

 2406
 2407

2408 Substituting the operator results in an expression for each dimensional component i

2409
 2410
$$[R_{1,b}]_i = \sum_{\nu=1}^n \int_{t_0}^t (t-u) \left(\sum_{j=1}^D \frac{\partial f_i}{\partial X^{(j)}} \sigma_{j\nu} \right) dW_u^{(\nu)}, \quad \text{for } i = 1, \dots, D. \quad (106)$$

 2411
 2412

2413 In matrix notation, this corresponds to

2414
 2415
$$R_{1,b} = \int_{t_0}^t (t-u) \mathbf{J}_f \boldsymbol{\sigma} d\mathbf{W}_u. \quad (107)$$

 2416
 2417

2418 The remainder $R_{1,b}$ is a stochastic integral with zero mean, but non-zero covariance, given by
 2419

2420
 2421
$$\text{Cov}(R_{1,b}) = \langle R_{1,b} R_{1,b}^\top \rangle = \int_{t_0}^t (t-u)^2 \mathbf{J}_f \boldsymbol{\sigma} \boldsymbol{\sigma}^\top \mathbf{J}_f^\top du. \quad (108)$$

 2422
 2423

2424 For sufficiently smooth \mathbf{J}_f and small time step $\tau = t - t_0$, this covariance scales on the order of τ^3 .
 2425

2426 The term $R_{1,b}$ quantifies the contribution to the remainder arising from stochastic fluctuations of
 2427 the noise acting through the spatial derivatives of the drift \mathbf{f} . It does not contribute to additional
 2428 systematic bias, but introduces variance in the drift estimator, especially when $\boldsymbol{\sigma}$ or \mathbf{J}_f are large.
 2429

2430 H.2.3 THIRD REMAINDER TERM $R_{1,c}$
 2431

2432 We denote the third remainder term by $R_{1,c}$ and re-write here for convenience
 2433

2434
$$R_{1,c} = \int_{t_0}^t \int_{t_0}^s \mathcal{L}_u^\dagger \boldsymbol{\sigma}(\mathbf{X}_u, u) du d\mathbf{W}_s. \quad (109)$$

 2435

2436 In the general case of time- and state- dependent diffusion the integrand of this term would be
 2437 expressed for the i -th row and ℓ -th column component of $\boldsymbol{\sigma}$ as follows
 2438

2439
$$[\mathcal{L}_u^\dagger \boldsymbol{\sigma}(\mathbf{X}_u, u)]_{i\ell} = \frac{\partial}{\partial u} \sigma_{i\ell}(\mathbf{X}_u, u) + \sum_{j=1}^D \frac{\partial \sigma_{i\ell}}{\partial X^{(j)}}(\mathbf{X}_u, u) f_j(\mathbf{X}_u, u) \quad (110)$$

 2440

2441
$$+ \frac{1}{2} \sum_{j,k=1}^D \frac{\partial^2 \sigma_{i\ell}}{\partial X^{(j)} \partial X^{(k)}}(\mathbf{X}_u, u) [\boldsymbol{\sigma} \boldsymbol{\sigma}^\top]_{jk}(\mathbf{X}_u, u). \quad (111)$$

 2442

2443 However, in our setting we consider state- and time-independent diffusion matrix, and thus
 2444 $\mathcal{L}_u^\dagger \boldsymbol{\sigma}(\mathbf{X}_u, u) = \mathbf{0}$, and by consequence $R_{1,c} = \mathbf{0}$
 2445

2446 H.2.4 FOURTH REMAINDER TERM $R_{1,d}$
 2447

2448 The fourth remainder term is
 2449

2450
$$R_{1,d} = \sum_{\nu=1}^n \int_{t_0}^t \int_{t_0}^s \mathcal{L}_{W,\nu} \boldsymbol{\sigma} dW_u^{(\nu)} d\mathbf{W}_s. \quad (112)$$

 2451

2452 For each component (i, ℓ) of $\boldsymbol{\sigma}$
 2453

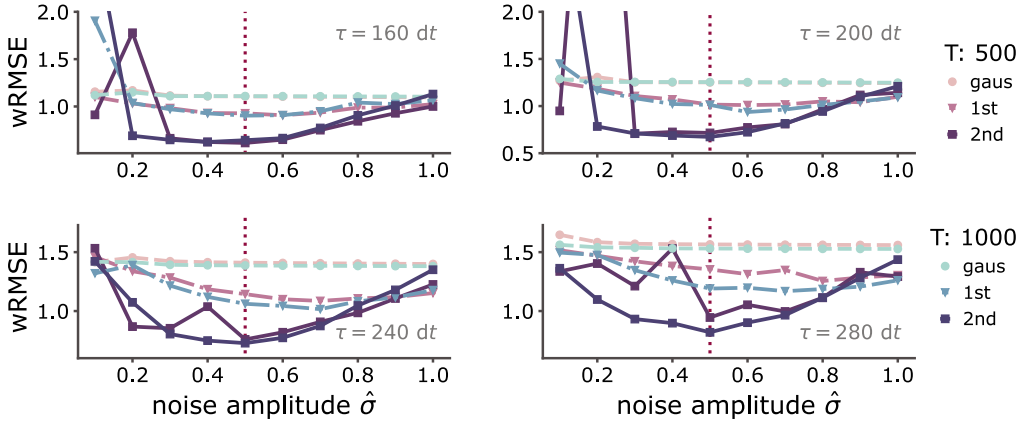
2454
$$[\mathcal{L}_{W,\nu} \boldsymbol{\sigma}]_{i\ell} = \sum_{j=1}^D \frac{\partial \sigma_{i\ell}}{\partial X^{(j)}} \sigma_{j\nu} = \mathbf{0}. \quad (113)$$

 2455

2456 Thus, the omission of this remainder term does contribute any bias or variance to the EuM-based
 2457 drift estimator.
 2458

2459
 2460
 2461
 2462
 2463
 2464
 2465
 2466
 2467
 2468
 2469
 2470
 2471
 2472
 2473
 2474
 2475
 2476
 2477
 2478
 2479
 2480
 2481
 2482
 2483

2484 I ADDITIONAL NUMERICAL RESULTS
2485

2486 I.1 INFERENCE WITH NOISE MISS-ESTIMATION
2487

2503 **Figure 6**

2504 **Small noise misestimation has small impact on estimation accuracy.** Weighted root mean
2505 square error (wRMSE) vs. noise amplitude σ employed in the augmentation for different inter-
2506 observation intervals with a.) $\tau = 160 \text{ dt}$ b.) $\tau = 200 \text{ dt}$, c.) $\tau = 240 \text{ dt}$ d.) $\tau = 280 \text{ dt}$.
2507 Pink-purple lines correspond to estimation with total simulation length $T = 500$ time units,
2508 and blue markers correspond to total simulation length of $T = 1000$ time units. Red dotted line
2509 identifies the noise amplitude employed in the simulation of the observations.

2510
2511 I.2 ABLATIONS WITH RESPECT TO METRIC LEARNING ALGORITHM
2512

2513 To probe the robustness of our framework, when we employ a different approach to estimate the
2514 metric, following (Kapusiak et al., 2024) we tested our method when we employ a radial based
2515 function approximation to estimate the diagonal metric, similar to Arvanitidis et al. (2017). In the
2516 table 1 we report the performance of our method when we employ the locally adaptive normal
2517 distribution framework (Geometric (our)) for approximation the metric Arvanitidis et al. (2019)
2518 and when we employ the radial basis function variant of the metric approximation (Geometric_{RBF}
2519 (our)) for the Van der Pol system for different inter-observation intervals and noise conditions. We
2520 observe that the resulting drift is accurate also with the RBF method for estimating the metric, yet
2521 the method proposed in the main text performs slight better across all inter-observation intervals and
2522 noise conditions.

2523 J DETAILS ON NUMERICAL EXPERIMENTS
2524

2525 We simulated a two dimensional Van der Pol oscillator with drift function

2526
$$f_1(x, y) = \mu(x - \frac{1}{3}x^3 - y) \quad (114)$$

2527
$$f_2(x, y) = \frac{1}{\mu}x, \quad (115)$$

2528 starting from initial condition $x_0 = [1.81, -1.41]$ and under noise amplitudes $\sigma = \{0.25, 0.50, 0.75, 1.00\}$ for total duration of $T = \{500, 1000\}$ time units. The employed inter-
2529 observation intervals $\tau = \{80, 120, 160, 200, 240, 280, 320\} \times dt$. The last inter-observation interval
2530 exceeds the half period of the oscillator and thus samples only a single state per period. This resulted
2531 in erroneous estimates. In this setting this indicates the upper limit of τ for which we can provide
2532 estimates. However for any inference method, if the observation process samples only one observa-
2533 tion per period, identifying the underlying force field without additional assumptions is not possible

with temporal methods. The discretisation time-step used for simulation of the ground truth dynamics, and path augmentation $\delta t = 0.01$. For sampling the controlled bridges we employed $N = 100$ particles evolving the associated ordinary differential equation as described in (Maoutsa and Opper, 2022). The logarithmic gradient estimator used $M = 40$ inducing points. The sparse Gaussian process for estimating the drift was based on a sparse kernel approximation of $S = 300$ points. In the presented simulation we have employed a weighting parameter $\beta = 0.5$ (Eq. 37). This provides a moderate pull towards the invariant density. The example in Figure 2 was constructed with $\beta = 1$ and provides a better approximation of the transition density, than $\beta = 0.5$.

For the **out-of-equilibrium process** with harmonic trapping and circulation and a Gaussian repulsive obstacle in the centre we followed the description presented in Frishman and Ronceray (2020) following the drift

$$f_\mu(\mathbf{x}) = -\Omega_{\mu\nu}x_\nu + \alpha e^{-x^2/2\sigma^2}x_\mu \quad \text{with} \quad \Omega = \begin{pmatrix} 2 & 2 \\ -2 & 2 \end{pmatrix}, \quad (116)$$

for $\alpha = 10$ and simulated the stochastic system with noise amplitude $\sigma = 0.5$ on a time grid of $dt = 0.01$ steps, observed at inter-observation intervals $\tau = \{150, 200, 250\} \times dt$ and for total duration $T = 1000$ time units.

For the **Hopf system** we used the drift

$$f_1(x_1, x_2) = z_2, \quad (117)$$

$$f_2(x_1, x_2) = -z_1 + (\mu - z_1^2)z_2, \quad (118)$$

with $\mu = 0.35$ and integrated the system with noise amplitude $\sigma = 0.15$ on a timegrid with $dt = 0.01$ resolution, observed at $\tau = \{200, 300, 400\} \times dt$ time intervals. This is the normal form of the Hopf bifurcation.

For the **Selkov glycolysis model** (Selkov, 1968) we employed the drift

$$f_1(x_1, x_2) = -x_1 + \alpha x_2 + x_1^2 x_2, \quad (119)$$

$$f_2(x_1, x_2) = 0.6 - \alpha x_2 - x_1^2 x_2, \quad (120)$$

with $\alpha = 0.06$ and noise amplitude $\sigma = 0.05$ for inter-observation intervals $\tau = \{100, 200\} \times dt$ and simulation time grid of $dt = 0.01$ spacing and for total duration $T = 1000$ time units.

This model is a minimal two-variable model of glycolytic oscillations, first introduced in (Selkov, 1968). It describes the autocatalytic feedback processes in the glycolysis pathway, focusing on how simple nonlinear interactions can give rise to oscillatory dynamics in concentrations of intermediates. The first state variable x_1 represents the concentration of adenosine diphosphate, while x_2 represents the concentration of a glycolytic intermediate.

J.1 ON COMPUTATION OF GEODESIC CURVES

For the computation of geodesic curves we followed the framework introduced in (Arvanitidis et al., 2019). The geodesic equation relies on a non-parametric estimation of the Riemannian metric, which is constructed using kernel-weighted local diagonal covariances, and has computational complexity $\mathcal{O}(ND)$, where D is the dimensionality of the problem and N denotes the number of samples. The computational cost of solving the geodesic equation scales sublinearly with increasing dimensionality.

J.2 DETAILS ON BASELINE METHODS

We compared the performance of our method against a series of competing methods for inference of stochastic dynamics. In particular, we compared our method against methods specifically designed for inference of stochastic systems from single trajectories, and against systems that infer population dynamics.

We employed the following methods that assume single trajectories for drift inference:

1. Gaussian process regression without state estimation (**GP**)

2592 2. path augmentation with Ornstein-Uhlenbeck dynamics with Gaussian process inference
 2593 (OU) (Batz et al., 2018)
 2594 3. sparse variational inference with state estimation (SVISE) (Course and Nair, 2023a)
 2595 4. basis function approximation of Kramers-Moyal coefficients, i.e. the drift function (KM-
 2596 basis) (Nabeel et al., 2025)
 2597 5. latent SDE inference with amortized reparameterization with (LatentSDE+GP-pre) and
 2598 without pre-training (LatentSDE) (Course and Nair, 2023b).

2600 We further compared our method with recent Schrödinger bridge generating frameworks that
 2601 primary aim to infer population dynamics from snapshot data. In particular we considered the following
 2602 frameworks:

2603 I. Metric Flow Matching (MFM) (Kapusniak et al., 2024)
 2604 II. Generalized Schrödinger Bridge Matching (GSBM) (Liu et al., 2023)
 2605 III. Wasserstein Lagrangian Flows-Action Matching (WLF-AM) (Neklyudov et al., 2023b)
 2606 IV. Simulation-free Schrödinger bridges via score and flow matching ([SF]² M) (Tong et al.,
 2607 2023a)

2610 For these methods, we clustered the observations of each system into *disjoint* subsets of adjacent
 2611 points. We employed the k-Nearest neighbours algorithm (Fix, 1985; Cover and Hart, 1967) to
 2612 construct the clusters as local neighbourhoods on the state space, comprising each at most 64 and
 2613 minimum 20 observations. We paired each cluster \mathcal{J}_b with the set $\mathcal{J}_b^+ \doteq \{ \mathcal{O}_{k+1} : \mathcal{O}_k \in \mathcal{J}_b \}$ of
 2614 the next observation of each cluster member. We then considered each cluster pair $(\mathcal{J}_b, \mathcal{J}_b^+)$ as the
 2615 initial and terminal condition for a Schrödinger bridge problem, i.e.

$$\pi_0^b \doteq \{ \mathcal{O}_k : \mathcal{O}_k \in \mathcal{J}_b \} \quad (121)$$

$$\pi_1^b \doteq \{ \mathcal{O}_\ell : \mathcal{O}_\ell \in \mathcal{J}_b^+ \}. \quad (122)$$

2620 These serve as samples of the densities required as boundaries conditions for the Schrödinger
 2621 bridges.

2622 For the multi-marginal setting, starting from the cluster that contained the observation \mathcal{O}_1 and sub-
 2623 sequently created a sequence of cluster following the time ordering of the observations, i.e.

$$\pi_i^0 = \{ \mathcal{O}_{k+i} : k \in \mathcal{J}_0 \}. \quad (123)$$

2626 We then employed a sequence of 50 marginal densities $\{\pi_i^0\}_{i=0}^{49}$ as snapshot observations required
 2627 by the framework.

2629 **Metric Flow Matching.** For the Metric Flow Matching framework, we trained on observations
 2630 resulting from total simulation length $T_{\text{MFM}} = 3T = 1500$ (time units) to ensure sufficient data
 2631 for each bridge. For each constructed bridge indexed by b , the flow network trained with the flow
 2632 matching objective represents the velocity of the samples $\mathbf{u}_b(\mathbf{x}, t)$ transferred within the normalised
 2633 time $t \in [0, 1]$ from the initial boundary condition to the terminal one. We approximate a time-
 2634 independent local drift $\hat{\mathbf{f}}_b(\mathbf{x})$ by rescaling the velocity field $\mathbf{u}_b(\mathbf{x}, t)$ with the inter-observation inter-
 2635 val τ , i.e.,

$$\hat{\mathbf{f}}_b(\mathbf{x}) = \frac{1}{\tau} \mathbf{u}_b(\mathbf{x}, t). \quad (124)$$

2638 To obtain a global drift estimate from the individual local estimates, we compute "responsibilities" or
 2639 weights of each individual drift for each point \mathbf{x}_m of a pre-defined two-dimensional evaluation grid
 2640 that covers the state space region occupied by the observations. These weights indicate how relevant
 2641 each bridge b was for estimating the drift at each grid point \mathbf{x}_m . For each bridge, we compute support
 2642 weights $\omega_b(\mathbf{x})$ on the grid employing kernel density estimation (KDE) over the bridge boundary
 2643 condition samples. Then, for each grid point \mathbf{x}_m , we compute bridge responsibilities as

$$\rho_b(\mathbf{x}_m) = \frac{\omega_b(\mathbf{x}_m)}{\sum_{j=1}^B \omega_j(\mathbf{x}_m)}, \quad \sum_{b=1}^B \rho_b(\mathbf{x}_m) = 1. \quad (125)$$

We estimate the global drift at each grid point by weighting the local estimated drifts with the corresponding bridge responsibility, i.e.,

$$\hat{\mathbf{f}}(\mathbf{x}_m) = \sum_{b=1}^B \rho_b(\mathbf{x}_m) \hat{\mathbf{f}}_b(\mathbf{x}_m). \quad (126)$$

K ALGORITHMIC DETAILS

Here we provide the outline algorithm for each constituent component of our work. Algorithm A1 provides the main skeleton of the framework. For the geometric approximation and the construction of the geodesics we defer the readers to Arvanitidis et al. (2019). Algorithm A2 outlines the solution of the control problem that implements the path augmentation. This part is an adapted version of the main algorithm proposed by Maoutsu and Opper (2021). Finally, Algorithm A3 describes the solution of the Gaussian process inference given the path augmentations (bridges) created for each augmentation pair. For the simulation of Fokker-Planck equation solutions we used the deterministic particle framework of Maoutsu et al. (2020).

Algorithm A1: Skeleton of the proposed framework.

Input: $\mathcal{O} = \{(\mathbf{x}_k, t_k)\}_{k=1}^K$: observed states at timepoint t_k

Output: \hat{f} : posterior estimate of the drift function

$B^{(j)}$: augmented paths of latent states (optional)

```
// initialise  $\hat{\mathbf{f}}$  with a coarse drift estimate
```

1 Initialise drift estimate $\hat{\mathbf{f}}^{(0)}$ according to Eq. 20

// Approximate Riemannian metric from observations (Eq. 34)

$$^2 H_{dd} = \text{ApproximateMetric}(\{\mathcal{O}_k\}_{k=1}^K)$$

11

```
2686 // Construct geodesics between  $\mathcal{O}_k$  and  $\mathcal{O}_{k+1}$  under the estimated metric
2687 as shortest paths
```

$\mathfrak{z}, \Gamma^{(\ell)} \equiv \text{ConstructGeodesics}(\mathcal{Q}_k, \mathcal{Q}_{k+1}, H_{\ell\ell})$

// $E^k = \{\gamma^k_{i,j} \mid i, j \in \{1, \dots, n\}, i \neq j\}$ geodesic curves between selected observation pairs

// $\mathbf{1} = \lfloor It' \rfloor$

// document paths along modules using module's file name

AugmentPaths($\{ \cup_{k=1}^n T^{(j)}, T^{(j-1)} \}$)
 // use the determined local variables to decide next edge

// uses the deterministic particle flow / bridge (Eq. 12) to sample connected trajectories with $\hat{\mathbf{c}}^{(j-1)}$

sample augmented trajectories with $\mathbf{f}^{(0,1)}$

$\hat{p}^{(l)} = \text{softmax}(z^{(l)})$ // Gaussian prior

= GDPdriftInference($\{\mathcal{O}\}_{k=1}^K, B^{(j)}\}$)

```
// update GP posterior over  $f$  using original and augmented data
```

7 **end**

—

Algorithm A3: Gaussian process drift inference from an augmented path measure (part I)

Input: $\mathcal{Z} = \{\mathbf{z}_i\}_{i=1}^S$: inducing points for the sparse GP (Sp)
 $\{\mathbf{X}_j(t_\ell)\}_{j=1,\dots,N}^{\ell=1,\dots,T'}$: particle positions from the path measure Q (BALL2)
 $\{\mathbf{g}(\mathbf{X}_j(t_\ell), t_\ell)\}$: effective drift evaluated along particles (gbALL2)
 k^f : kernel with lengthscales ℓ_1, ℓ_2, ℓ_3 (shared across dimensions)
 g : diffusion amplitude, $\sigma^2 = g^2$
 Δt : time step of the particle simulation
 d : state dimension, N : number of particles, T' : number of time steps

Output: Approximations $I_1^{(i)}, I_2^{(i)}$ of the integrals over $A(\mathbf{x})$ and $B(\mathbf{x})$

// 0. shorthand and initialisation

1 Set $S \leftarrow |\mathcal{Z}|$ (number of inducing points)
2 Initialise $I_1 \in \mathcal{R}^{S \times S \times d}$ and $I_2 \in \mathcal{R}^{S \times d}$ to zero
3 Initialise $\Lambda \in \mathcal{R}^{S \times S \times d}$ and $\mathbf{d} \in \mathcal{R}^{S \times d}$ to zero
// 1. compute kernel matrices on the inducing points

4 Construct the inducing-inducing kernel matrix

$$\mathcal{K}_S = k^f(\mathcal{Z}, \mathcal{Z}) \in \mathcal{R}^{S \times S}$$

and compute a regularised inverse

$$\mathcal{K}_S^{-1} = (\mathcal{K}_S + \varepsilon I)^{-1}, \quad \varepsilon \approx 10^{-3}.$$

5 Define the kernel map to inducing points

$$k^f(\mathcal{Z}, \mathbf{x}) = (k^f(\mathbf{z}_i, \mathbf{x}))_{i=1}^S \in \mathcal{R}^S.$$

// 2. sample-based approximation of $A(\mathbf{x})$ and $B(\mathbf{x})$

6 **for** $i = 1, \dots, d$ **do** // loop over state dimensions

7 **for** $\ell = 1, \dots, T'$ **do** // loop over time

8 Let $\mathbf{X}(t_\ell) \in \mathcal{R}^{d \times N}$ be the particle positions at time t_ℓ
9 For each particle position $\mathbf{X}_j(t_\ell)$, compute

$$\mathbf{k}_j = k^f(\mathcal{Z}, \mathbf{X}_j(t_\ell)) \in \mathcal{R}^S.$$

Stack them column-wise to obtain

$$K_\ell = [\mathbf{k}_1, \dots, \mathbf{k}_N] \in \mathcal{R}^{S \times N}.$$

10 Let $g_i(\mathbf{X}_j(t_\ell), t_\ell)$ denote the i -th component of the effective drift at particle j and time t_ℓ // accumulate Monte Carlo estimates of the integrals

11 Update

$$I_1^{(i)} \leftarrow I_1^{(i)} + K_\ell K_\ell^\top, \quad I_2^{(i)} \leftarrow I_2^{(i)} + K_\ell \mathbf{g}_i(t_\ell),$$

12 where $\mathbf{g}_i(t_\ell) = (g_i(\mathbf{X}_1(t_\ell), t_\ell), \dots, g_i(\mathbf{X}_N(t_\ell), t_\ell))^\top$.

13 **end** // normalise by time and number of particles

$$I_1^{(i)} \leftarrow \frac{\Delta t}{N} I_1^{(i)}, \quad I_2^{(i)} \leftarrow \frac{\Delta t}{N} I_2^{(i)}.$$

14 **end**

In this algorithm Here $I_1^{(i)}$ approximates $\int k^f(\mathcal{Z}, \mathbf{x}) A(\mathbf{x}) k^f(\mathbf{x}, \mathcal{Z}) d\mathbf{x}$, and $I_2^{(i)}$ approximates $\int k^f(\mathcal{Z}, \mathbf{x}) B_i(\mathbf{x}) d\mathbf{x}$.

Algorithm A4: Gaussian process drift inference from an augmented path measure (part II)

Input: Same inputs as Alg. 3

$I_1^{(i)}, I_2^{(i)}$: Monte Carlo approximations from Alg. 3

$\mathcal{K}_S, \mathcal{K}_S^{-1}$: inducing-inducing kernel matrix and its regularised inverse

Output: Component-wise drift estimators $\hat{f}_i(\mathbf{x}), i = 1, \dots, d$

Expected negative log data likelihood $\mathcal{L}_{\text{path}}$ under Q_f

// 3. compute Λ and \mathbf{d} for each component

1 **for** $i = 1, \dots, d$ **do**

// match Eq. equation 42 with sparse GP parametrisation

2

$$2819 \quad \Lambda^{(i)} \leftarrow \frac{1}{\sigma^2} \mathcal{K}_S^{-1} I_1^{(i)} \mathcal{K}_S^{-1}, \quad \mathbf{d}^{(i)} \leftarrow \frac{1}{\sigma^2} \mathcal{K}_S^{-1} I_2^{(i)}.$$

2820 3 **end**

2821 4 This matches the definitions

$$2823 \quad \Lambda = \frac{1}{\sigma^2} \mathcal{K}_S^{-1} \left(\int k^f(\mathcal{Z}, \mathbf{x}) A(\mathbf{x}) k^f(\mathbf{x}, \mathcal{Z}) d\mathbf{x} \right) \mathcal{K}_S^{-1}, \quad \mathbf{d} = \frac{1}{\sigma^2} \mathcal{K}_S^{-1} \left(\int k^f(\mathcal{Z}, \mathbf{x}) B(\mathbf{x}) d\mathbf{x} \right).$$

2826 // 4. define the component-wise drift estimators

2827 5 For each component $i = 1, \dots, d$, define

$$2829 \quad \hat{f}_i(\mathbf{x}) = k^f(\mathbf{x}, \mathcal{Z}) \left(I + \Lambda^{(i)} \mathcal{K}_S \right)^{-1} \mathbf{d}^{(i)},$$

2831 so that the full drift estimate is

$$2833 \quad \hat{\mathbf{f}}_S(\mathbf{x}) = (\hat{f}_1(\mathbf{x}), \dots, \hat{f}_d(\mathbf{x}))^\top.$$

2834 // 5. compute expected negative log data likelihood under Q_f

2835 6 Initialise accumulators $S_{\|f\|} \leftarrow 0, S_{\nabla \cdot f} \leftarrow 0, S_{f \cdot g} \leftarrow 0$

2836 7 **for** $\ell = 1, \dots, T'$ **do**

2837 8 For all particle positions $\mathbf{X}_j(t_\ell)$, evaluate $\hat{\mathbf{f}}_S(\mathbf{X}_j(t_\ell))$
2838 9 Accumulate

$$2840 \quad S_{\|f\|} \leftarrow S_{\|f\|} + \sum_{j=1}^N \|\hat{\mathbf{f}}_S(\mathbf{X}_j(t_\ell))\|^2,$$

$$2843 \quad S_{f \cdot g} \leftarrow S_{f \cdot g} + \sum_{j=1}^N \hat{\mathbf{f}}_S(\mathbf{X}_j(t_\ell))^\top \mathbf{g}(\mathbf{X}_j(t_\ell), t_\ell),$$

2846 and compute the trace of the Jacobian $\nabla \cdot \hat{\mathbf{f}}_S(\mathbf{X}_j(t_\ell))$ via automatic differentiation,
2847 accumulating it into $S_{\nabla \cdot f}$

2848 10 **end**

2849 11 Approximate the expected negative log data likelihood (up to constants) as

$$2851 \quad \mathcal{L}_{\text{path}} = \frac{\Delta t}{N} \left(\frac{1}{2} S_{\|f\|} + S_{\nabla \cdot f} + S_{f \cdot g} \right),$$

2853 which corresponds to evaluating the quadratic form in Eq. equation 42 under the approximate
2854 posterior Q_f .

2862 **L IMPACT STATEMENT**
2863

2864 The aim of this work is to advance the field of dynamical inference for stochastic systems. While we
2865 do not foresee any direct societal consequences directly impinging from our work, we recognize that
2866 stochastic systems could be applied in military contexts, financial engineering, or more recently in
2867 machine learning for data (such as image, audio, video) generation. Still, the proposed method does
2868 not propose interventions that might lead to unfavourable societal outcomes. Overdamped Langevin
2869 systems are widespread in areas such as physics, biology, neuroscience, and ecology. We anticipate
2870 that our contributions will thus help these disciplines by offering a tool to identify and further study
2871 relevant systems.

2872 Our contribution emphasises the importance of incorporating concepts from the evolving field of ge-
2873 ometric statistics into system identification methods for stochastic systems. Although geometric and
2874 topological properties of invariant densities have been extensively studied in the context of deter-
2875 ministic systems, comparable attention is lacking for their stochastic counterparts. Our work further
2876 highlights that in settings where the amount of augmented data exceeds the number of observations,
2877 data augmentation frameworks can enhance inference accuracy by incorporating domain knowledge
2878 or other relevant information, such as the geometry of the system's invariant density we consider
2879 here. Many algorithms used for data augmentation, including the expectation maximisation algo-
2880 rithm employed in our work (Romero et al., 2019), show only **local convergence**. As a result, when
2881 the initial estimate deviates significantly from the true value, naive data augmentation methods may
2882 converge to suboptimal solutions that fail to accurately identify the underlying system.

2883 **M LLMs USAGE STATEMENT**
2884

2885 During the preparation of this manuscript, we used general-purpose large language models (e.g.,
2886 the GPT family) for grammar and writing polishing, minor rephrasing and condensing parts of the
2887 text, for limited code assistance (such as handling error messages and for parallelising and speeding
2888 up parts of the code), and for getting feedback on the finished draft. We did not rely on LLMs
2889 to generate research ideas, methods, experimental designs, analyses, or conclusions. All technical
2890 content, experiments, and claims were designed, implemented, and verified by the authors, who take
2891 full responsibility for the paper. Moreover, we did not embed any executable instructions, hidden
2892 prompts, or other mechanisms intended to influence the peer-review process in the manuscript or its
2893 supplementary materials.

2894
2895
2896
2897
2898
2899
2900
2901
2902
2903
2904
2905
2906
2907
2908
2909
2910
2911
2912
2913
2914
2915